

# UC San Diego

## UC San Diego Electronic Theses and Dissertations

### Title

Non-Maximally Decimated Filter Bank and Its Applications in Wideband Signal Processing /

### Permalink

<https://escholarship.org/uc/item/4j80896n>

### Author

Chen, Xiaofei

### Publication Date

2014

Peer reviewed|Thesis/dissertation

UNIVERSITY OF CALIFORNIA, SAN DIEGO

SAN DIEGO STATE UNIVERSITY

**Non-Maximally Decimated Filter Bank and Its Applications in Wideband Signal  
Processing**

A dissertation submitted in partial satisfaction of the  
requirements for the degree Doctor of Philosophy

in

Engineering Science (Electrical and Computer Engineering)

by

Xiaofei Chen

Committee in charge:

University of California, San Diego

Professor Bhaskar Rao, Chair

Professor William Hodgkiss

Professor Truong Nguyen

San Diego State University

Professor fred harris, Co-Chair

Professor Christopher Paolini

2014

Copyright  
Xiaofei Chen, 2014  
All rights reserved.

The dissertation of Xiaofei Chen is approved, and it is acceptable in quality and form for publication on microfilm and electronically:

---

---

---

---

Co-Chair

---

Chair

University of California, San Diego

San Diego State University

2014

## DEDICATION

I would like to dedicate this dissertation to my family and all my friends.

## EPIGRAPH

*In theory, theory and practice are the same.*

*In practice, they are not.*

—Albert Einstein

## TABLE OF CONTENTS

Signature Page	. . . . .	iii
Dedication	. . . . .	iv
Epigraph	. . . . .	v
Table of Contents	. . . . .	vi
List of Figures	. . . . .	ix
List of Tables	. . . . .	xi
Acknowledgements	. . . . .	xii
Vita	. . . . .	xv
Abstract of the Dissertation	. . . . .	xvii
Chapter 1	Introduction . . . . .	1
	1.1 Motivation of This Dissertation . . . . .	7
	1.2 Dissertation Contributions . . . . .	8
	1.2.1 Wideband Digital Filtering Based on Non-Maximally Decimated Filter Banks . . . . .	8
	1.2.2 Realizable Linear / Non-linear Equalizer Structure for Wideband Single Carrier Transmission . . . . .	9
	1.2.3 Improved System and Implementation Architecture for Single Carrier Diversity Combiner over Frequency Selective Channels . . . . .	9
	1.2.4 Efficient Synchronization Techniques for Filter Bank based Wideband Single Carrier Transmission . . . . .	10
	1.2.5 Novel Channelization Techniques for Supporting Fu- ture Demand for Transmitting and Receiving Multi- ple Random Located Signals with Arbitrary Band- widths . . . . .	10
	1.3 Dissertation Outline . . . . .	11
Chapter 2	Non-Maximally Decimated Analysis / Synthesis Filter Banks: Ap- plications in Wideband Digital Filtering . . . . .	12
	2.1 Introduction . . . . .	13
	2.2 Analysis / Synthesis Filter Bank Model . . . . .	17
	2.2.1 Model Description . . . . .	17
	2.2.2 NMDFB with PR Support . . . . .	18

2.2.3	Low-Pass Prototype Filter Design . . . . .	20
2.3	Efficient Implementation of NMDFB via Polyphase Partition	21
2.3.1	Polyphase Analysis Channelizer(PAC) . . . . .	21
2.3.2	Polyphase Synthesis Channelizer (PSC) . . . . .	22
2.3.3	Spectral Shaping via Intermediate Processing Elements	25
2.3.4	Piecewise Constant Spectral Approximation . . . . .	27
2.3.5	Straight Line Spectral Approximation . . . . .	29
2.3.6	Minmax Optimization over Intermediate Processing	30
2.4	Design Examples and Workload Analysis . . . . .	34
2.4.1	Design Example: $M = 64$ and $D = 32$ . . . . .	34
2.4.2	Workload Analysis . . . . .	36
2.5	Applications . . . . .	38
2.5.1	Linear Phase FIR Filter . . . . .	38
2.5.2	Non-Linear Phase FIR Filter . . . . .	39
2.5.3	Fractional Delay Filter (FDF) . . . . .	39
2.5.4	Masking Filter . . . . .	40
2.5.5	Cascade Filtering . . . . .	40
2.6	Simulation Results . . . . .	41
2.6.1	Linear Phase FIR Filter . . . . .	41
2.6.2	Non-Linear Phase FIR Filter . . . . .	42
2.6.3	Fractional Delay Filter (FDF) . . . . .	45
2.6.4	Applications in Communications . . . . .	45
2.7	Acknowledgment . . . . .	48
Chapter 3	Equalizers for Wideband Digital Receivers Based on Non-Maximally Decimated Filter Banks . . . . .	49
3.1	Introduction . . . . .	50
3.2	Signal Model . . . . .	53
3.3	Equalizer Weights For Infinite Number of NMDFB Channels	54
3.3.1	Linear / Forward Equalizer Weights . . . . .	55
3.3.2	ISI Canceller Weights . . . . .	58
3.4	Finite Path NMDFB Spectral Shaping Error . . . . .	59
3.5	Practical Implementation . . . . .	62
3.6	Implementation Complexity . . . . .	64
3.7	Simulation Results . . . . .	66
3.8	Acknowledgment . . . . .	72
Chapter 4	Filter Bank Selection Diversity and Linear Equalization Over Highly Frequency Selective Channels for Single Carrier Transmission . .	73
4.1	Introduction . . . . .	74
4.2	Signal Model . . . . .	76
4.3	Diversity Combining and Channel Equalization . . . . .	78
4.4	Simulation Results . . . . .	81

	4.4.1	MMSE Study over Single Channel Realization . . . . .	81
	4.4.2	BER Results over Statistical Channel Model . . . . .	83
	4.4.3	Implementation Complexity . . . . .	83
	4.5	Acknowledgment . . . . .	84
Chapter 5		Non-Maximally Decimated Filter Bank Based Single Carrier Receiver: A Pathway to Next Generation Wideband Communication	85
	5.1	Introduction . . . . .	86
	5.2	PR-NMDFB Based Carrier Frequency Recovery . . . . .	88
	5.2.1	CFO Correction in FB Transformed Domain . . . . .	90
	5.2.2	CFO Detection in FB Transformed Domain . . . . .	92
	5.3	PR-NMDFB Based Symbol Timing Recovery . . . . .	94
	5.4	Full NMDFB based FBMC Receiver and Complexity Analysis	95
	5.5	Simulation Results . . . . .	98
	5.5.1	PR-NMDFB Implemented Filters . . . . .	98
	5.5.2	Carrier Frequency Offset (CFO) Recovery Results . . . . .	99
	5.5.3	Symbol Timing Recovery Results . . . . .	101
	5.6	Acknowledgment . . . . .	103
Chapter 6		Multi-Channel Channelization Technique . . . . .	105
	6.1	Introduction . . . . .	106
	6.2	Channelization via Polyphase Analysis Channelizer (PAC) and Polyphase Synthesis Channelizer(PSC) Processing . . . . .	109
	6.3	Proposed Multi-Channel Channelizer Receiver . . . . .	111
	6.3.1	Post Analysis Block and PSC . . . . .	113
	6.3.2	Arbitrary Interpolator . . . . .	114
	6.4	Simulation Results . . . . .	115
	6.5	Acknowledgment . . . . .	117
Chapter 7		Conclusions . . . . .	126
Bibliography		. . . . .	129

## LIST OF FIGURES

Figure 1.1:	Development of Integrated Circuit and Micro-Processor . . . . .	3
Figure 1.2:	Recent Development of Wireless Communication . . . . .	3
Figure 1.3:	2G, 3G, 4G Receiver Complexity . . . . .	4
Figure 1.4:	Moore Versus Cellular . . . . .	6
Figure 2.1:	Generalized M-path Non-Maximally Decimated Filter Bank Model	17
Figure 2.2:	Generalized $M$ -path, Decimation by $D$ , PAC . . . . .	23
Figure 2.3:	$M$ -Path, Decimation by $D = M/2$ PAC [1, 2, 3] . . . . .	23
Figure 2.4:	Generalized $M$ -path, Up Sample by $D$ , PSC . . . . .	24
Figure 2.5:	$M$ -Path, Up Sample by $D = M/2$ PAC [1, 2, 3] . . . . .	25
Figure 2.6:	Filtering Models: (a).Frequency Domain Filtering Model; (b).Time Domain Filtering Model . . . . .	26
Figure 2.7:	64-Path, $D=32$ , Rectangular Design . . . . .	34
Figure 2.8:	Impulse Response of the Analysis and Synthesis Filter Bank . . . . .	35
Figure 2.9:	64-Path, $D=16$ , Triangular Design . . . . .	36
Figure 2.10:	Impulse Response of the Analysis and Synthesis Filter Bank . . . . .	37
Figure 2.11:	64-Path Piecewise Constant Approximation $K_m = S(\omega_m)$ . . . . .	42
Figure 2.12:	64-Path Straight Line Sub-optimal Minimax Approximation . . . . .	43
Figure 2.13:	256-Path Straight Line Sub-optimal Minimax Approximation . . . . .	43
Figure 2.14:	64-Path Piecewise Constant Approximation $K_m = S(\omega_m)$ . . . . .	44
Figure 2.15:	64-Path Straight Line Sub-optimal Minimax Approximation . . . . .	44
Figure 2.16:	256-Path Straight Line Sub-optimal Minimax Approximation . . . . .	45
Figure 2.17:	Fractional Delay Filter . . . . .	46
Figure 2.18:	NMDFB and FIR Based SRRC Shaping Filter . . . . .	46
Figure 2.19:	QPSK Constellation Dispersion (1 <sup>st</sup> Quadrant) . . . . .	47
Figure 3.1:	Theoretical Model of PR-NMDFB Based Linear / Nonlinear Equalizer	54
Figure 3.2:	Adaptive Implementation of PR-NMDFB based Linear / Non-linear Equalizer . . . . .	63
Figure 3.3:	Signal and Equalizer Magnitude Responses . . . . .	67
Figure 3.4:	Learning Curve of the Linear / Non-Linear Equalizers . . . . .	68
Figure 3.5:	MMSE Performance of Proposed Equalizers . . . . .	69
Figure 3.6:	BER Performance over Low Delay Spread, Highly Distorted Chan- nel [4] . . . . .	70
Figure 3.7:	50MHz Symbol Rate QPSK Signal BER Results Over ITU-B Channel	71
Figure 3.8:	100MHz Symbol Rate QPSK Signal BER Results Over 802.11 AC Medbo Model B . . . . .	72
Figure 4.1:	Optimum Combiner / Linear Equalizer Structure . . . . .	75
Figure 4.2:	Filter Bank Based Diversity Combining Model . . . . .	75
Figure 4.3:	Magnitude response 1 <sup>st</sup> Chan, 2 <sup>nd</sup> Chan and Combined Channels . . . . .	82

Figure 4.4:	MMSE after Linear Equalization for 1 <sup>st</sup> Chan, 2 <sup>nd</sup> Chan and Combined Channels . . . . .	82
Figure 4.5:	BER over ITU-B Channel with 50 MHz Symbol Rate . . . . .	83
Figure 5.1:	High Level Architecture of FBMC Receiver . . . . .	87
Figure 5.2:	Band Edge Filter Frequency Locked Loop . . . . .	89
Figure 5.3:	(a).Spectra of SRRC MF, Corresponding Frequency MF, and Spectral Response of their Cascade; (b).Suboptimal BE Filters . . . . .	89
Figure 5.4:	FB Transformed Domain CFO Recovery . . . . .	91
Figure 5.5:	Analysis and Synthesis Low Pass Prototype Filter (LPPF) . . . . .	93
Figure 5.6:	FB Transformed Domain Symbol Timing Recovery . . . . .	95
Figure 5.7:	Proposed FBSC Receiver Block Diagram . . . . .	96
Figure 5.8:	Time and Channelizer Domain MF, and BE Filters . . . . .	99
Figure 5.9:	M = 240, D = 80, PR-NMDFB Implemented FDF . . . . .	100
Figure 5.10:	CFO Tracking Loop Profile . . . . .	101
Figure 5.11:	Constellation Phase Offset Removal Tracking Loop Profile . . . . .	102
Figure 5.12:	Constellation Before and After the Convergence of the Constellation Phase Offset Removal Loop . . . . .	102
Figure 5.13:	Symbol Timing Recovery Loop Profile . . . . .	103
Figure 5.14:	Constellation Before and After the Convergence of the Symbol Timing Recovery Loop . . . . .	104
Figure 6.1:	Possible Received Signal Spectrum . . . . .	107
Figure 6.2:	Block Diagram of Primary Signal Processing in a Typical Digital Receiver . . . . .	107
Figure 6.3:	Block Diagram of the Standard M-path Polyphase Channelizer; M-Port Input Commutator, M-Path Partitioned Filter and M-Point IFFT . . . . .	108
Figure 6.4:	PAC Output Sample Rate Relative to Channel Spacing . . . . .	110
Figure 6.5:	High Level Block Diagram of the Proposed Channelizer . . . . .	111
Figure 6.6:	Block Diagram of the Proposed Receiver; PAC, Post Analysis Block, PSC, Complex Frequency Rotators and Arbitrary Interpolators . . . . .	112
Figure 6.7:	Two Stage Arbitrary Interpolator . . . . .	114
Figure 6.8:	Polyphase Arbitrary Linear Interpolator . . . . .	115
Figure 6.9:	Channelized Received Spectrum and Zoom of One of the Received Signals . . . . .	119
Figure 6.10:	PAC Low Pass Prototype Filter: Nyquist Pulse . . . . .	120
Figure 6.11:	PAC Output Signal Spectrum . . . . .	121
Figure 6.12:	Post Analysis Filters and Filtered Signals for Channel 30 of the PAC . . . . .	122
Figure 6.13:	Log Magnitude of Synthesizer Outputs with Frequency Offsets in the Normalized Frequency Domain . . . . .	123
Figure 6.14:	Log Magnitude of the Heterodyned and Interpolated Spectra in the Frequency Domain [MHz] . . . . .	124
Figure 6.15:	Matched-Filtered and Timing Recovery Signal Constellation . . . . .	125

LIST OF TABLES

Table 3.1: Summary of PR-NMDFB LMS Adaptation . . . . . 64

## ACKNOWLEDGEMENTS

I would like to express my deep gratitude to my research advisors, Professor fred harris and Professor Bhaskar Rao, for their patient guidance, enthusiastic encouragement and insightful critiques. Their guidance and confidence sustained me through times of inspiration and times of difficulty. I met Professor harris in 2006, when I was 21 years old, a kid's age. I was alone and had just begun my study in U.S, a country I know only from movies. I feel grateful that for all these years he takes care of me as one of his family members. He not only taught me everything he knows about signal processing but also the surviving skills in this society. I am very glad to have him as my research advisor and parent. In 2009, Professor harris introduced me Professor Rao, who is a very strict and hands-on advisor, for joint advising of my Ph.D. research. I admit I once had hard times satisfying Professor Rao's requirements on rigorous and preciseness. Yet, I always understood these requirements are necessary and sufficient conditions to earn a doctorate degree. From him, I gained not only valuable expertise in the field, but also a rigorous style in conducting research. I would also like to thank the members of my Ph.D. committee, Professor William Hodgkiss, Professor Truong Nguyen and Professor Christopher Paolini. I am grateful for the time they spent tracking my progress, and for the feedback and direction they provided to my research.

I would like to thank my SDSU labmate, Dr. Elettra Venosa for her participation in my research; and for her accompany in daily research activities. I also want to thank Dr. Chris Dick from Xilinx for giving us interesting research problems and for sharing his opinions on industry level signal processing development. I also want to thank all current and former UCSD labmates, Furkan Kovasoglu, Sheusheu Tan, Bang Nguyen, Anh Nguyen and etc., for sharing their opinions and discussing research progresses.

I would like to thank my friends, Jing Wang, Aaron Tang, Da Sun, Tom Tang, Ryan Chan, Hao Wang, and etc. They have made my after work life colorful. I cannot imagine a life without them.

Finally, I would like to thank my parents for their endless support and encouragement. They are always by my side throughout all the ups and downs of my life. I feel guilty for not able to go home to see them for the past five years. Thanks for their understanding of my academic goal!

Chapter 2, in full, contains material that appeared in the following three published articles:

- Xiaofei Chen, fred harris, Elettra Venosa, and Bhaskar Rao, "Non-maximally decimated analysis / synthesis filter banks: Applications in wideband digital filtering," *IEEE Transactions on Signal Processing.*, vol. 62, no. 4, pp. 852 - 867, 2014.
- fred harris, Elettra Venosa, Xiaofei Chen, Bhaskar Rao, "Variable bandwidth M-path filter with fixed coefficients formed by M-path polyphase filter engines," *Circuit Theory and Design (ECCTD), 2011 20th European Conference on* , vol., no., pp.5,8, 29 - 31 Aug. 2011
- fred harris, Xiaofei Chen, Elettra Venosa, and Chris Dick, "Wideband 160-channel polyphase filter bank cable tv channeliser," *Signal Processing, IET*, vol. 5, pp. 325 - 332, June 2011.

Chapter 3, in part, is currently being prepared for submission for publication of the material:

- Xiaofei Chen, fred harris, Bhaskar Rao and Elettra Venosa, "Equalizers for Wideband Digital Receivers Based on Non-Maximally Decimated Filter Bank"

Chapter 4, in full, contains material that appears in the following article, accepted for publication:

- fred harris, Xiaofei Chen, Elettra Venosa, Bhaskar Rao, "Filter Bank Selection Diversity and Linear Equalization Over Frequency Selective Channels for Single Carrier Transmission", *International Conference on Acoustics, Speech, and Signal Processing (ICASSP) 2014 IEEE*.

Chapter 5, in full, contains material that appears in the following articles (both accepted and published):

- Xiaofei Chen, fred harris, Elettra Venosa and Bhaskar Rao, "Non-Maximally Decimated Filter Bank Based Single Carrier Receiver: A Pathway to Next Generation Wideband Communication", accepted by *EURASIP Journal on Advances in Signal Processing*.

- fred harris, Xiaofei Chen, Elettra Venosa, "A carrier recovery architecture for next generation wideband modems," Global Conference on Signal and Information Processing (GlobalSIP), 2013 IEEE, vol., no., pp.1262,1265, 3-5 Dec. 2013
- fred harris, Elettra Venosa, Xiaofei Chen, Chris Dick, "Band edge filters perform non data-aided carrier and timing synchronization of software defined radio QAM receivers," Wireless Personal Multimedia Communications (WPMC), 2012 15th International Symposium on , vol., no., pp.271,275, 24 - 27 Sept. 2012

Chapter 6, in full, contains material that appeared in the following three published articles:

- fred harris, Elettra Venosa, Xiaofei Chen "Multirate Signal Processing for Software Radio Architectures", Academic Press Library in Signal Processing: Volume 1: Signal Processing Theory and Machine Learning
- fred harris, Elettra Venosa, Xiaofei Chen, and Bhaskar Rao, "Polyphase analysis filter bank down-converts unequal channel bandwidths with arbitrary center frequencies," Analog Integrated Circuit and Signal Processing, vol. 71, no. 3, pp. 481 - 494, 2012.
- fred harris, Chris Dick, Elettra Venosa and Xiaofei Chen, "M-Path Channelizer with Arbitrary Center Frequency Assignments", Wireless Personal Multimedia Communications (WPMC), 2010 13th International Symposium on.

## VITA

- 2006 B. S. in Electrical Engineering, Xi'an University of Posts and Telecommunications, China
- 2008 M. S. in Electrical Engineering, San Diego State University
- 2014 Ph. D. in Engineering Science (Electrical and Computer Engineering), University of California, San Diego, and San Diego State University.

## PUBLICATIONS

- X. Chen, f. j. harris, B. D. Rao and E. Venosa, "Equalizers for Wideband Digital Receivers Based on Non-Maximally Decimated Filter Bank", Ready to Submit to IEEE Trans. Signal Process
- X. Chen, f. j. harris, E. Venosa, B. D. Rao, "Non-Maximally Decimated Analysis / Synthesis Filter Banks: Applications in Wideband Digital Filtering", IEEE Trans. Signal Process.
- X. Chen, f. j. harris, E. Venosa and B. D. Rao, "Non-Maximally Decimated Filter Bank Based Single Carrier Receiver: A Pathway to Next Generation Wideband Communication", Accepted by EURASIP Journal on Advances in Signal Processing
- f. j. harris, X. Chen, E. Venosa, B. D. Rao, "Filter Bank Selection Diversity and Linear Equalization Over Frequency Selective Channels for Single Carrier Transmission", ICASSP 2014
- f. j. harris, E. Venosa, X. Chen "Multirate Signal Processing for Software Radio Architectures", Academic Press Library in Signal Processing: Volume 1: Signal Processing Theory and Machine Learning
- f. j. harris, X. Chen and E. Venosa, "A Carrier Recovery Channelizer Architecture for Next Generation Wideband Modems", GlobalSIP 2013
- f. j. harris; E. Venosa, X. Chen and C. Dick, "Band edge filters perform non data-aided carrier and timing synchronization of software defined radio QAM receivers," WPMC. 2012
- f. j. harris, X. Chen, E. Venosa, B. D. Rao, "Polyphase Analysis Filter Bank Down-Converts Unequal Channel Bandwidths with Arbitrary Center Frequencies", Analog Integr Circ Sig Process
- f. j. harris, E. Venosa, X. Chen and B. D. Rao, "Variable Bandwidth M-Path Filter with Fixed Coefficients Formed by M-path Polyphase Filter Engines", ECCTD 2011.

f. j. harris, C. Dick, E. Venosa and X. Chen, "M-Path Channelizer with Arbitrary Center Frequency Assignments", WPMC 2010

f. j. harris, X. Chen, E. Venosa and C. Dick, "Wideband 160 Channel Polyphase Filter Bank Cable TV Channelizer", IET Signal Processing, Special Issue on Multirate Signal Processing

ABSTRACT OF THE DISSERTATION

**Non-Maximally Decimated Filter Banks and Its Applications in Wideband Signal Processing**

by

Xiaofei Chen

Doctor of Philosophy in Engineering Science  
(Electrical and Computer Engineering)

University of California, San Diego, 2014  
San Diego State University, 2014

Professor Bhaskar Rao, Chair  
Professor fred harris, Co-Chair

Throughput, spectral efficiency and power consumption are the three major factors that drive the evolution of the communication systems. The data rate of modern wireless communication has increased from 10 kb/s (1995 narrow band GSM) to over 100 Mb/s (2015 LTE Advanced) in just twenty years. The data rate of the wired communication has reached more than 2 Gb/s to accommodate the fast growing cellular data rates. The Moore's law is still in effect and the wideband communication era continues to become more entrenched in our daily lives!

Dealing with wideband signals poses great challenges to our existing signal pro-

cessing approaches. At a high sample rate, i.e., GHz level, any non-trivial signal processing, e.g., digital filtering, may saturate the processing resources. This is because the signal's sample rate has become comparable to the hardware's clock rate! At such high rate, significant amount of hardware resources or parallelism is needed to execute the required number of multiply and accumulation operations. This phenomenon is the bottleneck in our further pursuit of higher data rate communication and will raise the hardware cost significantly.

This dissertation tackles several challenging wideband signal processing problems in communication system design. In particular, we propose the non-maximally decimated filter bank (NMDFB) based digital filtering approach. A key attribute of this structure is that the filtering is achieved via the intermediated processing element (IPE) embedded in between a pair of analysis and synthesis NMDFB. The polyphase implementation of NMDFB has its workload on the same order as the FFT and is thus extremely efficient. This type of digital filter implementation not only allows the signal processing to be performed at a significantly reduced sampling rate but also exhibits significant savings in power consumption over the conventional approaches. The NMDFB based processing supports many if not all of the commonly used filtering tasks in communications, and therefore can be used to implement a wideband receiver. We demonstrate this by developing a NMDFB based efficient linear / non-linear equalization techniques for single carrier QAM signal. We also address the carrier and symbol timing synchronization problems based on NMDFB approach. Besides the filtering tasks, the NMDFB based architecture also enables several key signal processing tasks required by the future's communication systems. We show NMDFB can be used as the basis of an efficient wideband diversity combiner over frequency selective channels. We also demonstrate advanced channelization technique based on NMDFB. Unlike the existing channelizers that often pose constraints on either signal format or signal spectrum, the proposed channelizer is able to channelize multiple signals with arbitrary center frequency, arbitrary bandwidth and arbitrary format.

# **Chapter 1**

## **Introduction**

Both wired and wireless communications have experienced significant growth during the past century. The early development of the telegraph in 1837 and telephone in 1876 made the long distance communication possible. Telegraph and telephone quickly became the principle media for telecommunications for most of the 20th century. The commercialization of radio by Gulielmo Marconi in 1901 opened the door for wireless communication. It greatly increased the mobility of business and personal communication and made greater volumes of communication possible. Stepping into the mid-20th century, aided by the invention of transistor and the fast growing integrated circuit and micro-processor technologies, the telecommunication industry has experienced another round of extraordinary growth. Critics have predicted the imminent demise of Moore's law ever since Gordon Moore stated it in 1965. Electrical Engineers continue to defy physical challenges; squeezing ever more circuitry into less space and making information fly ever further and faster. Fig. 1.1 illustrates the growth in semiconductor complexity and capabilities described by Moore's law.

Driven by the demand of high data rate, modern communications have evolved across multiple generations in the past two decades. Fig.1.2 from [5] shows the rapid increasing data rate support for successive generations of major commercial wireless standards. It comes as no surprise that the Gb/s cellular network is rapidly coming our way. The key fact worth noting is the steady increase in bandwidth and data rate in evolution of physical layer architecture used for cellular communication as shown in Fig.1.2. The early 2<sup>nd</sup> generation mobile telecommunication standards (2G), i.e., Groupe Special Mobile (GSM) and General Packet Radio Service (GPRS) systems were based on Quadrature Amplitude Modulation (QAM) supporting  $\leq 100$  kb/s data rate. The Code Division Multiple Access (CDMA) based 3G systems, i.e., Universal Mobile Telecommunications System (UMTS), support around 10 Mb/s data rate. The currently used Orthogonal Frequency Division Multiplexing (OFDM) based 4G systems, i.e., Long Term Evolution (LTE), support between 10 Mb/s and 100 Mb/s data rate.

Based on Fig. 1.2, one might think OFDM based systems are much superior to others in terms of high data support. In fact, as pointed by many researchers [6] [7] and etc., that OFDM systems suffer from synchronization and peak to average power ratio (PAPR) problem which can dramatically degrade overall system performance and

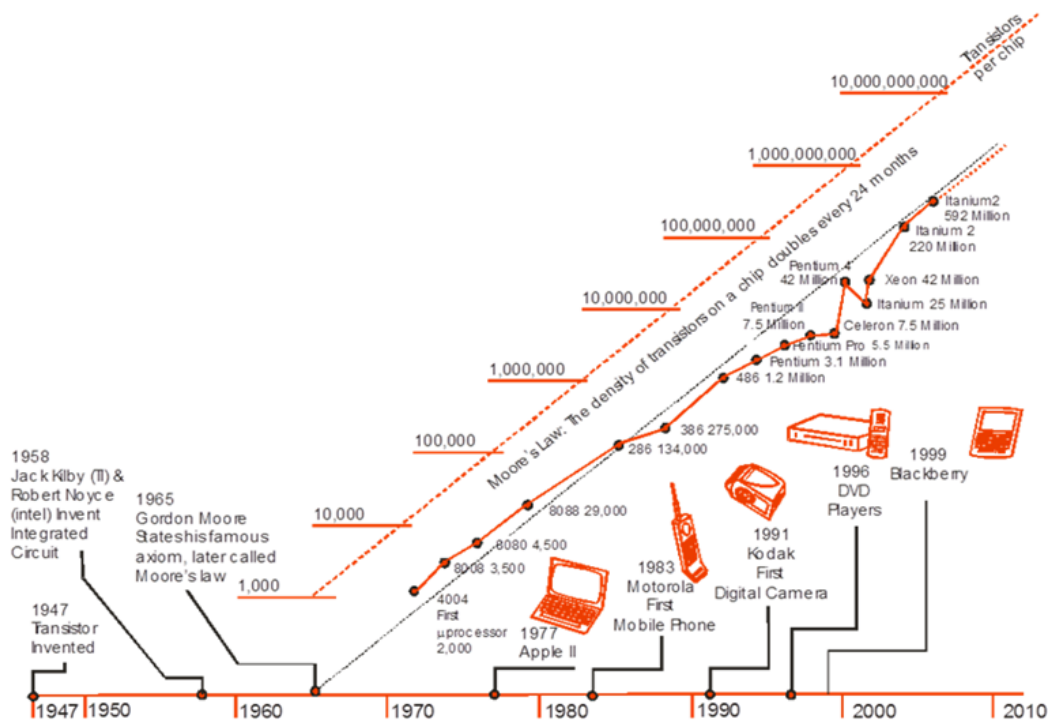


Figure 1.1: Development of Integrated Circuit and Micro-Processor

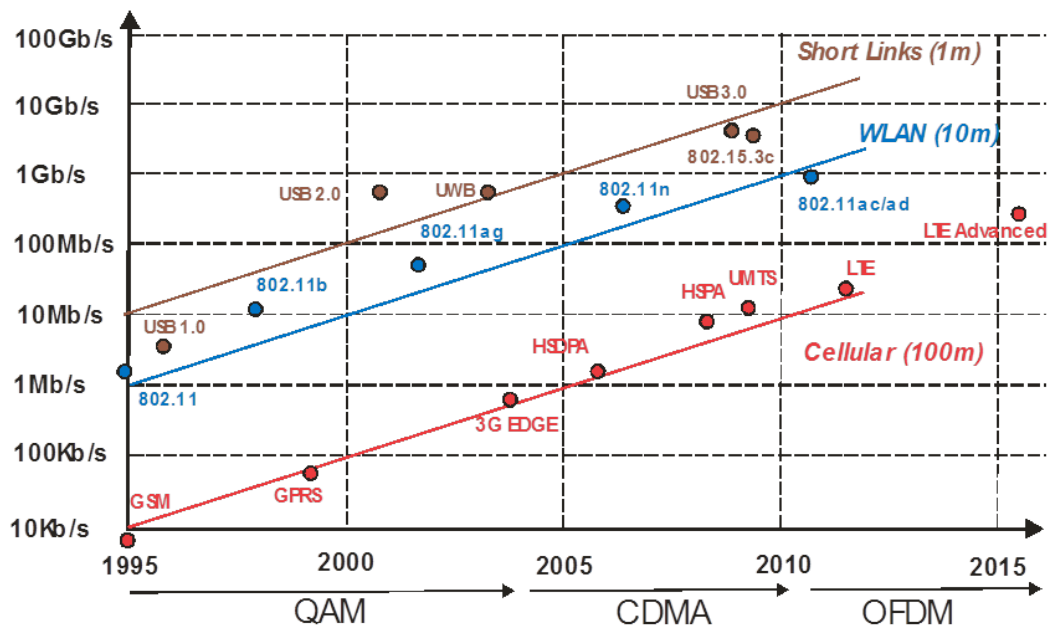


Figure 1.2: Recent Development of Wireless Communication



**Figure 1.3:** 2G, 3G, 4G Receiver Complexity

increase power consumption. Yet, we were taught that engineering is all about making trade-offs. A better question to ask might be "Why OFDM is chosen for commercial high data rate communication?" From a system point of view, the answer is that "OFDM offers lower equalization cost compared to other approaches when conducting wideband communication" [8] [9] [10]. The role of an equalizer is to combat any sort of channel distortion introduced between the transmitter and the receiver. Thus, it plays the most important role in any wideband communication systems. As a matter of fact, the cost of an equalizer has dominant impact on the overall receiver cost [9] [10] and this is especially true for QAM based systems. Fig. 1.3 briefly summarizes the equalization complexity for 2G, 3G and 4G systems. The 2G QAM based systems requires building maximum likelihood sequence estimation (MLSE) type of equalizer whose complexity grows exponentially with the length of channel echoes. The 3G CDMA systems utilizes RAKE receiver, whose complexity grows linearly with the number of channel echoes. The 4G OFDM systems are multi-carrier based system adopting frequency domain equalization via Fast Fourier Transform (FFT), one of the most, perhaps the most, efficient algorithms ever found. Therefore its complexity grows logarithmically with the length of channel echoes. Given this fact, OFDM is chosen from system design

perspective as the more capable candidate for wideband communication.

Another critical reason for adopting OFDM systems as commercial wideband communication platform is due to the hardware implementation cost. The modern digital signal processing (DSP) and micro-processor based modems rely on various digital filters to perform so-called first tier, second tier and third tier processing. The first tier processing includes shaping filters, spectral translation and signal conversion; the second tier processing covers any parameter estimation, carrier frequency and phase synchronization, timing recovery, automatic gain control and signal to noise ratio (SNR) estimation; the third tier processing often involves channel equalization, I-Q balancing, DC-canceling, PAPR control, signal pre-distortion, interference suppression, intrusion suppression and power amplifier linearization. Most of these necessary signal processing tasks are achieved via digital filters, e.g., Finite Impulse Response (FIR) filters. As the signal bandwidth grows, these filters need to run on higher speed proportional to the signal bandwidth; and this easily saturates the hardware's processing capability. As an example, assuming an FIR filter of 100 taps is used to process incoming signals with 1 GHz sample rate, then 100 multiplies needs to be performed within  $10^{-9}$  seconds interval. However, today's popular high-end hardware clock is only around 2-to-3 GHz. This implies significant hardware resource parallelism, i.e., 100 dedicated multipliers for this example, is needed to perform the high speed filtering task. This adds huge amount of implementation complexity and cost to the wideband system. On the other hand, the OFDM based system is entirely based on FFT which is a block processor and has low speed processing characteristic already built-in, i.e., the serial to parallel conversion for the FFT computation. Therefore, the OFDM type of modems has become dominant in today's wireless devices. Fig.1.4 obtained from [11] clearly shows the ratio between microchip clock rate and data rate has decreased from 2000 to 2 from 2G to 4G devices.

Besides wireless communication, the modern wired communication also suffers from the similar problems. One example is the backhaul modem used to communicate between base stations and the core networks. As the consequence of the increasing data rate for cellular devices, the throughput of the backhaul transmission should also be enhanced to accommodate the growing cellular data usage. The current generation backhaul modem utilizes the standard shaped QAM transmission and has symbol rate

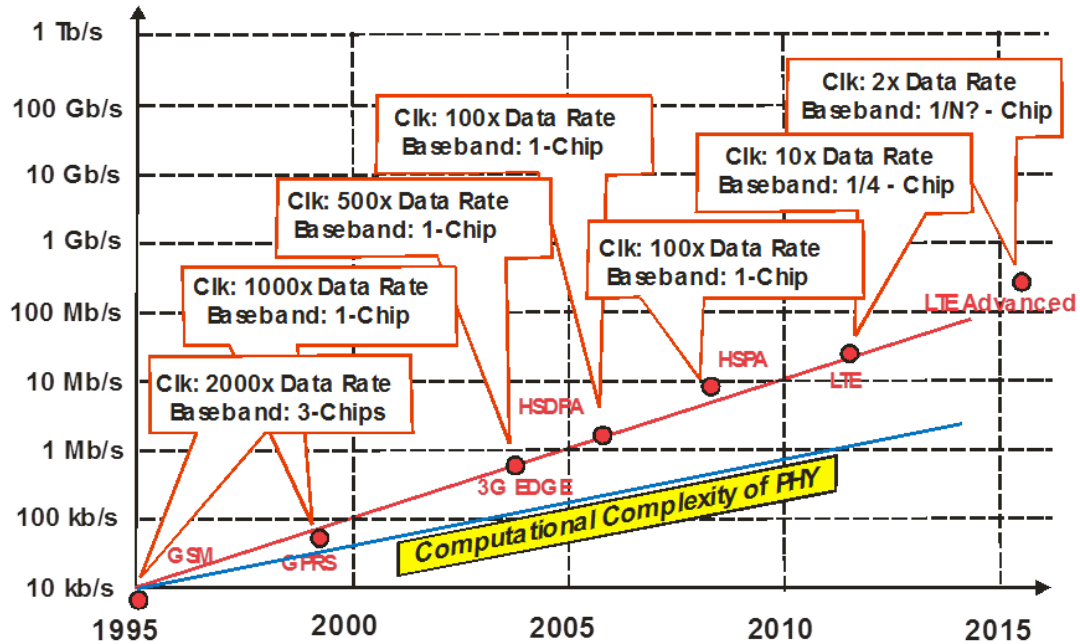


Figure 1.4: Moore Versus Cellular

around 200 Msym/s to 400 Msym/s. We have stated that signal processing at such high clock speed consumes lots of power, and requires significant amount hardware parallelism, both of which made the backhaul modems expensive. Moreover, according to Fig. 1.2, we are in need of backhaul modems capable of delivering data at 1 Gsym/s in the coming years.

The final fact on OFDM's superiority is its enhanced multiple access support compared to most of other existing waveforms. The OFDM by nature is a multi-carrier system. And, a multi-carrier scheme theoretically offers enhanced multiple access support. Ideally, different amount of sub-carriers can be assigned to a particular user based on its throughput request; moreover, the assigned sub-carrier frequencies do not need to be continuous. This scenario also fits very well with the future Cognitive Radio (CR) concept because one major requirement, except for spectral sensing, for implementing CR is the capability of transmitting and receiving multiple signals with arbitrary bandwidths and arbitrary frequencies [12]. However, the OFDM based systems requires that all sub-carriers arrive at the receiver to maintain orthogonality. This problem still remains to be solved before OFDM based systems becoming the physical layer for CR.

## 1.1 Motivation of This Dissertation

Several key factors can be extracted from our previous discussion: 1). OFDM based systems dominants today's major wireless standards because of its simple equalization scheme and low clock processing nature. 2). Although legacy waveforms, e.g., QAM transmission, have many nice properties, i.e., PAPR, synchronization, spectral efficiency and etc., their implementation cost grow exponentially with the signal bandwidth. 3). The hardware clock rate, which affects the number of operations per interval, is one of the limiting factors to the achievable data rate. The OFDM is FFT based block processor that requires much lower clock rate than legacy QAM waveform; or any waveforms requiring significant amount of digital filtering tasks. 4). The OFDM based multi-carrier systems may give better support for future's multiple access system and CR.

A question to ask at this point is "Can we take advantage of both OFDM and legacy waveforms?" or perhaps "Can we find any other candidates besides OFDM?". We know that OFDM type of systems suffer from severe problems in PAPR, synchronization, and throughput (when long cyclic prefix (CP) is involved to accommodate the channel delay spread). The impacts of any of these mentioned problems are non-trivial. The PAPR problem has made LTE based cellular headsets very power inefficient. The synchronization problem, especially for carrier offset, can dramatically degrade the quality of service or even ruin the entire communication. And, the CP takes at least 25% of the throughput (802.11a) based on channel conditions. Should we live with it just to avoid building less digital filters or should we find alternative solutions?

This dissertation aims at developing alternative signal processing solutions to all type of wideband signals. One must be clear that it is the lack of efficient digital filtering tools that prevents us from using alternative physical layer approaches other than OFDM. We also need to know that OFDM systems also need to perform regular digital filtering, except equalizer, to perform various tasks in the first tier, second tier and third tier signal processing tasks. Therefore, it is important to develop alternative digital filtering tools other than FIR filters, which requires very high clock speed support when processing wideband data. In this dissertation, we begin by proposing a new type of digital filters based on polyphase filters and FFT. This type of filter does not need high

clock frequency support and has its workload tied up with FFT. We shall demonstrate its capability in performing various filtering tasks that are often used in communications.

Based on the new filtering tool, we show that we can build both linear and non-linear equalizers for ordinary QAM signals with equalizer complexity that grow logarithmically with bandwidth, a relationship exhibited by OFDM systems! We show that the proposed digital filter offers enhanced diversity combining support for any single carrier wideband signals over severe frequency selective channels. We also present the full synchronization scheme via the proposed communication architectures. This single carrier wideband proposal allows us to enjoy properties such as low PAPR, better synchronization, high throughput and etc. Most importantly, we show that the proposed filtering tool also gives strong support to channelization tasks, i.e., transmit and receive multiple signals with arbitrary center frequencies and arbitrary bandwidths. We believe that the proposed wideband solution serves as a strong candidate to fulfill the future physical layer requirement side-by-side to OFDM.

## **1.2 Dissertation Contributions**

In the sequel, we summarize the main contribution of this dissertation.

### **1.2.1 Wideband Digital Filtering Based on Non-Maximally Decimated Filter Banks**

Current systems offer 100 Mb/s data rates in 20 MHz bandwidth links. We can expect future generation wireless systems to offer 1 Gb/s data rates with 500 MHz bandwidth links. Clock rates of signal processing engines in future devices will be comparable to the sample rates of the sampled input signal. At high sample rates even the simplest digital filtering task, i.e., FIR filtering, may saturate the hardware's processing limit. This is because the hardware operation speed is limited by its clock rate; and the number of operations required per clock interval is directly related to the signal's sampling rate and bandwidth. This dissertation presents very efficient wideband filtering tools that can enable the design of hardware realizable wideband transceivers. We propose a new class of digital filtering architecture that effectively handles various signal

processing tasks for wideband signals while operating the hardware at deeply reduced processing rates. This class of filter not only supports time invariant / varying filter operations; but also achieves special filtering tasks such as fractional delay and etc.

### **1.2.2 Realizable Linear / Non-linear Equalizer Structure for Wideband Single Carrier Transmission**

In this work, we propose filter bank based linear / non-linear block equalizer for single carrier, i.e., shaped Quadrature Amplitude Modulation (QAM) signals with time varying support. There are existing works addressing the filter bank based linear equalizer. In this dissertation, we introduce NMDFB with triangular shaped prototype filter. This option produces much lower spectral modeling error than the past works, thus having superiority in either system performance or in implementation cost. In addition, we introduce the novel non-linear block equalizer with variable block size. The non-linear equalizer part in the literature is either implemented via time domain transversal filter approach or via filter bank but subjected to causality issue, which often requires complicated initialization process. The proposed non-linear equalizer does not have causality problem and can be implemented via efficient adaptive algorithms. Compared to the existing OFDM based wideband systems, the proposed technique has well controlled PAPR, thus is power efficient; and is free of CP, thus is throughput efficient. We also derive the filter bank based equalizer's achievable minimum mean square error (MMSE) which was not addressed previously.

### **1.2.3 Improved System and Implementation Architecture for Single Carrier Diversity Combiner over Frequency Selective Channels**

The diversity combining techniques are crucial for maintaining reliable communication links. It is extensively used in narrow band single carrier systems as well as the modern wideband multicarrier systems. However, due to the extremely high implementation complexity, it is rarely used for single carrier wideband links. This dissertation explores the filter bank based implementation of a diversity combiner which efficiently

synthesizes the optimal maximum ratio combining (MRC) technique if the channel state information (CSI) is available at the receiver. In addition to MRC technique, the filter bank based diversity combiner also enables a new type of diversity technique called selection diversity over frequency selective channels. We show that the new selection diversity technique does not require CSI at the receiver while still providing performance close to the optimal MRC technique.

#### **1.2.4 Efficient Synchronization Techniques for Filter Bank based Wideband Single Carrier Transmission**

The single carrier receiver needs to perform carrier, timing and phase synchronization. These individual blocks are usually implemented via finite impulse response (FIR) filters. As the bandwidth grows, these tasks quickly become unaffordable due to the limited hardware resources. This dissertation presents the filter bank based carrier, timing and phase synchronization architecture for very wideband single carrier receiver. We shall show all the synchronization tasks can be efficiently embedded in the filter bank processor and enables significant workload reduction comparing to the traditional techniques.

#### **1.2.5 Novel Channelization Techniques for Supporting Future Demand for Transmitting and Receiving Multiple Random Located Signals with Arbitrary Bandwidths**

The channelization technique is an essential requirement for the near future's communication standards. This dissertation presents a novel channelization technique based on polyphase channelizers. The proposed channelization technique does not restrict the underlying received waveforms to be multi-carrier signals. The received signals can have arbitrary bandwidth, arbitrary center frequency and arbitrary format. Compared to the existing channelization techniques, the proposed solution has enhanced flexibility, and poses no constraints on signal format and received composite signal spectrum.

## 1.3 Dissertation Outline

The outline of this dissertation is as follows: In Chapter II, the Non-maximally Decimated Filter Bank (NMDFB) based digital filtering approaches are developed. The spectral approximation approach is used to synthesize various types of commonly used filters. In Chapter III, the NMDFB based linear and non-linear equalization techniques are presented for wideband single carrier transmissions. We will demonstrate the effectiveness of the proposed techniques from various perspectives and compare it to the existing solutions. In Chapter IV, the enhanced diversity combining technique for wideband single carrier signals over frequency selective channels is discussed. A new type of channelizer selection diversity approach is proposed and compared with the optimal MRC solution. In Chapter V, the synchronization technique for single carrier QAM signal based on NMDFB filters are discussed. We show that the complexity of the synchronization tasks can be much simplified with NMDFB based digital filters. In Chapter VI, the channelization technique based on analysis and synthesis NMDFB is presented. The receive of multiple randomly located signals with arbitrary bandwidths will be demonstrated. Chapter VII draws the conclusion.

## **Chapter 2**

# **Non-Maximally Decimated Analysis / Synthesis Filter Banks: Applications in Wideband Digital Filtering**

## 2.1 Introduction

This chapter develops high performance digital filtering architectures to deal with the significant increase in complexity, cost and possible performance losses that are likely to occur in dealing with the increasing bandwidth of communication signals in future wideband transceivers.

Successive generations of wireless communication systems have increased their bandwidths and data rates by more than an order of magnitude per generation. Current systems offer 100 M-bit/sec data rates in 20 MHz bandwidth links. We can expect future generation wireless systems to offer 1 G-bit/sec data rates with 500 MHz bandwidth links. Clock rates of signal processing engines in future mobile devices will be comparable to the sample rates of the sampled input signal. The signal processing algorithms, such as matched filtering, equalization, and synchronization will require significant parallelism to accomplish their processing tasks. At high sample rates even the simplest digital filtering task, i.e., FIR filtering, may saturate the hardware's processing limit. This is because the hardware operation speed is limited by its clock rate; and the number of operations required per clock interval is directly related to the signal's sampling rate or bandwidth. Historically, the efficient filtering problem is mainly solved via fast convolution [13], whereby the linear convolution is converted into circular convolution via either overlap-and-save or overlap-and-add algorithms. The circular convolution is then efficiently computed via the fast Fourier transform (FFT) algorithm. In practice, the fast convolution is rarely used in communication or real time systems, with the exception of Orthogonal Frequency Division Multiplexing (OFDM), in which the cyclic prefix (CP) symbol structure absorbs the channel transients and converts linear convolution into circular making the wireless channel equalization task simple [14]. Moreover, the block processing nature of the OFDM parallels the hardware's processing rate, i.e., serial to parallel conversion at FFT, which allows the hardware to operate on lowered processing rate thus significantly reducing the hardware cost. Despite all the advantages of OFDM systems, authors in [15, 6] have pointed out its disadvantages compared to legacy systems, for instance, high peak to average power (PAPR) ratio, CP overhead, sensitivity to frequency offset, etc. In the non-OFDM systems, the signal processing tasks often involve matched filtering, timing recovery, carrier/phase offset removal, channel equal-

ization [16, 17]. The current state of art requires these tasks to be performed over a sample by sample, or symbol by symbol basis due to their underlying signal structure as well as time varying channel nature; thus, it is difficult to apply fast convolution to these tasks. In addition, due to the boundary condition of the fast convolution, the linear convolution must be reconditioned via overlap add/save approaches [13], which imposes additional burdens. Considerable efforts have been spent on incorporating fast convolution into legacy receivers, and these works are mainly focused on channel equalization [15, 6, 4]. The purpose of this paper is to develop efficient wideband filtering tools that can enable the design of realizable wideband transceivers. We propose a new class of digital filtering architecture that effectively handles various signal processing tasks for wideband signals while operating the hardware at lowered processing rates. The proposed architecture is based on oversampled, uniform  $M$ -channel, discrete Fourier transform filter banks (DFT-FB) or DFT-NMDFBs, which includes a pair of analysis filter bank (AFB) and synthesis filter bank (SFB); as well as the intermediate processing elements (IPEs). It is important to emphasize that what we are describing here are a coupled analysis and synthesis filter bank pair and that the coupled filter bank pair resides at both the modulator side and at the demodulator side of the communication link. The coupled filter bank pair at each end of the link enables a unique set of signal processing options and opportunities not previously available in earlier signal processing architectures. For instance, the coupled filter bank pair can replace a high speed DSP engine applying a matched filter to a quadrature 1-GHz bandwidth signal with a 2-GHz sample rate. In one scenario the analysis filter partitions the 1-GHz bandwidth input signal into forty 25-MHz bandwidth segments with 50 MHz sample rates. These low data rate intermediate signals are processed and modified by forty parallel low speed processing engines to effect the spectral envelope change derived from the matched filter. The gain modified intermediate signals are recombined by the coupled synthesis filter bank to form the high bandwidth, high sample rate processed output signal. The theory of filter banks has been well studied from various perspectives. Pioneer works [18, 19, 20, 21, 22, 23, 24, 25, 26], etc., provided fundamental theory; derived the PR conditions; proposed general solutions to prototype filters design. The major application of PR filter banks is to serve source coding and data compression. Thus, critically sam-

pled PR filter banks, especially cosine modulated filter banks (CMFB) received major attention. Authors in [27, 28, 29] and etc. proposed prototype filter design algorithms for critically sampled CMFB; and [30, 31] discussed the practical implementation of M-channel PR filter bank. The oversampled filter banks [32, 33, 34, 1, 35] were introduced in late 90s, due to its various advantages as summarized in [32]. Our task in this paper is to introduce a new class of digital filters based on PR filter banks, whereby the filtering is achieved by altering the gain and phase over each spectral fragments presented at AFB outputs. In order to achieve this, several conditions on filter bank need to be met: 1) It must have PR or near PR property. 2) The aliasing cancellation should not involve other channels; as a counter example, CMFB [27] requires adjacent channels to cancel aliasing thus generally cannot be used; 3) Efficient polyphase implementation must exist, preferable with fixed channel size  $M$  and adjustable decimation factor  $D (D < M)$ . One filter bank design that meets these conditions is proposed by Karp, in Fig 9 of [1] under the name "DFT polyphase realization", which is served as intermediate step to derive the polyphase implementation of modified DFT (MDFT) [25, 1]. Note that, although MDFT is a critically sampled filter bank, the "DFT polyphase realization", denoted as DFT-NMDFB only performs  $D = M/2$  [1] decimation in an  $M$ -channel filter bank. The DFT-NMDFB itself may not offer competitive sample rate reduction from compression point of view. However, from waveform processing perspective, DFT-NMDFB efficiently implements a bank of band pass filters (BPFs) with PR support. As an example, a slightly different version of  $D = M/2$  based DFT-NMDFB is used by authors in [2, 3] to solve the channelization problem; simultaneously transmitting and receiving multiple communication signals with arbitrary bandwidths and center frequencies. Meanwhile, authors in [36] investigated efficient implementation of 2x oversampled, i.e.,  $D = M/2$ , from circuit design perspective. For other DFT-NMDFBs, authors in [37] recently proposed a general approach to construct PR paraunitary DFT-NMDFB. However, they focused on finding the minimal polyphase structure for a given  $M$  and  $D$ ; this cannot be used in our application which requires fixed  $M$ , adjustable  $D$ . Author in [38] also proposed design of NMDFB with PR. Yet, the prototype filter length is restricted to twice of the decimation factor  $D$  which impairs design flexibility. [39] investigated oversampled PR filter bank based on lattice structure, but from the perspective of suppressing

quantization noise. As a generalization of [1], an  $M$ -channel / path, decimation by  $D$  ( $D$  must divide  $M$ ) DFT-NMDFB with PR property will be derived. Later will be shown in the paper that the adjustable factor  $D$  decides how often the filter weights are updated; thus it offers time varying support to our NMDFB based filter. We also present our prototype filter design from Nyquist channel point of view, which provides both PR support and improved spectral shaping performance. Note that, Karp in [1] has used square root raised cosine (SRRC) pulse as prototype filters for both AFB and SFB; as a special case, its composite response produces a Nyquist channel. We shall further emphasize this idea in our derivation and offer insights from spectral shaping perspective. In our NMDFB, the AFB / SFB together with the IPEs are used to solve the spectral shaping / signal manipulation problem. This concept can be viewed as an enhanced version of the Frequency Response Masking (FRM) technique [17, 40, 41, 42, 43, 44]. Authors in [17, 40, 41, 42] used the filter banks to synthesize very sharp FIR masking filters; [?, 43, 44] proposed filter bank based variable bandwidth filter as well as BPFs. We will show, in addition to masking filter and BPF, the generalized NMDFBs with PR support can replace most of the conventional filters with enhanced benefits for both performance and implementation. The AFB can be thought as a bank of BPFs akin to the Fourier Transform [45], which offers access to the frequency domain. By properly controlling IPEs, i.e., the gain / phase applied at each AFB output, one can achieve arbitrary spectral shaping of the input data. Our filter design idea is also a generalization of the early frequency-sampling filter design technique seen in [46], where the desired frequency response is uniformly sampled and the corresponding time domain filter is produced. However, as will show later, by using NMDFB, not only the filtering task but also the filter design task is indeed transformed into the frequency domain. The performance comparison between NMDFB and FIR based design via representative examples will also be given; the future potential application will be discussed. The rest of this chapter is organized as: section 2.2 introduces the AFB/SFB model; section 2.3 describes the polyphase implementation of the NMDFB; section 2.4 describes the spectral manipulation via IPE; section 2.5 provides design examples of NMDFBs; and section 2.6 discusses the wideband filtering applications. Simulation results are given in section 2.7; section 2.8 draws the conclusion for this chapter.

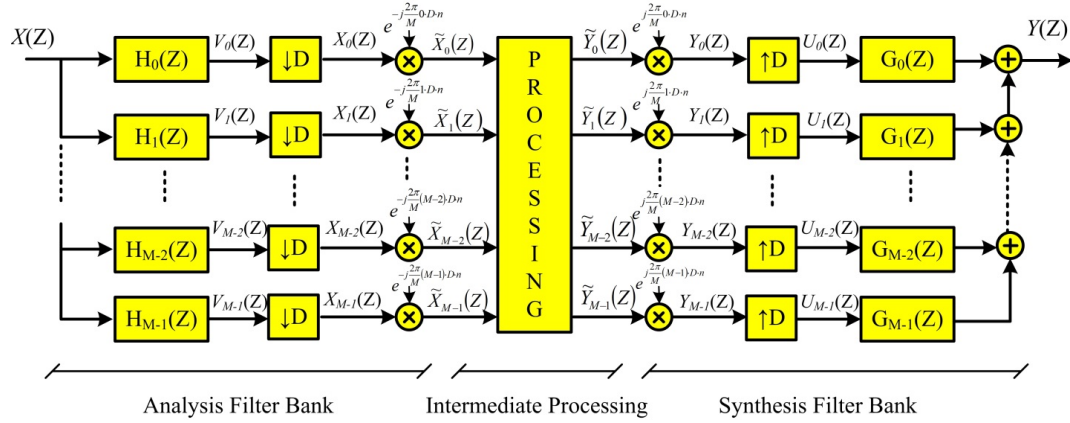


**Figure 2.1:** Generalized M-path Non-Maximally Decimated Filter Bank Model

## 2.2 Analysis / Synthesis Filter Bank Model

### 2.2.1 Model Description

We start derivation from the basic NMDFB model used in [33, 34]. Its high level basic block diagram is shown in Fig. 2.1.

The AFB contains  $M$  BPFs, whose  $Z$ -transforms are denoted as  $H_m(z)$ ,  $m = 0, 1, \dots, M-1$ . The BPFs have equal bandwidth, and each is centered on digital frequency  $\theta_m = \frac{2\pi}{M}m$ ,  $m = 0, 1, \dots, M-1$ . Let  $h(n)$  be the impulse response of the low pass prototype filter (LPPF). The  $m$ th BPF can then be represented as  $h_m(n) = h(n)e^{j\frac{2\pi}{M}mn}$ , whose  $Z$ -transform is  $H_m(z) = H\left(e^{-j\frac{2\pi}{M}m}z\right) = H(W_M^m z)$ , and  $W_M \triangleq e^{-j\frac{2\pi}{M}}$ . Similarly, the SFB filters  $G_m(z) = G(W_M^m z)$ ; and  $g_m(n) = g(n)e^{j\frac{2\pi}{M}mn}$ . A down sampling operation by a factor  $D$ , which is an integer that divides  $M$ , follows each BPF. After down sampling, on each output port of the AFB, the signal has to be centered on zero frequency. This task is accomplished by using a set of complex rotators whose values are  $e^{-j\frac{2\pi}{M}mnD}$ . With these definitions, the  $m^{\text{th}}$  BPF output signal is  $v_m(n) = x(n) * h_m(n)$ . The decimation by  $D$  causes  $D$ -fold aliases and can be written as  $x_m(n) = v_m(Dn)$  for  $n = 0, 1, \dots$ . The  $Z$ -transform of signal presented at the input to the IPE denoted as  $\tilde{X}_m(z)$  can be expressed as:

$$\tilde{X}_m(z) = \frac{1}{D} \sum_{d=0}^{D-1} X\left(z^{\frac{1}{D}} W_D^d W_M^{-m}\right) H\left(z^{\frac{1}{D}} W_D^d\right) \quad (2.1)$$

Denote the IPE transfer function for the  $m^{\text{th}}$  filter in the bank to be  $K_m(z)$ , for  $m = 0, 1, \dots, M-1$ . Thus the input to the  $m^{\text{th}}$  filter in the SFB is  $\tilde{Y}_m(z) = K_m(z) \tilde{X}_m(z)$ . Again, complex heterodyning  $\tilde{Y}_m(z)$  by  $e^{-j\frac{2\pi}{M}mnD}$ , one obtains  $Y_m(z) = \tilde{Y}_m(zW_M^{mD})$ . Using 2.1, we can express  $Y_m(z)$  as:

$$Y_m(z) = \frac{1}{D} K_m(zW_M^{mD}) \sum_{d=0}^{D-1} X\left(z^{\frac{1}{D}} W_D^d\right) H\left(z^{\frac{1}{D}} W_D^d W_M^m\right)$$

Signal  $U_m(z)$  is obtained by up sampling  $Y_m(z)$  by  $D$ , i.e.,  $U_m(z) = Y_m(z^D)$ . The final output of the SFB  $Y(z)$  is:

$$Y(z) = \frac{1}{D} \sum_{d=0}^{D-1} X\left(zW_D^d\right) \sum_{m=0}^{M-1} K\left(z^D W_M^{mD}\right) H\left(zW_D^d W_M^m\right) G\left(zW_M^m\right) \quad (2.2)$$

## 2.2.2 NMDFB with PR Support

Equation 2.2 can be compactly expressed in matrix form. Let us define the following column vectors:

$$\begin{aligned} \mathbf{G}(z) &= [G(zW_M^0) \dots G(zW_M^{M-1})]^T \\ \mathbf{H}(z) &= [H(zW_M^0) \dots H(zW_M^{M-1})]^T \\ \tilde{\mathbf{X}}(z) &= [X(zW_D^1) \dots X(zW_D^{D-1})]^T \\ \mathbf{X}(z) &= [X(zW_D^0) \tilde{\mathbf{X}}(z)]^T \end{aligned}$$

We also define matrices:

$$\mathbb{H} = \begin{pmatrix} H(zW_M^0 W_D^0) & \dots & H(zW_M^0 W_D^{D-1}) \\ \vdots & \ddots & \vdots \\ H(zW_M^{M-1} W_D^0) & \dots & H(zW_M^{M-1} W_D^{D-1}) \end{pmatrix}_{M \times D} = [\mathbf{H}_{M \times 1} \tilde{\mathbb{H}}_{M \times (D-1)}]_{M \times D}$$

$$\begin{aligned}\mathbb{K}(z) &= \text{diag} \left\{ K(z^D W_M^{0D}), \dots, K(z^D W_M^{(M-1)D}) \right\} \\ &= \begin{pmatrix} K(z^D W_D^{0D}) & \cdots & 0 \\ \vdots & \ddots & \vdots \\ 0 & \cdots & K(z^D W_D^{(M-1)D}) \end{pmatrix}_{M \times D}\end{aligned}$$

Then, the matrix representation of Eq. 2.2 can be written as:

$$Y(z) = \frac{1}{D} \mathbf{G}_{1 \times M}^T(z) \mathbb{K}_{M \times M}(z) \mathbb{H}_{M \times D}(z) \mathbf{X}_{D \times 1}(z) = \frac{1}{D} \mathbf{T}_{1 \times D}^{\mathbb{K}}(z) \mathbf{X}_{D \times 1}(z) \quad (2.3)$$

where

$$\mathbf{T}_{1 \times D}^{\mathbb{K}}(z) \triangleq \mathbf{G}_{1 \times M}^T(z) \mathbb{K}_{M \times M}(z) \mathbb{H}_{M \times D}(z) = \begin{bmatrix} T_S^{\mathbb{K}}(z) & \mathbf{T}_A^{\mathbb{K}}(z) \end{bmatrix}$$

is the total transfer function for the  $M$ -path, decimate by  $D$ , AFBs and SFBs,

$$T_S^{\mathbb{K}}(z) \triangleq \mathbf{G}_{1 \times M}^T(z) \mathbb{K}_{M \times M}(z) \mathbf{H}_{M \times 1}(z)$$

is the desired signal transfer function; and

$$\mathbf{T}_A^{\mathbb{K}}(z) \triangleq \mathbf{G}_{1 \times M}^T(z) \mathbb{K}_{M \times M}(z) \bar{\mathbb{H}}_{M \times (D-1)}(z)$$

is the undesired aliasing transfer function. We then rewrite Eq. 2.3 as:

$$Y(z) = \frac{1}{D} T_S^{\mathbb{K}}(z) X(z) + \frac{1}{D} \mathbf{T}_A^{\mathbb{K}}(z) \bar{X}(z) \quad (2.4)$$

If the aliasing transfer function  $\mathbf{T}_A^{\mathbb{K}}(z) = \mathbf{0}_{1 \times (D-1)}$ , the aliasing energy would be completely cancelled:

$$\sum_{m=0}^M K(z^D W_M^{mD}) H(z W_D^d W_M^m) G(z W_M^m) = 0, \forall d = 1, \dots, D-1$$

Thus, the aliasing cancellation condition becomes:

$$\sum_{m=0}^M H(z W_D^d W_M^m) G(z W_M^m) = 0, \forall d = 1, \dots, D-1$$

Because the AFBs and SFBs are essentially the modulated version of their baseband LPPF, we can remove the constant modulation  $W_M^m$  as well as the summation over  $m$ . Therefore, the condition that ensures aliasing cancellation is:

$$H(zW_D^d)G(z) = 0, \forall d = 1, \dots, D-1 \quad (2.5)$$

Note that, Eq. 2.5 holds regardless of the IPE operation. This nice aliasing cancellation property is inherited from DFT-NMDFB. Examine the 1st term in Eq. 2.4, the condition for producing a distortionless response for input signal  $X(z)$  is:

$$T_S^{\mathbb{K}}(z) = \sum_{m=0}^M K(z^D W_M^{mD}) H(zW_M^m) G(zW_M^m) = z^{-n_D}$$

where  $n_D$  is a positive integer representing the total delay introduced by the AFBs / SFBs, plus the intermediate processing. We do not require the intermediate processing matrix  $\mathbb{K}_{M \times M}$  to participate in distortionless response, thus setting it to identity  $\mathbb{K}_{M \times M} = \mathbb{I}_{M \times M}$ , the distortion-less condition then becomes:

$$\sum_{m=0}^M H(zW_M^m) G(zW_M^m) = z^{-n_D} \quad (2.6)$$

Therefore, in the absence of the intermediate processing matrix  $\mathbb{K}_{M \times M}$ , the PR condition for a NMDFB has to simultaneously satisfy Eq. 2.5 and 2.6.

### 2.2.3 Low-Pass Prototype Filter Design

In general, the choices for a PR-NMDFB LPPFs  $H(z)$  and  $G(z)$  are not unique. Non-maximally decimation offers certain degrees of freedom for designing LPPF because it makes the aliasing cancellation task simple. From Eq.2.5, it can be seen that as long as  $H(zW_D^d)$  and  $G(z)$ ,  $\forall d = 1, \dots, D-1$  do not share common pass band and certain part of their transition bands, the aliasing energy can be made arbitrarily small by increasing the prototype filters' stop-band performance. Furthermore Eq.2.6 is satisfied when the composite response of  $H(z)$  and  $G(z)$  forms a Nyquist channel. Author in

[1] suggested letting both  $H(z)$  and  $G(z)$  to be identical SRRC filters. In our observation, if channelization [2, 3] is the desired operation,  $H(z)$  and  $G(z)$  may be chosen to be identical SRRC filters yielding a paraunitary filter bank. The SRRC filters appeared frequently in communications serving as a pair of fixed shaping and matched filter for the purpose of suppressing noise injected in between transmitter and receiver and maximizing the signal to noise ratio. However, due to the poor stop-band performance of SRRC filters [17]; and also account for the fact no noise is injected between AFB and SFB, we can let the analysis prototype  $H(z)$  itself be any Nyquist pulses while letting the synthesis prototype  $G(z)$  be designed via Remez algorithm satisfying Eq. 2.5 and 2.7

$$H(z)G(z) = H^{NYQ}(z) \quad (2.7)$$

where  $H^{NYQ}(z)$  is any Nyquist channel. Summarizing, the analysis/synthesis LPPF design strategy should give considerations to both in-band aliasing error Eq.2.5, as well as the distortionless condition Eq.2.6. The in-band aliasing error can be bounded using proper filter design specification. The distortionless condition is met by simply forcing the product  $H(z)G(z)$  to be a Nyquist channel.

## 2.3 Efficient Implementation of NMDFB via Polyphase Partition

The direct implementation of the theoretical model shown in Fig. 2.1 is impractical because building all BPFs for each AFB / SFB is computationally prohibitive. We next discuss the generalized polyphase implementation for AFB and SFB.

### 2.3.1 Polyphase Analysis Channelizer(PAC)

In the AFB, the down sampling operation can be transferred to the input side of AFB via Noble identity [17], which leads to the polyphase implementation. The M-path partition of the  $m^{\text{th}}$  analysis filter bank can be written as:

$$H_m(z) = H(zW_M^m) = \sum_{k=0}^{M-1} z^{-k} W_M^{-km} E_k(z^M) \quad (2.8)$$

where  $E_k(z^M)$  is the  $k^{\text{th}}$  polyphase component obtained from the 2-D partition of the prototype low pass filter  $H(z)$ . Use Noble Identity to transfer the down-sampling operation through filter  $H_m(z)$ ; and we obtain the polyphase form of  $H_m(z)$ , denoted as  $H_m^P(z)$ , which can be written as:

$$H_m^P(z) = \sum_{k=0}^{M-1} z^{-k} W_M^{-km} E_k\left(z^{\frac{M}{D}}\right) \quad (2.9)$$

Here we require  $D$  divides  $M$ . Note that, the complex rotator  $W_M^{-km}$  in Eq. 2.9 can be implemented via IFFT simultaneously servicing all  $M$  channels [17]. Also note from Fig. 2.1 that a complex heterodyne  $e^{-j\frac{2\pi}{M}mnD}$  is applied to the  $m^{\text{th}}$  AFB. The complete block diagram of a generalized  $M$ -path, decimation by  $D$ , PAC is shown in Fig. 2.2. In the case of  $D = M/2$ , the complex rotators  $e^{-j\frac{2\pi}{M}mnD}$ , followed by each polyphase component vanish if  $m$  is even; or they reduce to  $(-1)^n$  when  $m$  is odd [1]. This phase rotation array can be offset by using a two-state circular shift buffer [2, 3] at the input to the FFT. In the first state (Flag = 0), all channels are weighted by 1, thus an  $M$ -point IFFT is performed. In the second stage (Flag = 1), all odd channels are weighted by -1, and even channels are weighted by 1. The phase offset is absorbed by switching the upper half outputs with the bottom half outputs. Similar arrangement can be made for other decimation factors to avoid the complex shifters. Based on Fig. 2.2, The block diagram for the  $M$ -Path, decimation by  $D = M/2$  PAC used in [1, 2, 3] is shown in Fig. 2.3. Notice that, we have again used the Noble Identity to further exchange the  $D=M/2$  down sampler with delay element resulting in a two-port input commutator.

### 2.3.2 Polyphase Synthesis Channelizer (PSC)

The PSC is the dual system of the PAC and its high level block diagram is shown in Fig.2.4. The  $M$ -path polyphase partition of the synthesis filter for the  $m^{\text{th}}$  channel can be written as:

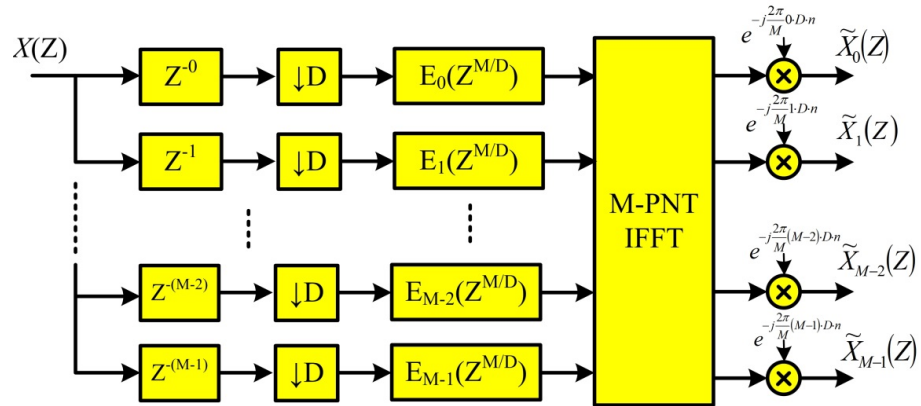


**Figure 2.2:** Generalized  $M$ -path, Decimation by  $D$ , PAC

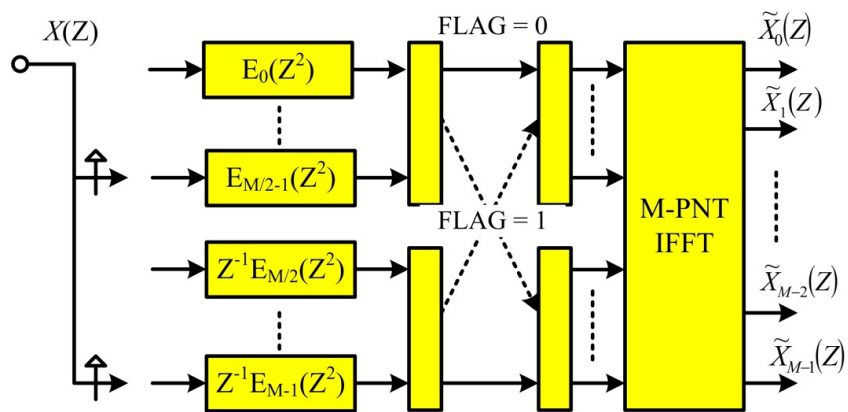


**Figure 2.3:**  $M$ -Path, Decimation by  $D = M/2$  PAC [1, 2, 3]

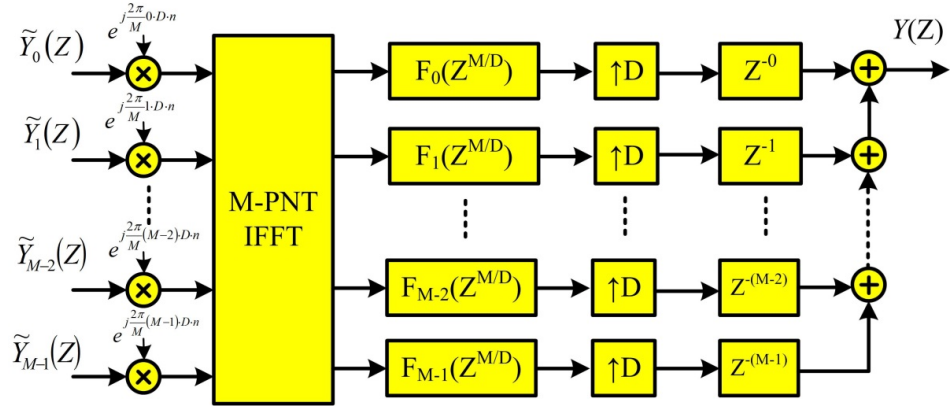


**Figure 2.4:** Generalized  $M$ -path, Up Sample by  $D$ , PSC

$$G_m(z) = G(zW_M^m) = \sum_{k=0}^{M-1} z^{-k} W_M^{-km} F_k(z^M) \quad (2.10)$$

where  $F_k(z^M)$  is the  $k^{\text{th}}$  polyphase component. Sliding the up sampling operation through the partitioned filter  $G_m(z)$ , we obtain the polyphase representation  $G_m^P(z)$ .

$$G_m^P(z) = \sum_{k=0}^{M-1} z^{-k} W_M^{-km} F_k\left(z^{\frac{M}{D}}\right) \quad (2.11)$$

Again, an IFFT block is placed in front of the synthesis polyphase filter servicing all  $M$  channels. Setting  $D = M/2$ , and carrying out similar arrangement as for the PAC, we obtain the efficient implementation of the PSC which is shown in Fig. 2.5, [1, 2, 3].

The polyphase implementations significantly reduce the computation complexity and allow building realizable systems based on Fig .2.1. One now only needs one FFT and one polyphase partitioned LPPF to achieve either AFB or SFB. Examining the polyphase form shown in Fig. 2.2 to 2.5, in each AFB/ SFB operation interval,  $D$  pieces of data from the incoming serial signal are processed;  $M$  pieces of data are generated in the IPE stage; and  $D$  pieces of output data are produced. Although the incoming signal seems to be partitioned into length  $D$  segments, the entire process is still continuous. Moreover, by varying decimation factor  $D$ , one has the freedom to decide how frequently the IPEs are applied. This flexibility is important since building block filters

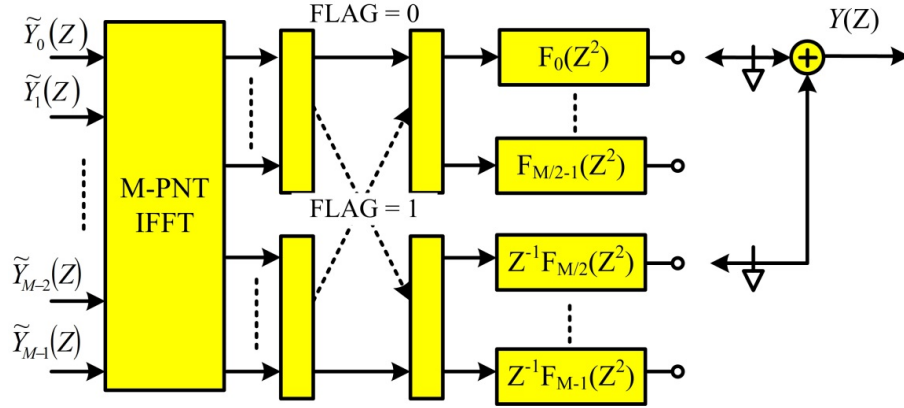


**Figure 2.5:**  $M$ -Path, Up Sample by  $D = M/2$  PAC [1, 2, 3]

with time varying update support is one of our goals.

### 2.3.3 Spectral Shaping via Intermediate Processing Elements

An  $M$ -path PR-NMDFB is constructed when the IPE matrix  $\mathbb{K}_{M \times M}$  is identity matrix. Because the AFB are essentially a bank of digital BPFs centered on multiples of  $\frac{2\pi}{M}$ , and it may be viewed as the filtered bank interpretation of the input signal spectrum. The  $M$  outputs of the AFB offer access to the frequency domain. Therefore, spectrum shaping is made possible via IPE matrix  $\mathbb{K}_{M \times M}$ .

Given the discrete time Fourier transform (DTFT) of an arbitrary signal spectrum  $S(\omega)$  and its corresponding finite time duration or truncated impulse response  $s(n)$ ,  $n = 0, 1, \dots, N_{Max}$ , the goal is to synthesize or approximate it via an  $M$ -path PR-MNDFB. Let us consider the frequency domain and time domain filtering models which are shown in Fig. 6.

In Fig. 5.3a the input signal  $x(n)$  is passed through an  $M$ -path, decimation by  $D$ , AFB/SFB with diagonal IPE matrix  $\mathbb{K}_{M \times M}$ , whose  $(m, m)^{\text{th}}$  entry is a complex scalar denoted as  $K_m$ , for  $m = 0, 1, \dots, M - 1$ . In Fig. 5.3b, the same signal  $x(n)$  is fed into an FIR filter  $S(z) = \mathcal{L}\{s(n)\}$ , and then delayed by  $n_D$ , where  $n_D$  is the total delay introduced by the  $M$ -path, decimation by  $D$ , AFB/SFB. Using Eq. 2.4, the  $Z$ -transform of the output signal  $y^f(n)$  corresponding to Fig. 5.3a is written as  $Y^f(z) = T_S^{\mathbb{K}}(z)X(z) + T_A^{\mathbb{K}}(z)\bar{X}(z)$ . As mentioned earlier, the aliasing energy can be made arbitrarily small by increasing

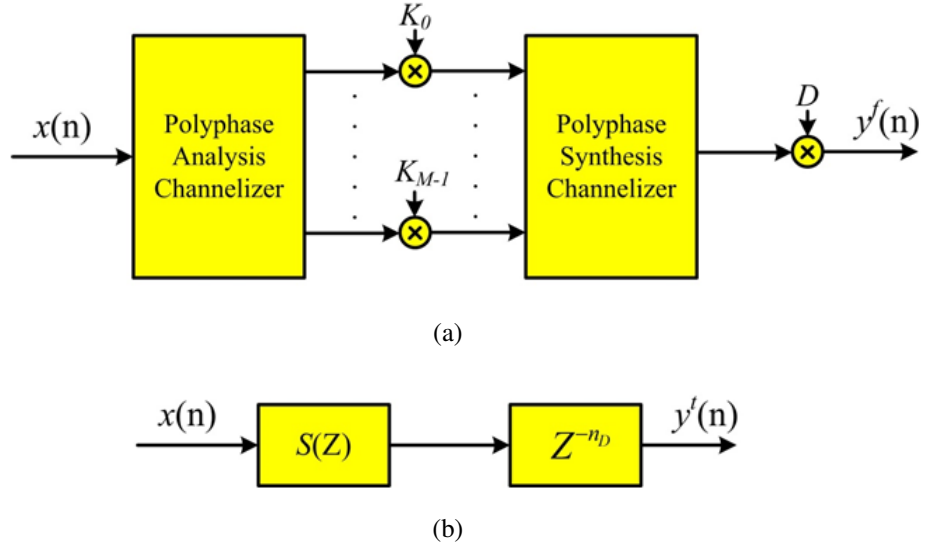


**Figure 2.6:** Filtering Models: (a).Frequency Domain Filtering Model; (b).Time Domain Filtering Model

AFB/SFB's stop band attenuation. We now assume the aliasing energy is small and ignore it in the analysis. Therefore, we rewrite  $Y^f(z)$  as:

$$Y^f(z) = T_S^{\mathbb{K}}(z)X(z) \quad (2.12)$$

The Z-transform of the output signal  $y^f(n)$  corresponding to the time domain filtering model shown in Fig 6 (b) can be written as:

$$Y^t(z) = S(z)z^{-n_D}X(z) \quad (2.13)$$

The difference between the two filtering models can be defined as:

$$\mathcal{E}(z) = \left[ T_S^{\mathbb{K}}(z)z^{n_D} - S(z) \right] X(z)z^{-n_D} \quad (2.14)$$

Following Eq. 2.14, we further define error transfer function to be:

$$T_{\mathcal{E}}(z) = T_S^{\mathbb{K}}(z) z^{n_D} - S(z) = \sum_{m=0}^{M-1} K_m H^{NYQ}(zW_M^m) z^{n_D} - S(z) \quad (2.15)$$

Since the goal is to use AFB and SFB along with the IPE to manipulate arbitrary spectrum  $S(\omega)$ , the error transfer function  $T_{\mathcal{E}}(z)$  must be made zero or, if acceptable by the application requirements, close to zero. Recall that  $n_D$  is total delay of the Nyquist pulse  $H^{NYQ}(zW_M^m)$ . Thus, term  $H^{NYQ}(zW_M^m) z^{n_D}$  is the zero phase version of the chosen Nyquist pulse that has a real spectrum. Let us denote the zero phase Nyquist channel to be  $\tilde{H}^{NYQ}(zW_M^m)$ . We can further split Eq. 2.15 into real and imaginary parts as shown in Eq. 2.16.

$$T_{\mathcal{E}}(\omega) = \begin{bmatrix} \sum_{m=0}^{M-1} \text{Re}\{K_m\} \tilde{H}^{NYQ}(\omega - \omega_m) - \text{Re}\{S(\omega)\} \\ + j \left[ \sum_{m=0}^{M-1} \text{Im}\{K_m\} \tilde{H}^{NYQ}(\omega - \omega_m) - \text{Im}\{S(\omega)\} \right] \end{bmatrix} \quad (2.16)$$

Equation 2.16 suggests the real and imaginary part of  $K(m)$  can be independently designed based on the real and imaginary part of the target spectrum  $S(\omega)$ . In addition,  $\tilde{H}^{NYQ}(\omega)$ , is also a design parameter, since any waveforms satisfying Nyquist channel condition can be used to design the analysis/synthesis LPPF. We next explore a few options:

### 2.3.4 Piecewise Constant Spectral Approximation

Let us select the Nyquist pulse to be a *SINC* function. The magnitude response of the *SINC* pulse covers  $1/M$  of the total bandwidth, and overlaps with its adjacent neighbors at its half power transition band, i.e.,  $\tilde{h}^{NYQ}(n) = \frac{1}{M} \text{SINC}\left(\frac{1}{M}n\right)$ , for  $-n_D \leq n \leq n_D$ . For simplicity of analysis, we assume the magnitude response of the *SINC* pulse is a perfect rectangular window

$$\tilde{H}^{NYQ}(\omega - \omega_m) = \begin{cases} 1, & \omega \in \left[\omega_m - \frac{\pi}{M}, \omega_m + \frac{\pi}{M}\right], m = 0, 1, \dots, M-1 \\ 0, & \text{otherwise} \end{cases}$$

Examine Eq.2.15 and consider that the chosen Nyquist pulse only covers the  $m^{\text{th}}$  band, i.e  $\left[\omega_m - \frac{\pi}{M}, \omega_m + \frac{\pi}{M}\right]$ . Therefore, the error transfer function for the  $m^{\text{th}}$  band is

$$T_{\mathcal{E},m}(\omega) \triangleq K_m \widetilde{H}^{NYQ}(\omega - \omega_m) - S(\omega), \text{ for } \omega \in \left[\omega_m - \frac{\pi}{M}, \omega_m + \frac{\pi}{M}\right] \quad (2.17)$$

Using midpoint approximation method, we let

$$K_m = S(\omega_m) \quad (2.18)$$

which results in a piecewise constant approximation of the given spectrum  $S(\omega)$ . In order to evaluate the approximation performance, we assume the given spectrum  $S(\omega)$  is an analytic function, and twice differentiable. Therefore, we may expand  $S(\omega)$  using Taylor series around frequency  $\omega_m$  for  $\omega \in \left[\omega_m - \frac{\pi}{M}, \omega_m + \frac{\pi}{M}\right]$  such that

$$S(\omega) = S(\omega_m) + \dot{S}(\eta)(\omega - \omega_m) \quad (2.19)$$

for some  $\eta \in \left[\omega_m - \frac{\pi}{M}, \omega_m + \frac{\pi}{M}\right]$ . Using Eq. 2.17 to 2.19 and the zero phase property of the chosen Nyquist pulse, we can find  $T_{\mathcal{E},m}(\omega)$  as

$$T_{\mathcal{E},m}(\omega) = S(\omega_m) - S(\omega_m) - \dot{S}(\eta)(\omega - \omega_m) = -\dot{S}(\eta)(\omega - \omega_m) \quad (2.20)$$

Therefore, we arrive at the inequality:

$$|T_{\mathcal{E},m}(\omega)| \leq \underset{\omega \in \left[\omega_m - \frac{\pi}{M}, \omega_m + \frac{\pi}{M}\right]}{\text{Max}} |\dot{S}(\omega)| \cdot \frac{\pi}{M} = B_{\mathcal{E},m} \quad (2.21)$$

We then find the maximum gain distortion due to the piecewise constant approximation as  $B_{\mathcal{E},m}$ . Because the low energy section of  $S(\omega)$  is more sensitive to the phase distortion, the upper bound for the maximum phase distortion can be obtained by considering the smallest magnitude response within region  $\omega \in \left[\omega_m - \frac{\pi}{M}, \omega_m + \frac{\pi}{M}\right]$ . Let

$\gamma_{s,m} \triangleq \underset{\omega \in [\omega_m - \frac{\pi}{M}, \omega_m + \frac{\pi}{M}]}{\text{Max}} |S(\omega)|$ , the maximum phase distortion  $\phi_m$  can be readily obtained as:

$$\phi_m \leq \text{atan} \left( \frac{B_{\mathcal{E},m}}{\sqrt{\gamma_{s,m}^2 - B_{\mathcal{E},m}^2}} \right), \text{ for } \gamma_{s,m} > B_{\mathcal{E},m} \quad (2.22)$$

Note that, if  $\gamma_{s,m} \leq B_{\mathcal{E},m}$ , the phase distortion is from  $-\pi$  to  $\pi$ . However, this also implies the target spectrum  $S(\omega)$  has significant attenuation at  $\omega_m$  and the signal around frequency  $\omega_m$  may not have significant value, i.e., the stop band of the target spectrum. Notice, from Eq. 2.21 2.22, that the gain and phase distortion is related to the 1st derivative of the target spectrum and the filter bank's path number  $M$ . This implies that a fast variation in the target spectrum causes/increases both magnitude and phase distortion. However, increasing the path number  $M$  can always help in reducing the magnitude and phase errors.

### 2.3.5 Straight Line Spectral Approximation

Inspired by the piecewise constant approximation, the spectral approximation may be viewed as an interpolation problem. An immediate improvement over the piecewise constant approximation is to let Nyquist pulse,  $\tilde{H}^{NYQ}(\omega)$ , have a triangular magnitude response, which yields frequency domain linear interpolation between adjacent filter banks. We then define the Nyquist pulse as:

$$\tilde{h}^{NYQ}(n) = \frac{1}{M} \text{SINC}^2 \left( \frac{1}{M} n \right), \text{ for } -n_D \leq n \leq n_D$$

$$\tilde{H}^{NYQ}(\omega - \omega_m) = \begin{cases} 1 - \left| \frac{\omega - \omega_m}{\frac{2\pi}{M}} \right|, & \omega \in [\omega_m - \frac{2\pi}{M}, \omega_m + \frac{2\pi}{M}] \\ 0, & \text{otherwise} \end{cases}$$

Due to the underlying triangular pulse shape, the approximated spectrum by  $K_m, K_{m+1}$  for  $\omega \in [\omega_m, \omega_{m+1}]$ , can be written as  $(\omega_{m+1} - \omega) \cdot K_m + \omega \cdot K_{m+1}$ . Using Eq. 2.15, and only considering region  $\omega \in [\omega_m, \omega_{m+1}]$ , we can define the error transfer function on the interval  $\omega \in [\omega_m, \omega_{m+1}]$  as:

$$T_{\mathcal{E},m}(\omega) \triangleq (\omega_{m+1} - \omega) \cdot K_m + \omega \cdot K_{m+1} - S(\omega) \quad (2.23)$$

Set  $K_m = S(\omega_m)$  and  $K_{m+1} = S(\omega_{m+1})$ , and expand  $S(\omega)$  using Taylor series around  $\omega = \omega_m$ , we find

$$S(\omega) = S(\omega_m) + \dot{S}(\eta)(\omega - \omega_m) + \frac{1}{2}\ddot{S}(\eta)(\omega - \omega_m)^2 \quad (2.24)$$

for some  $\eta \in [\omega_m, \omega_{m+1}]$ . Now the maximum gain within region  $[\omega_m, \omega_{m+1}]$  can be bounded by:

$$|T_{\mathcal{E},m}(\omega)| \leq \underset{\omega \in [\omega_m, \omega_{m+1}]}{\text{Max}} |\dot{S}(\omega)| \cdot \frac{1}{2} \left(\frac{\pi}{M}\right)^2 = B_{\mathcal{E},m} \quad (2.25)$$

And the bound for the maximum phase error can be obtained via Eq. 2.22. Notice that the magnitude and phase distortion is directly proportional to the 2<sup>nd</sup> derivative of the target spectrum, and inversely proportional to the squared analysis/synthesis path number  $M$ .

### 2.3.6 Minmax Optimization over Intermediate Processing

Motivated by the interpolation technique, we assigned the IPE  $K_m$  to be equal to  $S(\omega_m)$  for  $m = 0, 1, \dots, M-1$ . Yet, we would like to determine the optimum IPE matrix that minimizes the peak magnitude distortion or the  $L^\infty$ -norm in each approximation interval. This leads us to the minimax polynomial approximation for each interval. For the piecewise constant approximation, the  $L^\infty$ -norm minimization is:

$$\underset{K_m \in \mathcal{C}}{\text{arg min}} \|T_{\mathcal{E},m}(\omega)\|_\infty = \underset{K_m \in \mathcal{C}}{\text{arg min}} \max_{\omega \in [\omega_m - \frac{\pi}{M}, \omega_m + \frac{\pi}{M}]} |T_{\mathcal{E},m}(\omega)| \quad (2.26)$$

Examine Eq. 2.16, the optimization is equivalent to independent minimization for the real and imaginary parts of  $T_{\mathcal{E},m}(\omega)$ . The solution to Eq. 2.26 can be easily determined using 0<sup>th</sup> order minimax polynomial:

$$\begin{aligned}
Re\{K_m\} &= \frac{1}{2} \left[ \max_{\omega \in [\omega_m - \frac{\pi}{M}, \omega_m + \frac{\pi}{M}]} S^{Re}(\omega) + \min_{\omega \in [\omega_m - \frac{\pi}{M}, \omega_m + \frac{\pi}{M}]} S^{Re}(\omega) \right] \\
Im\{K_m\} &= \frac{1}{2} \left[ \max_{\omega \in [\omega_m - \frac{\pi}{M}, \omega_m + \frac{\pi}{M}]} S^{Im}(\omega) + \min_{\omega \in [\omega_m - \frac{\pi}{M}, \omega_m + \frac{\pi}{M}]} S^{Im}(\omega) \right]
\end{aligned} \tag{2.27}$$

And, the maximum magnitude distortions for real and imaginary parts are:

$$\begin{aligned}
B_{\mathcal{E},m}^{Re} &= \frac{1}{2} \left[ \max_{\omega \in [\omega_m - \frac{\pi}{M}, \omega_m + \frac{\pi}{M}]} S^{Re}(\omega) - \min_{\omega \in [\omega_m - \frac{\pi}{M}, \omega_m + \frac{\pi}{M}]} S^{Re}(\omega) \right] \\
B_{\mathcal{E},m}^{Im} &= \frac{1}{2} \left[ \max_{\omega \in [\omega_m - \frac{\pi}{M}, \omega_m + \frac{\pi}{M}]} S^{Im}(\omega) - \min_{\omega \in [\omega_m - \frac{\pi}{M}, \omega_m + \frac{\pi}{M}]} S^{Im}(\omega) \right]
\end{aligned} \tag{2.28}$$

The maximum magnitude distortion can be bounded as:

$$|T_{\mathcal{E},m}| \leq \sqrt{\left(B_{\mathcal{E},m}^{Re}\right)^2 + \left(B_{\mathcal{E},m}^{Im}\right)^2} = B_{\mathcal{E},m} \tag{2.29}$$

For the triangular approximation case, the  $L^\infty$  optimization can be thought as having a straight line in each segment, e.g.,  $\omega \in [\omega_m, \omega_{m+1}]$ , such that the maximum amplitude error is minimized. The constraint is that each line segment must be connected with its left and right neighbors. The optimization problem is summarized in Eq.2.30, where  $K_m^{Left}$  is the optimum value obtained from interval  $\omega \in [\omega_{m-1}, \omega_m]$  and  $K_{m+1}^{right}$  is the optimum value obtained from interval  $\omega \in [\omega_{m+1}, \omega_{m+2}]$ .

$$\begin{aligned}
\arg \min_{Re\{K_m\}, Re\{K_{m+1}\}} \left\| \overline{T}_{\mathcal{E},m}^{Re}(\omega) \right\|_\infty &= \arg \min_{Re\{K_m\}, Re\{K_{m+1}\}} \max_{\omega \in [\omega_m, \omega_{m+1}]} \left| \overline{T}_{\mathcal{E},m}^{Re}(\omega) \right| \\
\arg \min_{Im\{K_m\}, Im\{K_{m+1}\}} \left\| \overline{T}_{\mathcal{E},m}^{Im}(\omega) \right\|_\infty &= \arg \min_{Im\{K_m\}, Im\{K_{m+1}\}} \max_{\omega \in [\omega_m, \omega_{m+1}]} \left| \overline{T}_{\mathcal{E},m}^{Im}(\omega) \right|
\end{aligned} \tag{2.30}$$

Subject to:  $K_m = K_m^{Left}$ ,  $K_{m+1} = K_{m+1}^{Right}$

The direct solution to this problem is difficult due to the optimization constraint. However, we can find a sub-optimum solution in two steps. We first ignore the optimization

constraint and obtain the optimum values of  $K_m$  and  $K_{m+1}$  for each section. Then, a weighted average is applied between  $K_m$  and  $K_m^{Left}$  as well as  $K_{m+1}$  and  $K_{m+1}^{Right}$ . Ignoring the constraint, the optimization problem stated in Eq. 2.30 is equivalent to the construction of a degree one minimax polynomial or Chebyshev line within region  $\omega \in [\omega_m, \omega_{m+1}]$  for both real and imaginary parts with respect to the target spectrum  $S(\omega)$ . And, argument  $K_m$  and  $K_{m+1}$  can be evaluated on the constructed minimax polynomial. The real and imaginary parts of the constructed line have slopes

$$A_m^{Re,Im} = \frac{S^{Re,Im}(\omega_{m+1}) - S^{Re,Im}(\omega_m)}{\omega_{m+1} - \omega_m} = \dot{S}^{Re,Im}(\alpha_m) \quad (2.31)$$

for  $\alpha_m \in [\omega_m, \omega_{m+1}]$  and passes through point  $(\alpha_m, L_m^{Re,Im}(\alpha_m))$ , where:

$$L_m^{Re,Im}(\alpha_m) \triangleq \frac{1}{2} [S^{Re,Im}(\alpha_m) + A_m^{Re,Im}(\alpha_m - \omega_m) + S^{Re,Im}(\omega_m)] \quad (2.32)$$

Thus the line functions for the real and imaginary parts are:

$$L_m^{Re,Im}(\omega) = A_m^{Re,Im}(\omega - \alpha_m) + L_m^{Re,Im}(\alpha_m) \quad (2.33)$$

And the optimum solution for interval  $[\omega_m, \omega_{m+1}]$ , without considering the constraint condition, denoted as  $K_m^*$  and  $K_{m+1}^*$ , are obtained by evaluating  $L_m^{Re,Im}(\omega)$ :

$$\begin{aligned} K_m^* &= L_m^{Re}(\omega_m) + jL_m^{Im}(\omega_m) \\ K_{m+1}^* &= L_m^{Re}(\omega_{m+1}) + jL_m^{Im}(\omega_{m+1}) \end{aligned} \quad (2.34)$$

Based on the minimax polynomial property, the maximum real and imaginary part magnitude errors for  $\omega \in [\omega_m, \omega_{m+1}]$  are:

$$\begin{aligned} B_{\mathcal{E},m}^{Re} &= |Re\{K_m^*\} - S^{Re}(\omega_m)| = |Re\{K_{m+1}^*\} - S^{Re}(\omega_{m+1})| = |L_m^{Re} - S^{Re}(\alpha_m)| \\ B_{\mathcal{E},m}^{Im} &= |Im\{K_m^*\} - S^{Im}(\omega_m)| = |Im\{K_{m+1}^*\} - S^{Im}(\omega_{m+1})| = |L_m^{Im} - S^{Im}(\alpha_m)| \end{aligned} \quad (2.35)$$

And, the sub-optimum solution, denoted as  $K_m^{sub}$ , is defined as the weighted average shown in Eq. 2.36

$$K_m^{sub} = \frac{B_{\mathcal{E},m}^{*Re} \cdot Re\{K_m^*\}}{B_{\mathcal{E},m-1}^{*Re} + B_{\mathcal{E},m}^{*Re}} + j \frac{B_{\mathcal{E},m}^{*Im} \cdot Im\{K_m^*\}}{B_{\mathcal{E},m-1}^{*Im} + B_{\mathcal{E},m}^{*Im}} \quad (2.36)$$

The sub-optimum solutions modify the edge amplitudes of each interval so that the adjacent segments agree at their boundaries. The modification introduces excess amplitude error to the optimum solution. If both ends shift up or down, the excess magnitude error equals to the largest change of either end. And, if one end shifts up and the other end shift down, the excess magnitude error equals the absolute sum of the two changes. The expressions for the sub-optimum maximum magnitude distortion are summarized in Eq. 2.37.

$$B_{\mathcal{E},m}^{Sub,Re} = \begin{cases} B_{\mathcal{E},m}^{*Re} + \max(|Re\{K_m^*\} - Re\{K_m^{Sub}\}|, |Re\{K_{m+1}^*\} - Re\{K_{m+1}^{Sub}\}|) \\ \text{for } (Re\{K_m^*\} - Re\{K_m^{Sub}\})(Re\{K_{m+1}^*\} - Re\{K_{m+1}^{Sub}\}) \geq 0 \\ B_{\mathcal{E},m}^{*Re} + |Re\{K_m^*\} - Re\{K_m^{Sub}\}| + |Re\{K_{m+1}^*\} - Re\{K_{m+1}^{Sub}\}| \\ \text{otherwise} \end{cases}$$

$$B_{\mathcal{E},m}^{Sub,Im} = \begin{cases} B_{\mathcal{E},m}^{*Im} + \max(|Im\{K_m^*\} - Im\{K_m^{Sub}\}|, |Im\{K_{m+1}^*\} - Im\{K_{m+1}^{Sub}\}|) \\ \text{for } (Im\{K_m^*\} - Im\{K_m^{Sub}\})(Im\{K_{m+1}^*\} - Im\{K_{m+1}^{Sub}\}) \geq 0 \\ B_{\mathcal{E},m}^{*Im} + |Im\{K_m^*\} - Im\{K_m^{Sub}\}| + |Im\{K_{m+1}^*\} - Im\{K_{m+1}^{Sub}\}| \\ \text{otherwise} \end{cases} \quad (2.37)$$

Following Eq. 2.37, one can readily use Eq. 2.22, 2.29 to determine the maximum gain and phase distortion. The triangular minimax sub-optimal approximation effectively handles the curvatures in the target spectrum compared to the non-optimized version. In fact, it is very close to the optimal minimax approximation. This will be further shown in the simulation section.

## 2.4 Design Examples and Workload Analysis

### 2.4.1 Design Example: $M = 64$ and $D = 32$

In this section, the design of a 64-path PR-NMDFB, with decimation factors  $D = M/2$  (piecewise constant approximation) and  $D = M/4$  (straight line approximation), will be presented. We begin with the 64-path, decimation by 32, rectangular design for a 100 dB dynamic range system. The AFB's prototype filter can be designed as a Kaiser windowed *SINC* function, with normalized bandwidth equal to  $1/M = 1/64$ . The design of the synthesis filter must satisfy Eq. 2.5 to 2.7. The nearest modulated image is located at  $H(zW_{32}^1) = H(zW_{64}^2)$  (same in the negative frequency direction). Therefore, the pass band edge of the synthesis prototype filter is  $\frac{\pi}{M}$ , and stop band edge is  $\frac{3\pi}{M}$ . If we normalize each channel spacing to be one, i.e.,  $f_s = 64$ , then the pass band edge is from 0 to 0.5, and stop band from 1.5 to 32. Fig. 2.7 shows the magnitude

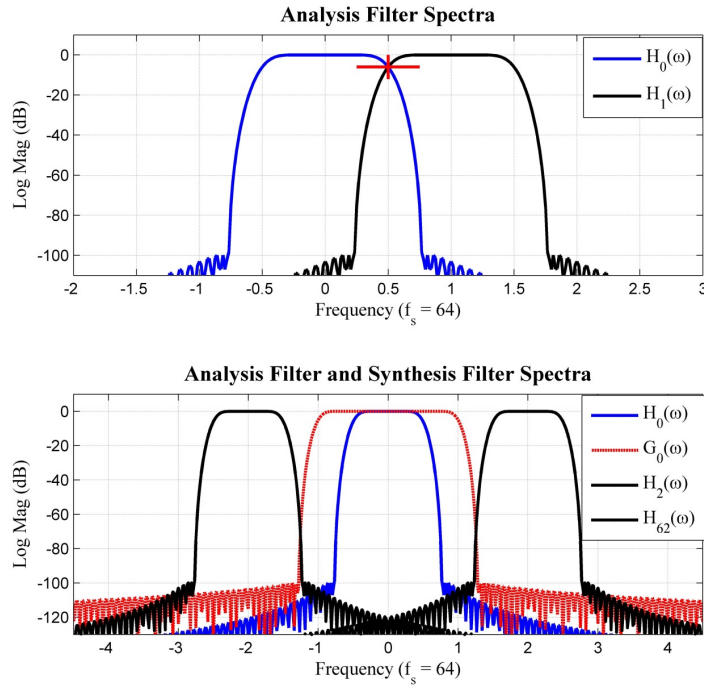


**Figure 2.7:** 64-Path, D=32, Rectangular Design

response of the designed analysis and synthesis prototype filters. The upper subplot of

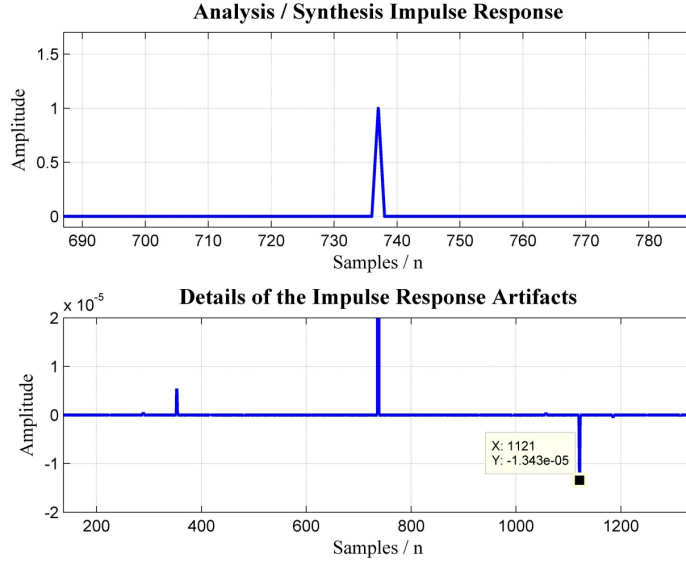


**Figure 2.8:** Impulse Response of the Analysis and Synthesis Filter Bank

Fig. 2.7 shows the magnitude response of the designed analysis filter  $H_0(\omega)$  along with its shifted version  $H_1(\omega) = H_0(\omega - \frac{2\pi}{M})$ . The two responses overlap at their half-power point and they are even symmetric around  $\omega = \frac{\pi}{M}$ , which makes them Nyquist pulse. The lower subplot of Fig. 7 shows the magnitude response of the designed synthesis filter. We can see its pass bank fully covers  $H_0(\omega)$ , while rejecting all other modulated images. The pass band of this synthesis prototype filter is from 0 to 0.725, and stop band from 1.275 to 32. The length of this filter is 769 taps, same to the analysis prototype filter. Figure. 2.8 shows the total impulse response of the designed analysis/synthesis filter bank with the IPE being an identity matrix. Since it is a PR filter bank, the ideal output is simply the delayed version of the input impulse. In this case, as shown in the upper subplot, the total latency is 736 samples, which is equal to the composite latency of analysis and synthesis prototype filter subtracted by 32, i.e.,  $(769-1)-32$ . The subtraction by 32 is due to the polyphase implementation as it has been shown in Fig. 2.3. The zoomed lower subplot shows the artifacts in the impulse response due to the reconstruction error and in-band aliasing. We can see that the highest artifact has amplitude of  $-1.343 \times 10^{-5}$ , which is -97 dB.

The design of 64-path, decimation by 16, triangular analysis / synthesis PR-

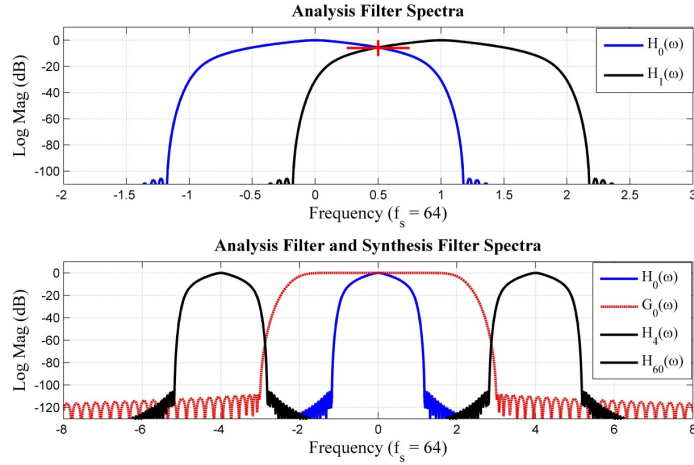


**Figure 2.9:** 64-Path,  $D=16$ , Triangular Design

NMDFB is presented in Fig. 2.9 and 2.10. The analysis LPPF has a triangular magnitude response and bandwidth of  $\frac{4\pi}{M}$ . This filter can be simply generated by windowing a squared *SINC* function. The synthesis LPPF has its theoretical pass band from 0 to 1 and stop band from 3.5 to 32 in the normalized frequency domain. The designed synthesis LPPF shown in subplot 2 of Fig. 2.9 has pass band from 0 to 1.1 and stop band from 3 to 32. And, the resulting filter only has 257 taps. Fig. 2.10 shows the impulse response of the triangular design. Because the synthesis filter is shorter than the  $\frac{M}{2}$  case, the latency in the example is 496, i.e.,  $(\frac{257-1}{2} + \frac{769-1}{2} - 16)$  samples. And, the highest artifact level is  $-4.975 \times 10^{-6}$ , which is -106 dB. It is worth noting that the synthesis filter length is significantly reduced in the  $D = \frac{M}{4}$  case compared to the  $D = \frac{M}{2}$ . This is because the modulated analysis image is further apart from its baseband copy, which widens the synthesis filter's transition bandwidth, thus resulting a shorter filter.

## 2.4.2 Workload Analysis

We now analyze the workload of the proposed analysis/synthesis filter bank. Denote  $L_A$  and  $L_S$  to be the length of the analysis and synthesis LPPF. Let the input data be complex, i.e., In-phase/Quadrature communication paths. For every  $D$  input data, the AFBs / SFBs operate once which cost  $2 \times (L_A + L_S)$  real multiplies. The  $M$  point FFT is

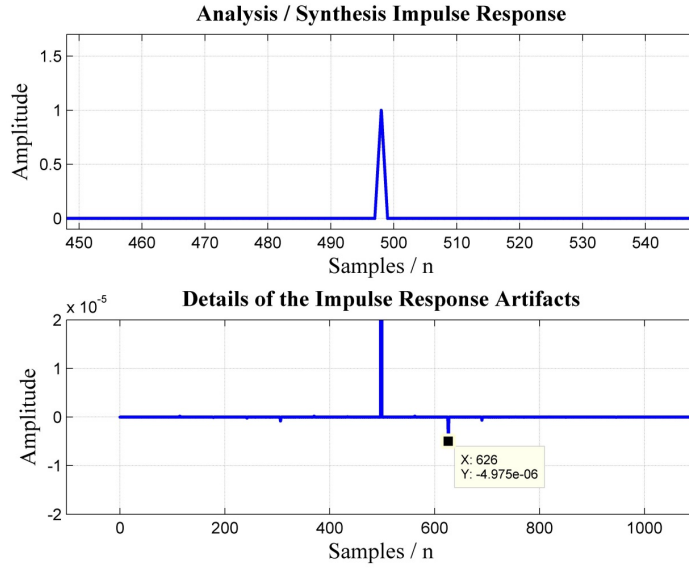


**Figure 2.10:** Impulse Response of the Analysis and Synthesis Filter Bank

used twice, which cost  $2 \times 4 \times \frac{M}{2} \log_2 M$  real multiplies via Radix-2. Suppose there are  $N$  IPE matrices, which cost additional  $4 \times N \times M$  real multiplies. Then, the number of real multiplies for  $D = \frac{M}{2}$  and  $D = \frac{M}{4}$  per input data can be summarized as:

$$\begin{aligned} \left( \frac{\text{ops}}{\text{input}} \right)_{M/2} &= \frac{4}{M} (L_A + L_S) + 8 \log_2 M + 8N \\ \left( \frac{\text{ops}}{\text{input}} \right)_{M/4} &= \frac{8}{M} (L_A + L_S) + 16 \log_2 M + 16N \end{aligned} \quad (2.38)$$

Using the filters designed in section 2.4.1 as example, we find the number of total real multiplies for 64-path, decimation by 32, rectangular design is  $144 + 8 \times N$ , where 144 accounts for the real multiplies without intermediate processing. Similarly, the number of real multiplies for 64-path, decimation by 16, triangular design is  $224 + 16 \times N$ . Note that, 144 real multiplies per input sample corresponds to a 72 taps FIR filter with real coefficients processing complex data. In our case, the 144 real multiplies is spent on analysis/synthesis PR-NMDFB, yet the rest of the filtering processing, i.e., IPE, only cost 8 real multiplies per filter / IPE. Clearly, the more filters put in cascade, the more efficient PR-NMDFB becomes! Another interesting fact is the relationship between

the number of paths,  $M$ , and the PR-NMDFB filtering complexity. Recall from earlier discussion, the performance of the spectral approximation increases as  $M$  gets larger. In the meantime, the length of the LPPF for the AFB/ SFB also grows. Yet this growth is proportional with  $M$ , because for an FIR filter, the filter length grows linearly with its sampling frequency for a given fixed transition bandwidth [17]. Given this fact, the 1st term of Eq. 2.38 is essentially a constant determined by the desired system dynamic range. This implies that increasing the number of paths  $M$  only affects the workload in FFT computation. Therefore, the system performance is essentially proportionally to the FFT complexity as  $M$  becomes large!

## 2.5 Applications

In the previous section, we have analyzed the feasibility of using IPEs embedded in the PR-NMDFB to synthesize target spectrum  $S(\omega)$ . We now address the applications of spectrum approximation in filtering. Any filters' phase responses can be separated into the combination of linear phase and non-linear phase component. We restrict all the filters to be approximated to have only non-linear phase component. Part of the reason is because the IPE matrix  $\mathbb{K}$  is a diagonal matrix, which is essentially a complex multiplier array across each filter bank; and does not contribute any integer delay. Therefore, it corresponds to a spectrum with no linear phase component. Unlike time domain filters, which require latency to make the system causal, the IPE can be treated as frequency domain processing, which does not require causality. Another reason for restricting linear phase component is because it introduces phase shift which modulates the real and imaginary parts of the spectrum and degrades the spectrum approximation performance.

### 2.5.1 Linear Phase FIR Filter

The linear phase FIR filter is perhaps the most commonly used digital filter in signal processing tasks. The type I and III linear phase FIR filters have odd number of taps [13, 17], which give integer delay and guarantees a zero phase structure. Let  $s(n)$ ,  $n = 0, 1, \dots, N_{max}$  be the impulse response of a linear phase FIR filter of odd number of taps. The DTFT of  $s(n)$  is  $S(\omega) = e^{j\omega \frac{N_{max}}{2}} \sum_{n=0}^{M-1} s(n) e^{-j\omega n}$ . Due to the sym-

metry of the impulse response, the zero phase spectrum  $S(\omega)$  is either a pure real or imaginary spectrum. Using Eq. 2.18 and 2.36 one can determine the IPEs  $K_m$  for,  $m = 0, 1, \dots, M - 1$ . And, use Eq. 2.21, 2.22, 2.25, 2.29 to determine the filter approximation performance based on the chosen LPPF and  $M$ . Finally, the PR-NMDFB with specifically designed IPE behaves like an FIR filter, with fixed delay  $n_D$ .

## 2.5.2 Non-Linear Phase FIR Filter

For the linear phase FIR filter, the intermediate processing elements are either real or imaginary. In the case of non-linear phase FIR filtering, they become complex scalars. Again, let  $s(n)$ ,  $n = 0, 1, \dots, N_{max}$  be the impulse response of any non-linear phase FIR filter. We also require sequence  $s(n)$  to be free of linear phase component, i.e, integer number of delays. The spectrum to be approximated can be computed as:  $S(\omega) = \sum_{n=0}^{M-1} s(n) e^{-j\omega n}$ . Then, the IPE can be determined based on the proposed approximation methods.

## 2.5.3 Fractional Delay Filter (FDF)

An FDF by its name is a filter that delays the digital samples by any fraction of its sampling period, say  $\tau = \delta T$ , where  $\tau$  is the fractional delay;  $\delta$  is the fraction  $|\delta| \leq 1$ ; and  $T$  is the sampling period. It is an important class of filter which is extensively used in communication systems, e.g. timing recovery. The legacy design of any FDF falls in line with the interpolators, among which polynomial interpolation and polyphase filters are the two most commonly used techniques [47]. The interpolation error is directly related with the filter's dynamic range. In order to reduce interpolation error, either higher order polynomial or higher oversampling ratio should be considered, which increases the computations as well as memory size.

The time domain perspective has led us to build interpolators acting on the desired time grid between available samples. Notice that, the basic Fourier transform property states that time delay is phase shift. And the phase shifter has frequency response  $S(\Omega) = e^{j\Omega\tau}$ , where  $\Omega$  is the continuous frequency in Fourier transform. Using  $K_m = S(\omega_m)$ , for  $\omega_m = \frac{2\pi}{M}$ , for,  $m = 0, 1, \dots, M - 1$ , gives  $K_m = e^{j\frac{2\pi}{M}m\tau}$ ,  $|\tau| \leq 0.5, m \neq \frac{M}{2}$ .

Note that, the DTFT must have a periodic spectrum. Therefore, we force  $K_{\frac{M}{2}}$ , the channel located on the half sample rate, to be the average of its adjacent neighbors:  $K_{\frac{M}{2}} = \frac{1}{2} (K_{\frac{M}{2}-1} + K_{\frac{M}{2}+1})$ . Doing so, we made the  $K_m, m = 0, 1, \dots, M-1$  periodic; but, we also sacrificed the half sample rate channel. The operation bandwidth for this fractional delay filter becomes  $\omega \in [-\pi + \frac{\pi}{M}, \pi - \frac{\pi}{M}]$

$$K_m = \begin{cases} e^{j(\frac{2\pi}{M}m\tau)}, & \text{for } m \neq \frac{M}{2} \\ \frac{1}{2} (K_{M/2-1} + K_{M/2+1}), & \text{for, } m = \frac{M}{2} \end{cases} \quad (2.39)$$

From the spectral approximation point of view, the problem becomes using  $M$  spectral samples to approximate complex sinusoid  $e^{j(\frac{2\pi}{M}m\tau)}$  up to half a cycle. In the case of straight line approximation and  $M = 64$ , we use Eq. 2.22 through Eq. 2.25 to determine the maximum magnitude error to be -70 dB, and maximum phase distortion to be  $3.012 \times 10^{-4} rad$ . It is clear that the spectral approximation provides a very good fractional delay filter with only 64-path filter banks.

## 2.5.4 Masking Filter

The digital masking filter is frequently used in systems which require very sharp filter transition bandwidth as well as stop band attenuation [40, 41, 42]. Note that, setting IPE  $K_m$  to 0 or 1 can either disable or enable the  $m^{\text{th}}$  filter bank. Clearly, by enabling and disabling the  $K_m$ , we can synthesize low pass and band pass filters. Moreover, the synthesized masking filter has the same transition bandwidth with the analysis LPPF, thus they are of the same length [17]. For example, the LPPF designed in section 2.4.1 has 769 taps. Then a 769 taps time domain FIR masking filter is expected, which costs  $768 \times 2 = 1538$  real multiples per complex input. Recall the filter bank approach only requires approximately 144 operations with,  $M = 64, D = 32$ . This gives 90% workload reduction.

## 2.5.5 Cascade Filtering

Consider cascade filtering task for  $N$  filters denoted as  $S_1(\omega), \dots, S_N(\omega)$ . It is clear that the frequency response of the cascade is  $S(\omega) = \prod_{i=1}^N S_i(\omega)$ . he correspond-

ing IPE can be designed based on  $S(\omega)$ . However, in communication systems, where time varying filter, i.e., equalizer, is engaged after fixed receiver filter, one should then design separate IPEs, i.e.,  $\mathbb{K}(\omega) = \prod_{i=1}^N \mathbb{K}_i(\omega)$ , where  $\mathbb{K}_i$  is the IPE matrix corresponding to the  $i^{\text{th}}$  filter  $S_i(\omega)$ , that subjected to different functionalities, e.g., equalization, timing recovery and etc. Furthermore, the additional IPEs cost trivially comparing to the analysis and synthesis tasks Eq. 2.38. And, since the cascaded filters are free of linear phase component, the overall filtering latency is imposed by the analysis/synthesis filter banks' latency  $n_D$ .

## 2.6 Simulation Results

### 2.6.1 Linear Phase FIR Filter

Let us consider the task of approximating a low pass filter having pass band from 0 to 0.2 in the normalized frequency domain ( $f_s = 1$ ); stop band from 0.3 to 0.5 with 100 dB stop band attenuation. Fig. 2.11 shows the piecewise constant approximation result using  $K_m = S(\omega_m)$ . The upper subplot of Fig. 2.11 shows the overlaid magnitude responses of the original filter (in blue) and the approximated filter (in red). The middle subplot shows the error spectrum (in blue) between the original filter and the approximated filter. The red curve is the error bound drawn using Eq.2.21. In this approximation, the error is proportional to the 1<sup>st</sup> derivative. The highest error magnitude is at -14 dB, located on frequency 0.25 which is the mid-point of the filter transition band. It should be noted that this error is a measure of the difference between the target spectrum and the synthesized spectrum rather than the filtering error caused by the synthesized filter. The lower subplot in the same picture shows the phase error in normalized angle  $\frac{\text{radians}}{2\pi}$  between the two responses and their theoretical bound drawn using Eq. 2.22. It is easy to notice that the pass-band phase error is well below  $10^{-4}$ . Fig. 2.12 shows the result of 64-path straight line sub-optimal minimax approximation working under  $D = \frac{\pi}{4}$ . Seen from the upper subplot, the approximation is at about -40 dB. And, this error resides in the transition band of the filter, where signal energy has been significantly attenuated. The red dashed curve shown in the second subplot is the optimal minimax bound (cannot achieve) and the black curve is the sub-optimal minimax bound.

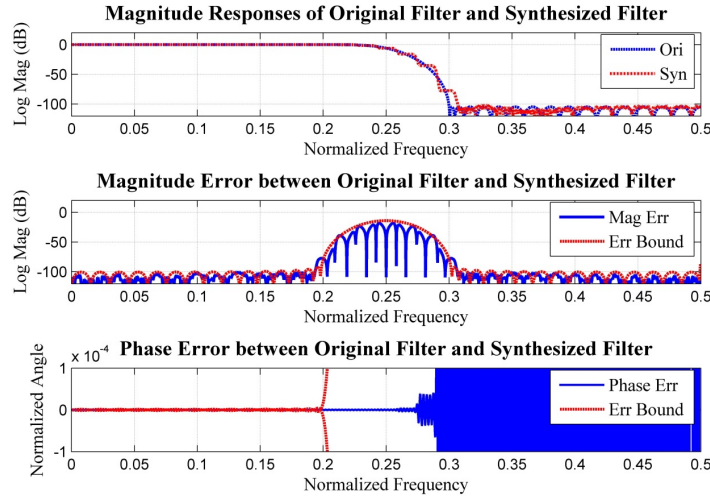


**Figure 2.11:** 64-Path Piecewise Constant Approximation  $K_m = S(\omega_m)$

The error spectrum lies in between the two bounds. Note the bound becomes inaccurate if the error is smaller than the filter's dynamic range (100 dB), where the aliasing energy becomes dominant. Similarly, Fig. 2.13 shows the sub-optimal minimax straight line approximation result for  $M = 256, D = 64$ ; and, the error spectrum is at -60 dB, We can see that increasing  $M$  dramatically increases the performance.

## 2.6.2 Non-Linear Phase FIR Filter

Consider a FIR filter with coefficients  $[1 \ 0 \ -0.5j \ 0.3 \ 0.1 \ 0 \ 0 \ 0 \ 0.01]$ , which is a typical tapped delay line channel having a deep notch (-19 dB) at frequency 0.16. Fig. 2.14 shows the result of the 64-path piecewise constant approximation. Although the gain approximation result is satisfactory, the phase error is enormous. Fig. 2.15 and Fig.2.16 show the similar result but using 64-path and 256-path suboptimal minimax straight line method. And we can see that both have good magnitude and phase approximation performance. In particular for the 256-path, the magnitude error is below -58 dB, and maximum phase error is below  $5 \times 10^{-4}$  on the normalized angle scale.

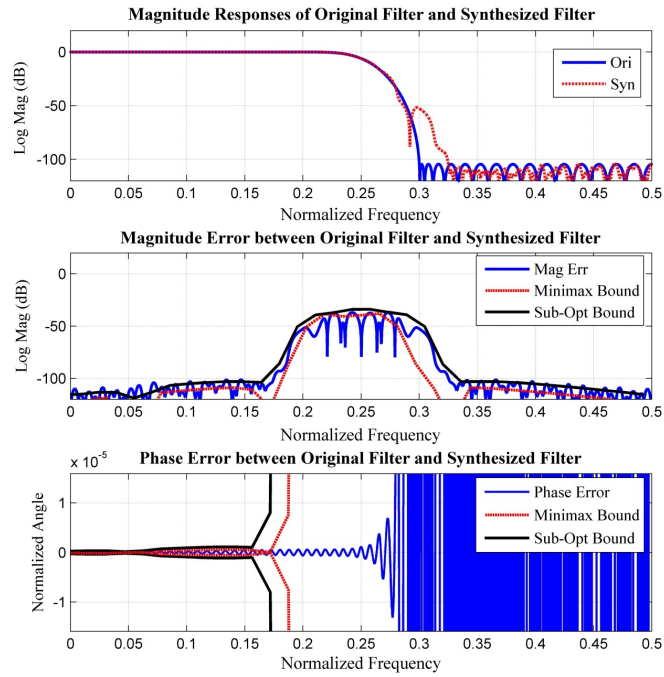


**Figure 2.12:** 64-Path Straight Line Sub-optimal Minimax Approximation

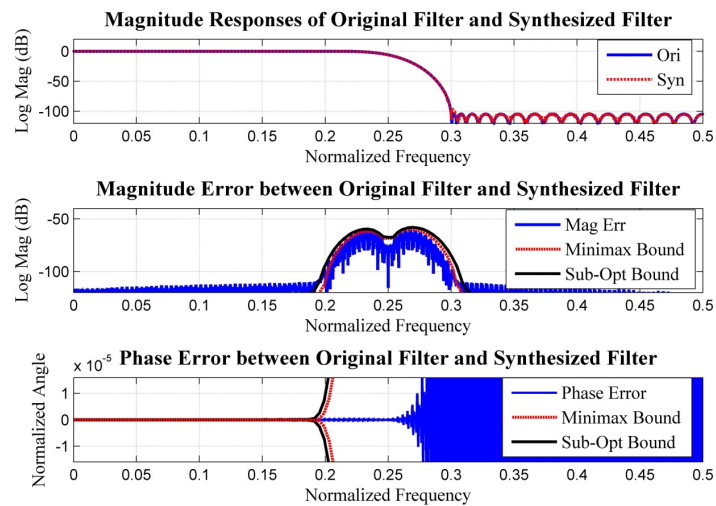


**Figure 2.13:** 256-Path Straight Line Sub-optimal Minimax Approximation

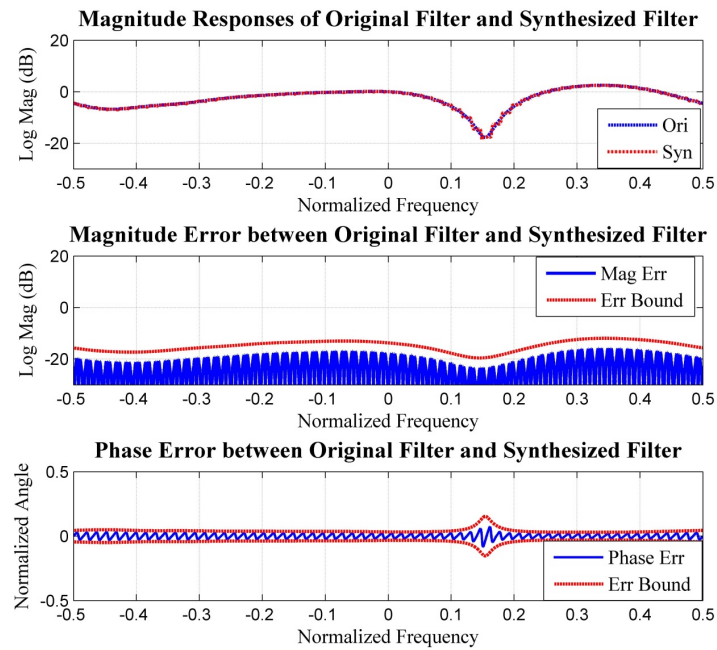


**Figure 2.14:** 64-Path Piecewise Constant Approximation  $K_m = S(\omega_m)$

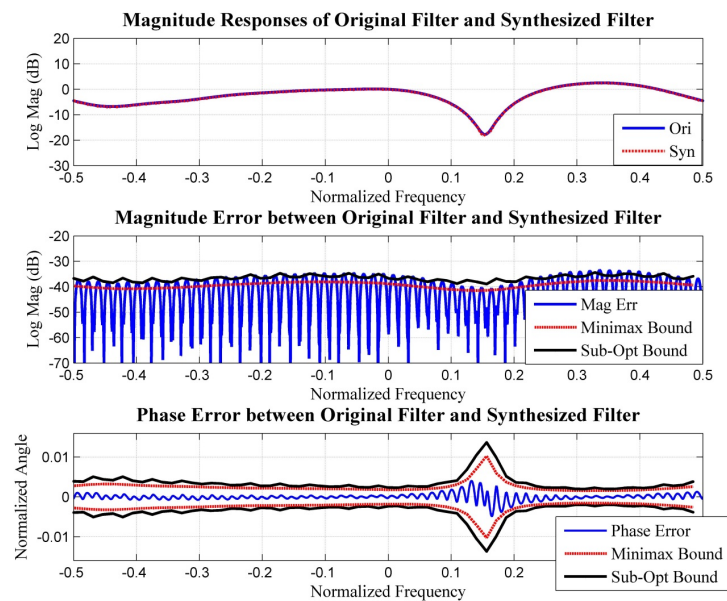


**Figure 2.15:** 64-Path Straight Line Sub-optimal Minimax Approximation

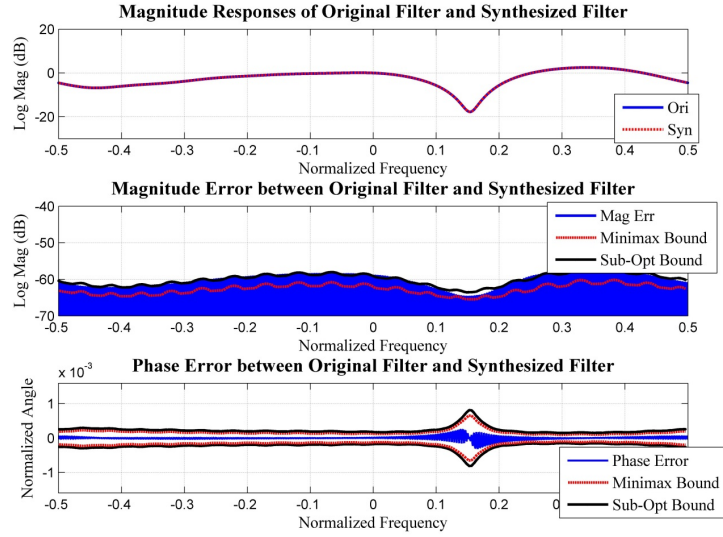


**Figure 2.16:** 256-Path Straight Line Sub-optimal Minimax Approximation

### 2.6.3 Fractional Delay Filter (FDF)

The FDF is simulated based on 64-path, decimation by 16, straight line approximation model. The IPE matrix is determined using Eq. 2.39. Figure 2.17 shows the result for delaying the impulse response by 0, 0.5, and -0.5 samples. The left column figures show the impulse responses, while the right column figures show the magnitude responses. Note that, we have subtracted the parasitic delay  $n_D$  caused by AFBs / SFBs from the impulse responses. Thus we see the impulse response for delaying 0 sample sits on index 0. And, the impulses for delaying  $\pm 0.5$  samples become sampled Nyquist pulses. Noted that, the magnitude response for delaying  $\pm 0.5$  samples have larger in-band distortion. This is due to the use of IPEs to approximate the complex sinusoid of the phase shifter (see Eq. 2.39). Clearly, the worst case distortion happens when delaying  $\pm 0.5$ , since all one needs is fractional delay within one sample.

### 2.6.4 Applications in Communications

Consider SRRC pulse shaping and matched filtering (MF) processes in the absence of channel and noise. An  $M = 240, D = M/3, L_A = L_S = 1920$  (8 taps per polyphase

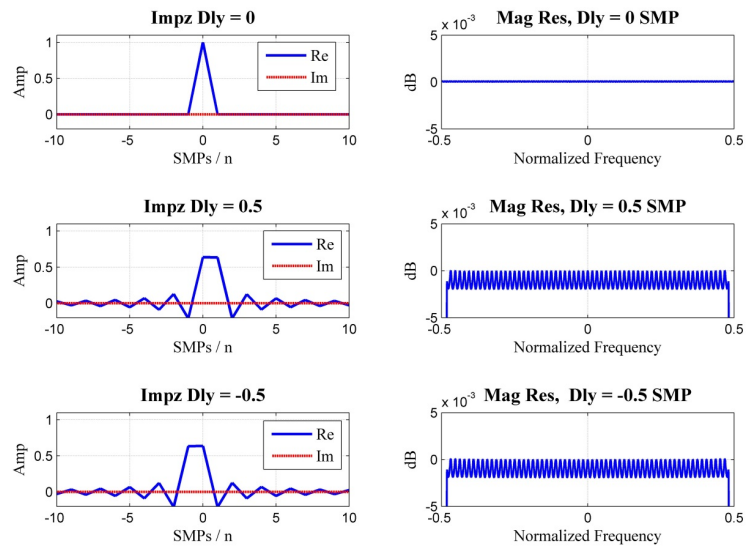


**Figure 2.17:** Fractional Delay Filter

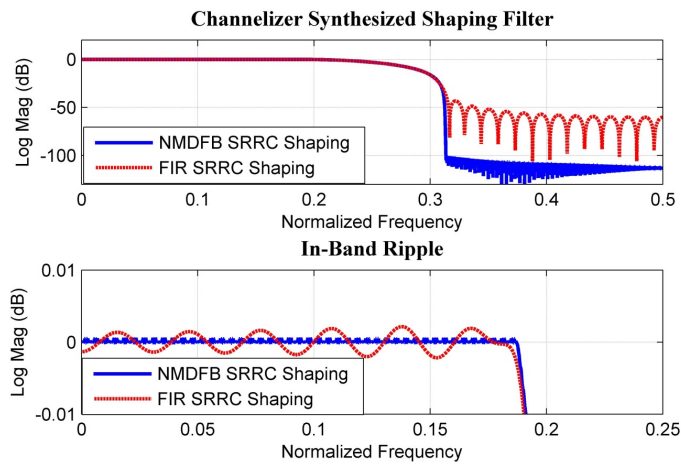


**Figure 2.18:** NMDFB and FIR Based SRRC Shaping Filter

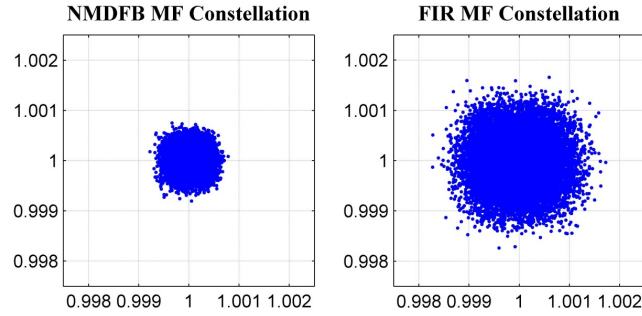


**Figure 2.19:** QPSK Constellation Dispersion (1<sup>st</sup> Quadrant)

arm) triangular design based NMDFB is constructed with target spectrum  $S(\omega)$  being the well-known ideal SRRC spectrum at 2 samples / symbol. The number of real multiplies per input data spent on PAC and PSC filtering is  $\frac{6}{M}(L_A + L_S)$ , which is 96. The 240-point FFT can be designed via Good Thomas algorithm costs 1100 real multiplies for complex input, i.e., Table 2-6 of [48]; two 240-point FFT operate once for every  $D = 80$  inputs, which is 27.5 real multiplies per input. The IPE costs 12 real multiplies per input. In total, the NMDFB implementation costs 135.5 real multiplies per input sample, which roughly corresponds to a real coefficient FIR filter with 67 taps processing complex data. Fig. 2.18 shows the magnitude response of the NMDFB and FIR based SRRC shaping filters. The comparison shows NMDFB based design has its highest side lobe level at -100.03 dB while the FIR based design is at -43.3 dB; the maximum in-band ripple levels for NMDFB and FIR are  $\pm 0.00061$  dB and  $\pm 0.0021$  dB respectively. Clearly, for the same nominal computation cost, the proposed approach has significant advantage, i.e., over 56 dB stop-band performance improvement and significant smaller in-band ripple. It should be noted that improved stop-band performance came from the NMDFB structure's designed dynamic range. This improved stop-band attenuation allows us to build high quality receivers and enhance immunity to near far problem. The conventional approach requires a second masking filter in cascade with

SRRC filter to achieve this performance. To further consolidate the result, we have generated SRRC shaped and SRRC matched filtered QPSK constellation ( $\pm 1 \pm j$ ). Fig.2.19 shows the constellation dispersion in the 1<sup>st</sup> Quadrant. The measured error vector magnitude (EVM) [49] for NMDFB based approach is -73.02 dB or 0.022%; and for FIR based approach is -65.95 dB, or 0.050%.

## 2.7 Acknowledgment

Chapter 2, in full, contains material that appeared in the following three published articles:

- Xiaofei Chen, fred harris, Elettra Venosa, and Bhaskar Rao, "Non-maximally decimated analysis / synthesis filter banks: Applications in wideband digital filtering," IEEE Transactions on Signal Processing., vol. 62, no. 4, pp. 852 - 867, 2014.
- fred harris, Elettra Venosa, Xiaofei Chen, Bhaskar Rao, "Variable bandwidth M-path filter with fixed coefficients formed by M-path polyphase filter engines," Circuit Theory and Design (ECCTD), 2011 20th European Conference on , vol., no., pp.5,8, 29 - 31 Aug. 2011
- fred harris, Xiaofei Chen, Elettra Venosa, and Chris Dick, "Wideband 160-channel polyphase filter bank cable tv channeliser," Signal Processing, IET, vol. 5, pp. 325 - 332, June 2011.

## **Chapter 3**

# **Equalizers for Wideband Digital Receivers Based on Non-Maximally Decimated Filter Banks**

### 3.1 Introduction

The history of communication has always been driven by the development of equalizers [9], which facilitate the performance of the communication link. The equalization task was traditionally implemented by time domain linear / nonlinear filters, usually via transversal structures. As the demands for high data rate communications rapidly grows, the conventional equalizer becomes unaffordable when dealing with highly dispersive channels or in wideband legacy systems. This phenomenon pushed the development of many broadband techniques [10], such as OFDM, CDMA techniques. Although the OFDM [14] suffers from problems like poor spectral efficiency and high PAPR [6, 7], it still becomes dominate because of its simple equalizer structure for highly frequency selective channels. Another hidden advantage of OFDM is its block processing nature [14], which achieves low speed processing on hardware, i.e., serial/parallel conversion at the transmitter (Tx) and receiver (Rx). Comparing with the legacy systems, e.g., shaped QAM, where filtering is performed at the input rate, the OFDM is much more economical to deploy as a wideband system.

Previous works have been proposed to overcome the drawbacks of OFDM systems over the past decade. The authors in [6] studied the frequency domain equalization (both feedforward and feedback equalization) problem for single carrier (SC) transmission with circular convolution technique. They showed the performance improvement via iterative block decision feedback equalizer (IB-DFE). However, their DFE requires parameter estimation which is still problematic [50, 4, 51] in a real system. And, their underlying modulation scheme is essentially close to OFDM in the sense that certain transmission redundancy is added to force linear convolution to be circular. In this paper, we focus on the design of block linear / nonlinear equalizer via PR-NMDFBs and our proposed technique does not pose any constrains on the modulation format as long as the channel distortion information can be extracted and updated via IPE. As a born cousin to FFT based technique, the filter bank (FB) based transceiver approach has also drawn lots of attention. The authors in [52, 53] studied the blind channel identification and equalization problem by adding redundancy via FB precoder at Tx and decoder at the Rx. The design considers joint optimization of FBs at both Tx and Rx. The authors in [54] proved PR is the necessary and sufficient condition for parameterable FBs jointly

at Rx/Tx. In our work, since standard high throughput, wideband signals, i.e., shaped QAM are considered, the transmitted signal does not contain redundancy and the equalization is achieved via PR AFBs / SFBs only at the Rx independent of the transmitted signals. In the more recent time, the authors in [55, 56, 57] studied equalizing multicarrier OQAM, which is an alternative transmission technique for OFDM, also called filter bank multicarrier (FBMC). And complex FIR filter per channel equalization scheme was adopted. Author in [58] made the detailed comparison between OFDM and FBMC. The results shows FB based system has advantage in spectral efficiency as well as in synchronization. Most recently, author in [59] studied subband chip level equalization problem for MIMO downlink DS-UWB. Yet, a direct usage of subband FB design [23] and various standard block adaptive algorithms [60] were examined. Comparing with the mentioned multi-carrier techniques, our focus is on equalizing a wideband SC signal regardless of the modulation format.

The idea of equalizing of a SC signal via FBs is sometimes coupled with subband processing [60]. This idea was briefly seen in [61], where the author showed a preliminary example of channel identification using FBs. And, the author in [62, 63], have used a pair of PR-NMDFB (i.e., AFB & SFB) to mitigate narrowband interference. They proposed similar linear equalization idea to [61], but via a 2x oversampled PR-NMDFBs; and have used all-pass / complex FIR filter per channel as IPE to perform linear equalization. Note that the 2x oversampled FB is first seen in [1], where a 2x oversample Modified Discrete Fourier Transform (MDFT) FB was derived for image coding. Authors in [2] also arrived at slightly different structure when performing Rx channelization tasks. In this work, a recently proposed, generalized M-path, decimation by  $D$  ( $D = \frac{M}{2}$  corresponding to 2x oversampled MDFT-FB), NMDFB [64] is considered. The importance of including generalized decimation factor  $D$  is to control the coefficient update rate of the block equalizer, which leads to the implementation of a time varying block equalizer that has not been proposed previously. We will analytically show combining with properly designed low pass prototype filter (LPPF) plus sufficiently large number of channels, the 1-tap per channel scalar IPE is sufficient to accomplish both equalization and spectral shaping tasks; more rigor performance analysis and filter design methods shall be provided to support this fact. Furthermore, based

on the spectral shaping property of NMDFB [64], one can embed other major filtering tasks besides equalizer, i.e., matched filtering (MF), timing and carrier recovery and etc., into the NMDFB processing in the form of IPE vectors. This arrangement not only enables a cost effective equalizer but indeed producing an entire modem. As demonstrated in [64], the NMDFB based cascade IPE processing implements a chain of filters at the cost of one, which dramatically decreases the implementation complexity of a SC FB transceiver as well as the power consumption due to high speed filtering.

Besides linear equalizer, it is crucial to include nonlinear equalizers in the system to deal with more complicated channels; especially for channels with very deep nulls. Several attempts of building block DFEs were made; however, as detailed in [6] that the block DFEs often impose causality problems and can hardly be achieved. As a result, a time domain DFE is used in hybrid with the FB based linear equalizer [6, 65, 66]. Author in [67] derived the time domain block DFE solution from theoretical point, however it still suffers from high complexity; and adaptive algorithm cannot be easily applied. Author in [68] show another approach for designing frequency domain block DFE, but the algorithm involves very complicated initialization process to overcome causality problem, which limits the implementation in highly dispersive channel or in higher order QAM modulations; and efficient FBs are not employed. To solve this issue, the author in this paper derive an FB based ISI canceller to serve as nonlinear equalizer. And, we find it is closely connected to the time domain ISI canceller derived by Gersho & etc in [69, 70] used for mitigating ISI in highly distorted Volterra channels. We will rigorously derive the FB based ISI canceller and draw its connection as well as performance limit to its time domain correspondence.

Another problem remains unclear in the context of FB based equalizers is to determine the achievable MMSE after applying proper equalization techniques. Authors in [71, 72] studied the MMSE of the subband adaptive filters (SAF) as well as its modeling accuracy. However, their analysis is restricted to the performance degradation caused by the aliasing inherited from the FBs; and the question on how many subbands are needed to equalize a given channel remains unanswered. In this paper, we adopt the PR-NMDFB derived in Chapter 2 which has almost zero aliasing, leaving only the modeling error; and we will analytically show the MMSEs of the FB based linear and

nonlinear equalizer.

The contributions of this chapter are: 1) Propose FB based block linear / nonlinear equalizer for SC signal. 2) Detailed MMSE analysis for FB based linear and nonlinear equalizers. 3) Introducing PR-NMDFB based receiver structure, emerging all time domain filters into the FB domain to achieve significant workload reduction. This chapter is organized as follows. Section 2 sets up the signal model; Section 3 solves the optimum equalizer weights; Section 4 introduces the spectral shaping NMDFB; Section 5 gives the adaptive implementation of the proposed equalizer; Section 6 shows complexity analysis; Section 7 shows the simulation result; and Section 8 gives the conclusion.

## 3.2 Signal Model

Let us examine a baseband equivalent system for a QAM signal with complex notation for the in-phase ( $I$ ) and quadrature ( $Q$ ) branches, e.g.,  $\text{Re}(\cdot)$  and  $\text{Im}(\cdot)$  respectively. Denoting the  $k^{\text{th}}$  complex QAM data symbol as  $S_k$ , with symbol period  $T$  seconds. We assume the data symbols are stationary and uncorrelated,  $[S_k S_{k'}] = \sigma_s^2 \delta_{kk'}$ , where  $\delta_{kk'}$  is the Kronecker delta function. At the transmitter (Tx), the symbol stream first experiences 1-to-2 zero packing / up-sampling process and then were passed onto a square-root raised cosine (SRRC) digital shaping filter  $h_{tx}(n)$ , which produces the shaped digital waveform sampled at 2 samples-per-symbol. Assuming the usage of an ideal discrete-to-continuous (D/C) conversion, i.e., via a brick-wall reconstruction filter with 0 dB in-band gain, the emitted signal has power spectral density (PSD)  $\frac{1}{2} \sigma_s^2 |H_{tx}(\Omega)|^2$ , where  $\Omega$  is the analog frequency. The multipath channel used in this paper is assumed to be frequency selective and stationary. We denote the complex baseband equivalent channel as  $h_c(t)$ . The additive white noise  $n(t) = n_I(t) + n_Q(t)$ , of two-sided power spectral density  $\frac{N_0}{2}$  W/Hz per complex components is introduced at the output of the channel. The received continuous signal at the input to the receiver is written as:

$$r(t) = \sum_{k=-\infty}^{\infty} S_k h_{tc}(t - kT - t_0) + n(t) \quad (3.1)$$

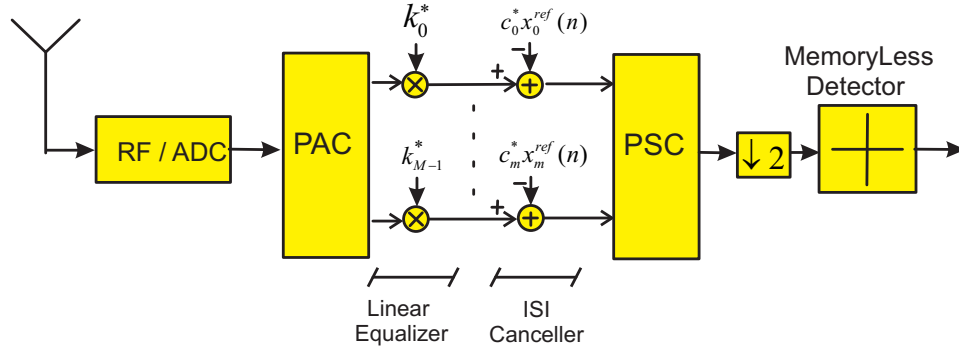


**Figure 3.1:** Theoretical Model of PR-NMDFB Based Linear / Nonlinear Equalizer

where,  $h_{tc}(t) \triangleq h_{tx}(t) * h_c(t)$ ; and  $t_0$  is the channel delay or the sampler phase. In this paper, we assume the channel  $h_c(t)$  is free of linear phase component, and set  $t_0 = 0$ . Digitizing the received signal at sampling speed  $T_s = \frac{T}{2}$ , i.e., 2 samples-per-symbol, we find digitized signal as:

$$r(n) = \sum_{k=-\infty}^{\infty} S_k h_{tc}(n - 2k) + n(n) \quad (3.2)$$

### 3.3 Equalizer Weights For Infinite Number of NMDFB Channels

The most well-known approach for equalizing a QAM signal is to use the combination of a linear equalizer and a decision feedback equalizer (DFE) [73, 8]. In general, the linear equalizer synthesizes the inverse of the channel based on either zero-forcing or MMSE criteria; the DFE cancels the post cursors based on the correctly detected symbols. The LE becomes unsatisfactory when channel nulls present since the noise power is amplified dramatically. The DFE, on the other hand, is a nonlinear equalizer operating on detected symbols, which does not amplify noise. An alternative approach for DFE is the so-called ISI canceller first derived by Gersho [69, 70], which was used to cope with highly non-linear Volterra channels. The authors in [37] have shown that the ISI canceller is also a nonlinear equalizer which cancels both pre and post cursors; and has comparable performance with DFE.

In this paper, we present the idea of linear / nonlinear equalizer in the context of channelizer transformed domain. The mathematical model block diagram is shown in Fig. 3.1. The forward or linear equalizer occurs after PAC, where a set of multiplicative scalar equalization coefficients are applied to each PAC outputs modifying the gain and phase for each frequency band, which will be shown later as a spectral shaping process. A copy of the PAC transformed reference signal, i.e., received / matched filtered signal free of channel distortion and additive noise, is assumed available for now. The path-wise ISI is generated via filtered or complex scaled path-wise reference signal. And, the ISI cancellation is achieved by subtracting the ISI off from the forward equalized signal in the PAC domain. We will later show under infinite number of PAC/PSC path assumption, the ISI can be completely removed leaving only the noise component. This two-step equalization arrangement utilizes similar transformed domain nonlinearity idea with authors in [6, 7, 50, 4]. However, FB based structure does not require CP / redundancy, and does not require parameter estimation. And, comparing with the legacy approach, the crucial advantages for this arrangement are: 1) the broadband signal is transformed onto sufficiently large amount of narrow band signals, which made the ISI cancellation work easy since the frequency selective channel has nearly flat frequency response over each signal at the output of PAC. 2) The PAC/PSC is a block processor. It not only has low workload when performing spectral shaping, i.e., on the order of FFT computation, but also permitting signal processing to be performed on deeply decimated clock rate, since the incoming broadband signal is first decimated via PAC [2, 65]. This feature allows us to build affordable hardware for processing very wideband signals.

### 3.3.1 Linear / Forward Equalizer Weights

The decimated by  $D$  and frequency translated output signal observed at the  $m^{\text{th}}$  AFB output is:

$$x_m(n) = (\downarrow D) \left[ \sum_k S_k h_{a,m}(n-2k) e^{-j\theta_m n} + v_m(n) e^{-j\theta_m n} \right] \quad (3.3)$$

where,  $h_{a,m}(n) \triangleq h_{tc}(n) * a_m(n)$ , and  $v_m(n) \triangleq n(n) * a_m(n)$ . Note that  $a_m(n)$  is the  $m^{\text{th}}$  AFB, i.e.,  $a_m(n) = a(n) e^{j\frac{2\pi}{M}mn}$ , where  $a(n)$  is the low pass prototype filter of the

AFB. The Discrete Time Fourier Transform (DTFT) of  $h_{a,m}(n)$  and  $a_m(n)$  is denoted as  $H_{a,m}(\theta)$  and  $A_m(\theta)$  respectively. We then have  $H_{a,m}(\theta) = H_{tx}(\theta)H_c(\theta)A_m(\theta)$ . Assuming the number of AFBs is large, i.e.,  $M \rightarrow \infty$ , the bandwidth of filter  $A_m(\theta)$  becomes arbitrarily narrow. The DTFT of  $h_{a,m}(n)$  can be rewritten as:

$$H_{a,m}^\infty(\theta_m) \triangleq \gamma_m \beta_m A_m(\theta) \xrightarrow{IDTFT} \gamma_m \beta_m a_m(n) \triangleq h_{a,m}^\infty(n) \quad (3.4)$$

where,  $\gamma_m = H_{tx}(\theta_m)$ ,  $\beta_m = H_c(\theta_m)$ . As  $M \rightarrow \infty$ , we find the  $m^{\text{th}}$  channel AFB output data as:

$$x_m^\infty(n) = e^{-j\theta_m n D} \left[ \sum_k S_k \gamma_m \beta_m \bar{a}_m(n-2k) + \bar{v}_m(n) \right] \quad (3.5)$$

where,  $\bar{a}_m(n) = a_m(nD)$ ,  $\bar{v}_m(n) = v_m(nD)$ . Assuming a perfect copy of the matched filtered signal, denoted as  $x_m^{\text{ref}}(n)$ , is available at the output of the AFBs, i.e., free of channel and noise. And, it can be written as:

$$x_m^{\text{ref}}(n) = (\downarrow D) \left[ \sum_k S_k h_{a,m}^{\text{ref}}(n-2k) e^{-j\theta_m n} \right] \quad (3.6)$$

where,  $H_{a,m}^{\text{ref}} = H_{tx}(\theta)A_m(\theta)H_{tx}^*(\theta) \xrightarrow{IDTFT} h_{a,m}^{\text{ref}}(n)$ . Use the assumption that  $M \rightarrow \infty$ , we have

$$H_{a,m}^{\text{ref}} = H_{tx}(\theta)A_m(\theta)H_{tx}^*(\theta) \stackrel{M \rightarrow \infty}{=} |\gamma_m|^2 A_m(\theta) \quad (3.7)$$

$h_{a,m}^{\text{ref}}(n)$  can be rewritten as  $h_{a,m}^{\text{ref}}(n) = |\gamma_m|^2 a_m(n)$ . Thus, the data observed at the  $m^{\text{th}}$  AFB for the reference path is

$$x_m^{\text{ref}}(n) = e^{-j\theta_m n D} \sum_k S_k |\gamma_m|^2 \bar{a}_m(n-2k) \quad (3.8)$$

Define the AFB transformed received signal column vector  $X^\infty(n) \triangleq [x_0^\infty(n), x_1^\infty(n), \dots, x_{M-1}^\infty(n)]^T$ ; and the reference signal vector  $X^{\text{ref}}(n) \triangleq [x_0^{\text{ref}}(n), x_1^{\text{ref}}(n), \dots, x_{M-1}^{\text{ref}}(n)]^T$ ,

the NMDFB based MMSE linear equalization problem is defined as the optimization problem shown below

$$\arg \min_{\mathbf{K}} \mathbf{J}^{f,\infty}(\mathbf{K}) = \arg \min_{\mathbf{K}} E \left\| \mathbf{K}^H X^\infty(n) - X^{\text{ref}}(n) \right\|_2^2 \quad (3.9)$$

where,  $\mathbf{K} \triangleq \text{diag} \{k_0, k_1, \dots, k_{M-1}\}$  is the to be determined equalizer coefficient. Since the AFB has decoupled the input signal into  $M$  outputs. The optimization problem can be solved by examining one channel, say the  $m^{\text{th}}$  channel. In the case  $M \rightarrow \infty$ , the equalizer weight for the  $m^{\text{th}}$  channel can be solved by minimizing the following function:

$$\arg \min_{k_m} J_m^{f,\infty}(k_m) = \arg \min_{k_m} E \left\| k_m^* x_m^\infty(n) - x_m^{\text{ref}}(n) \right\|_2^2 = \arg \min_{k_m} E \left[ \varepsilon_m^f \varepsilon_m^{f*} \right] \quad (3.10)$$

where  $\varepsilon_m^f \triangleq k_m^* x_m^\infty(n) - x_m^{\text{ref}}(n)$ . Coefficient  $k_m$  can be solved by taking derivative to  $J_m^{f,\infty}(k_m)$  with respect to  $k_m$ , and set to zero. After simple steps, the optimum coefficient  $k_m^{\text{opt}}$  can be written as:

$$k_m^{\text{opt}} = \frac{E \{x_m(n) x_m^{\text{ref}*}(n)\}}{E \{x_m(n) x_m^*(n)\}} \quad (3.11)$$

And, one may calculate quantities:

$$\begin{aligned} E \{ \bar{v}_m(n) \bar{v}_m^*(n) \} &= \sigma_n^2 \sum_k |\bar{a}_m(n-k)|^2 = \sigma_n^2 \eta_1 \\ E \{ x_m(n) x_m^*(n) \} &= |\gamma_m|^2 |\beta_m|^2 \sigma_s^2 \eta_2 + \sigma_n^2 \eta_1 \\ E \{ x_m(n) x_m^{\text{ref}*}(n) \} &= |\gamma_m|^2 \gamma_m \beta_m \sigma_s^2 \eta_2 \end{aligned}$$

where  $\eta_1 \triangleq \sum_k |\bar{a}_m(n-k)|^2$ ;  $\eta_2 \triangleq \sum_k |\bar{a}_m(n-2k)|^2$ . Note,  $\eta_1$  is the decimated AFB prototype filter norm; we also have  $\eta_2 = \frac{\eta_1}{2}$ , i.e.,  $\bar{a}_m(2k)$  is the two path polyphase partition of  $\bar{a}_m(k)$ . We then find the optimum  $k_m^{\text{opt}}$  as

$$k_m^{\text{opt}} = \frac{\gamma_m \beta_m}{|\beta_m|^2 + \frac{\sigma_n^2 \eta_1}{\sigma_s^2 \eta_2} |\gamma_m|^{-2}} = \frac{\gamma_m \beta_m}{|\beta_m|^2 + \frac{\sigma_n^2}{0.5 \sigma_s^2 |\gamma_m|^2}} \quad (3.12)$$

Note that the PSD of  $x_m(n)$  is  $\frac{1}{2}\sigma_s^2|\gamma_m|^2$ , where the factor 1/2 comes from the 1-to-2 zero-packing in the shaping process. Eq. 3.12 can be viewed as the composite response of MF (The term matched filter in this paper is a fixed receiver SRRC filter matching to the transmitter only. Note, we do not assume the receiver has prior channel knowledge so that a true matched filter matching to the shaping pulse and the channel can be applied to maximize the SNR.) and equalizer applied at the  $m^{\text{th}}$  AFB. The term  $\gamma_m$  is simply the fixed MF part; and the rest part is the MMSE equalizer w.r.t to the channel and received signal's PSD. The minimum value of  $J_m^{f,\infty}(k_m)$  can be found by plugging in  $k_m^{\text{opt}}$  in to Eq. 3.10, doing so we find the minimum error energy as:

$$J_m^{f,\infty}(k_m^{\text{opt}}) = \frac{\sigma_n^2 |\gamma_m|^2 \eta_1}{|\beta_m|^2 + \frac{\sigma_n^2}{0.5\sigma_s^2 |\gamma_m|^2}} \quad (3.13)$$

### 3.3.2 ISI Canceller Weights

The conventional DFE or canceller equalizer utilizes the linear combination of the detected symbols to generate the current ISI and subtract it off from the current symbol. In our case, although the frequency selective channel introduces ISI to the broadband signal, the signal observed at the AFB transformed domain have little or no ISI due to the narrow band nature. This is because the channel has approximately flat frequency response when the bandwidth of  $A_m(\theta)$  is sufficiently narrow, see Eq. 3.4. Define the column vectors  $Y^\infty(n) \triangleq [y_0^\infty(n), y_1^\infty(n), \dots, y_{M-1}^\infty(n)]^T$  as the linear equalizer output, i.e,  $y_m^\infty(n) = k_m^* x_m^\infty(n)$ . Consider the optimization problem:

$$\arg \min_{\mathbf{C}} \mathbf{J}^{c,\infty}(\mathbf{C}) = \arg \min_{\mathbf{C}} E \left\| X^{ref}(n) - \left[ Y^\infty(n) - \mathbf{C}^H X^{ref}(n) \right] \right\|_2^2 \quad (3.14)$$

where,  $\mathbf{C} \triangleq \text{diag}\{c_0, c_1, \dots, c_{M-1}\}$  is the to be determined canceller coefficient. Again, since the optimization is decoupled, only one path is considered.

$$\begin{aligned} \arg \min_{c_m} J_m^{c,\infty}(c_m) &= \arg \min_{c_m} E \left\| x_m^{\text{ref}}(n) - \left[ y_m^\infty(n) - c_m^* x_m^{\text{ref}}(n) \right] \right\|_2^2 \\ &= E \{ \boldsymbol{\varepsilon}_m^c(n) \boldsymbol{\varepsilon}_m^{c*}(n) \} \end{aligned} \quad (3.15)$$

where  $\boldsymbol{\varepsilon}_m^c(n) \triangleq x_m^{\text{ref}}(n) - \left[ y_m^\infty(n) - c_m^* x_m^{\text{ref}}(n) \right]$ . Solving for  $c_m$ , we have:

$$c_m^{\text{opt}} = \frac{E \{ x_m^{\text{ref}}(n) y_m^{\infty*}(n) \}}{E \{ x_m^{\text{ref}}(n) x_m^{\text{ref}*}(n) \}} - 1 \quad (3.16)$$

Plug in  $E \{ x_m^{\text{ref}}(n) x_m^{\text{ref}*}(n) \} = |\gamma_m|^4 \sigma_s^2 \eta_2$ ,  $E \{ x_m^{\text{ref}}(n) y_m^{\infty*}(n) \} = \gamma_m^* \beta_m^* k_m |\gamma_m|^2 \sigma_s^2 \eta_2$ ; and set  $k_m = k_m^{\text{opt}}$ , we find  $c_m^{\text{opt}}$  as

$$c_m^{\text{opt}} = \frac{|\beta_m|^2}{|\beta_m|^2 + \frac{\sigma_n^2}{0.5\sigma_s^2|\gamma_m|^2}} - 1 = \frac{\beta_m^*}{\gamma_m} k_m^{\text{opt}} - 1 \quad (3.17)$$

Examining the above expression, the optimal ISI canceller weights is simply the overall channel minus 1, regardless the shaping and fixed receiver response  $y_m$ . This coincides with the frequency response of the well-known results for adaptive canceller. The optimal error energy can then be found by plugging Eq. 3.17 into Eq. 3.15:

$$J_m^{c,\infty}(c_m^{\text{opt}}) = |k_m^{\text{opt}}|^2 \sigma_n^2 \eta_1 \quad (3.18)$$

Equation 3.18 suggests under the assumption of infinite number of AFB; and the possession of perfect reference signal, the ISI can be completely eliminated leaving only the noise component. Note the noise is colored by the linear equalizer; yet within each sufficiently narrow channel, it is still white.

### 3.4 Finite Path NMDFB Spectral Shaping Error

We have derived the PR-NMDFB based equalizer weights based on infinite number of paths / BPFs. It is important to understand the equalizer's performance for a finite

path NMDFB. In this section, we utilize the previous developed NMDFB spectral shaping property to analyze the linear / non-linear equalizer performance. Based on the BPF interpretation of the Fourier transform [45], the weight vector  $K$  eventually becomes the continuous frequency response of the desired MMSE linear equalizer as  $M \rightarrow \infty$ . Therefore, we find the DTFT of the optimum MMSE equalizer based on criteria defined in Eq.3.9 to be:

$$K(\theta) = \left( \frac{H_{tx}(\theta) H_c(\theta)}{|H_c(\theta)|^2 + \frac{\sigma_n^2}{0.5\sigma_s^2 |H_{tx}(\theta)|^2}} \right)^* \quad (3.19)$$

Similarly, we find the DTFT of the optimum ISI canceller based on criteria defined in Eq. 3.14 to be:

$$C(\theta) = \frac{H_c^*(\theta)}{H_{tx}(\theta)} K(\theta) - 1 \quad (3.20)$$

The continuous spectrum  $K(\theta)$  or  $C(\theta)$  can be viewed as an ideal target spectrum or filter's frequency response applied to the input broadband signal. Provided with any ideal continuous target spectrum, the goal is to synthesize it via an  $M$ -path PR-MNDFB developed in Chapter. 2. Also note that, target spectrum does not necessarily only be the linear / non-linear equalizer responses. Based on the spectral shaping property presented in Chapter. 2, one can ideally synthesize any spectral shapes needed in the receiver's signal processing chain. For instance, besides equalizer and MF, one can also design fractional delay filter via IPE as part of the timing recovery process [64].

Given the  $M$ -Path NMDFB AFB matrix:

$$\mathbb{A} = \begin{pmatrix} A(zW_M^0 W_D^0) & \cdots & A(zW_M^0 W_D^{D-1}) \\ \vdots & \ddots & \vdots \\ A(zW_M^{M-1} W_D^0) & \cdots & A(zW_M^{M-1} W_D^{D-1}) \end{pmatrix}_{M \times D} = [A_{M \times 1} \quad \bar{\mathbb{A}}_{M \times (D-1)}]_{M \times D}$$

and the SFB vector

$$\mathbf{G}(z) = [G(zW_M^0) \dots G(zW_M^{M-1})]^T$$

Assuming the aliasing caused by PR-NMDFB is negligible, therefore the linear and non-linear equalized signal can be represented as:

$$\begin{aligned}
Z(z) &= \frac{1}{D} \mathbf{G}_{1 \times M}(z) \left[ \mathbb{K}_{M \times M} \mathbf{A}_{M \times D}(z) \mathbf{R}_{D \times 1}(z) - \mathbb{C}_{M \times M} \mathbf{A}_{M \times D}(z) \mathbf{R}_{D \times 1}^{\text{ref}}(z) \right] \quad (3.21) \\
&= \frac{1}{D} \mathbf{G}_{1 \times M}(z) \mathbb{K}_{M \times M} \mathbf{A}_{M \times D}(z) \mathbf{R}_{D \times 1}(z) - \frac{1}{D} \mathbf{G}_{1 \times M}(z) \mathbb{C}_{M \times M} \mathbf{A}_{M \times D}(z) \mathbf{R}_{D \times 1}^{\text{ref}}(z) \\
&= \frac{1}{D} T_s^{\mathbb{K}}(z) R(z) - \frac{1}{D} T_s^{\mathbb{C}}(z) R^{\text{ref}}(z)
\end{aligned}$$

where  $T_s^{\mathbb{K}}(z)$  and  $T_s^{\mathbb{C}}(z)$  is the NMDFB signal transfer function defined in Eq. (2.3, 2.4);  $\mathbf{R}(z) = [R(zW_D^0), R(zW_D^1), \dots, R(zW_D^{D-1})]^T = [R(zW_D^0) \ \bar{\mathbf{R}}(z)]^T$  is the modulated versions of the input signal;  $\mathbf{R}^{\text{ref}}(z) = [R^{\text{ref}}(zW_D^0), R^{\text{ref}}(zW_D^1), \dots, R^{\text{ref}}(zW_D^{D-1})]^T = [R^{\text{ref}}(zW_D^0) \ \bar{\mathbf{R}}^{\text{ref}}(z)]^T$  is the modulated versions of the reference signal. Since we have assumed the PR-NMDFB has zero aliasing error, these modulation terms disappears in Eq. 3.21, i.e.,  $\mathbf{T}_A^{\mathbb{K}}(z) = \mathbf{0}$  and  $\mathbf{T}_A^{\mathbb{C}}(z) = \mathbf{0}$ .

The error signal due to linear equalization is defined as  $E_m(\theta) \xrightarrow{IDTFT} e_m(n) \triangleq r(n) * t_{\varepsilon,m}(n)$ , where  $t_{\varepsilon,m}(n) \xrightarrow{DTFT} T_{\varepsilon,m}(\theta)$ . Note that,  $T_{\varepsilon,m}(\theta)$  is the  $m^{\text{th}}$ -channel spectral shaping error transfer function defined in Eq. 2.20 and 2.23. The scalar  $1/D$  can be omitted because it only affects the gain of the received signal; and have no influence on SNR. Using Parseval's Theorem, we can readily determine the error energy due to finite  $M$ , denoted as  $\varepsilon_{E,m}^f$ :

$$\begin{aligned}
\varepsilon_{E,m}^f &= \frac{1}{2\pi} \int_{-\pi}^{\pi} |E_m(\theta)|^2 d\theta \quad (3.22) \\
&= \frac{1}{2\pi} \int_{\theta_m}^{\theta_{m+1}} |R(\theta)|^2 |T_{\varepsilon,m}^{\mathbb{K}}(\theta)|^2 d\theta \\
&\leq \frac{1}{4} \left( \ddot{B}_{\varepsilon,m}^{\mathbb{K}} \right)^2 \left( \frac{\pi}{M} \right)^4 \frac{1}{2\pi} \int_{\theta_m}^{\theta_{m+1}} |R(\theta)|^2 d\theta \\
&= \frac{1}{4} \frac{1}{M} \left( \ddot{B}_{\varepsilon,m}^{\mathbb{K}} \right)^2 \left( \frac{\pi}{M} \right)^4 \left( \frac{1}{2} \sigma_s^2 |\gamma_m|^2 |\beta_m|^2 + \sigma_n^2 \right)
\end{aligned}$$

where  $\ddot{B}_{\varepsilon,m}^{\mathbb{K}} \triangleq \underset{\theta \in [\theta_m - \frac{\pi}{M}, \theta_m + \frac{\pi}{M}]}{\text{Max}} |\ddot{K}(\theta)|$  implying that the straight line approximation error

bound Eq. 2.25 is used. We also assumed the target spectrum is analytic and twice differentiable. We also used the assumption that the PSD of the received signal is a constant  $\frac{1}{2}\sigma_s^2 |\gamma_m|^2 |\beta_m|^2 + \sigma_n^2$  within the integral region. Therefore, the total error energy due to forward equalizer finite approximation is:

$$\begin{aligned}\epsilon_E^f &= \sum_{m=0}^{M-1} \epsilon_{E,m}^f \\ &\leq \frac{1}{4} \frac{1}{M} \sum_{m=0}^{M-1} \left( \ddot{B}_{\epsilon,m}^{\mathbb{K}} \right)^2 \left( \frac{\pi}{M} \right)^4 \left( \frac{1}{2} \sigma_s^2 |\gamma_m|^2 |\beta_m|^2 + \sigma_n^2 \right)\end{aligned}\quad (3.23)$$

Similarly, one can derive the total error energy due to ISI canceller approximation as:

$$\begin{aligned}\epsilon_E^c &= \sum_{m=0}^{M-1} \epsilon_{E,m}^c \\ &\leq \frac{1}{4} \frac{1}{M} \sum_{m=0}^{M-1} \left( \ddot{B}_{\epsilon,m}^{\mathbb{C}} \right)^2 \left( \frac{\pi}{M} \right)^4 \left( \frac{1}{2} \sigma_s^2 |\gamma_m|^4 \right)\end{aligned}\quad (3.24)$$

If we make the assumption that the forward equalization spectral shaping error and ISI cancellation shaping error are independent, then the total excess error due to finite path PR-NMDFB is

$$\epsilon_E = \epsilon_E^f + \epsilon_E^c \quad (3.25)$$

Examining Eq. 3.25, the total excess error  $\epsilon_E$  can be bounded via Eq. 3.23 3.24; and can be reduced by increasing path number  $M$ , since  $\epsilon_E$  is inversely proportional to  $M^4$ .

### 3.5 Practical Implementation

In practice, we desire the receiver shown in Fig . 3.1 to be implemented via adaptive algorithms. Comparing to other proposed block transmission / equalizers [6, 7, 50, 4, 67, 68], our proposed technique can obtain equalizer update via simple adaptive

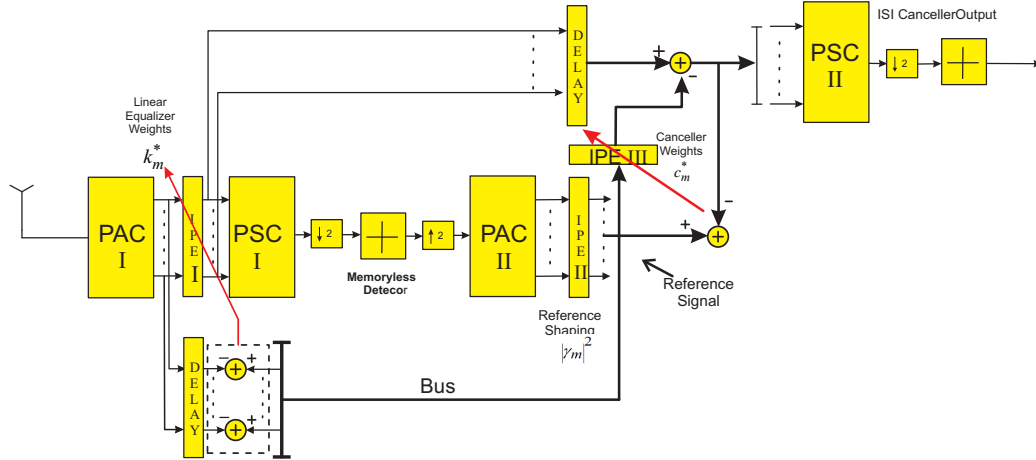


**Figure 3.2:** Adaptive Implementation of PR-NMDFB based Linear / Non-linear Equalizer

algorithms, i.e., Least Mean Square (LMS) algorithm making the system realization much more practical. Moreover, utilizing the ISI canceller as the non-linear equalizer avoids the causality problem occurred in block equalizers [67, 68].

The proposed adaptive implementation of block equalizer is shown in Fig. 3.2. The forward or linear equalizer occurs after PAC-I via IPE-I, where a set of equalization coefficients are applied to each PAC-I outputs performing the spectral shaping. The reference signal is defined in the PAC transformed domain and can be created via three steps: synthesize the forward equalized signal via PSC-I; make symbol decisions via memoryless detector, where the 1st stage tentative decisions are made [69, 70]; locally perform spectral shaping via PAC-II and IPE-II. The ISI canceller subtracts the ISI, which is generated from the filtered referenced signal via IPE-III, from the forward equalized signal in the PAC domain. It should be noted that non-ideal tentative decisions will degrade the overall BER performance [74], similar to the error propagation problem in DFE.

The data observed at the output of the PAC-I was previously defined as  $X(n) = [x_0(n), \dots, x_{M-1}(n)]^T$ ; put it in diagonal form  $\mathbb{X}(n) \triangleq \text{diag}\{x_0(n), \dots, x_{M-1}(n)\}$ . The reference signal at IPE-II output is  $X^{\text{ref}}(n) = [x_0^{\text{ref}}(n), \dots, x_{M-1}^{\text{ref}}(n)]^T$  and also define  $\mathbb{X}^{\text{ref}}(n) \triangleq \text{diag}\{x_0^{\text{ref}}(n), \dots, x_{M-1}^{\text{ref}}(n)\}$ . The forward equalizer and ISI canceller weight

**Table 3.1:** Summary of PR-NMDFB LMS Adaptation

INITIALIZATION
$K_{M \times 1}(0) = [1, 1, \dots, 1]^T$
$C_{M \times 1}(0) = [0, 0, \dots, 0]^T$
FOR EACH NEW OUTPUT VECTOR AT AFBs
$Y(n) = \mathbb{X}(n)K_{M \times 1}$
$E^f(n-L) = X^{ref}(n) - Y(n-L)$
$E^c(n) = X^{ref}(n) - [Y(n-L) - \mathbb{X}^{ref}(n)C_{M \times 1}(n)]$
$K_{M \times 1}(n+1) = K_{M \times 1}(n) + 2\mu_f \mathbb{N}_f \mathbb{X}^H(n)E^f(n)$
$C_{M \times 1}(n+1) = C_{M \times 1}(n) + 2\mu_c \mathbb{N}_c \mathbb{X}^{ref H}(n)E^c(n)$

is rewritten as  $K_{M \times 1}(n) = [k_0(n), \dots, k_{M-1}(n)]^T$ ,  $C_{M \times 1}(n) = [c_0(n), \dots, c_{M-1}(n)]^T$  respectively. The error vector is  $E^f(n-L) = X^{ref}(n) - \mathbb{X}(n-L)K_{M \times 1}(n-L) = X^{ref}(n) - Y(n-L)$ , where  $L$  is the delay caused by the PAC and PSC; and  $Y(n) \triangleq \mathbb{X}(n)K_{M \times 1}(n)$ . Using LMS algorithm [75], the gradient is  $\mathbb{X}^H(n)E^f(n)$ ; and the weights can be updated as:  $K_{M \times 1}(n+1) = K_{M \times 1}(n) + 2\mu_f \mathbb{N}_f \mathbb{X}^H(n)E^f(n)$ , where  $\mu_f$  is diagonal matrix containing step sizes; and  $\mathbb{N}_f$  is a diagonal matrix representing the constrain on the gradient. We set the  $(m, m)^{\text{th}}$  diagonal element of  $\mathbb{N}_f$  to be  $|\gamma_m|^2$ , since we only have to update the spectral portion that contains signal energy w.r.t the signal's PSD. Similarly, the ISI canceller error vector is  $E^c(n) = X^{ref}(n) - [Y(n-L) - \mathbb{X}^{ref}(n)C_{M \times 1}(n)]$ , and the gradient is  $\mathbb{X}^{ref H}(n)E^c(n)$ . The weights are updated as:  $C_{M \times 1}(n+1) = C_{M \times 1}(n) + 2\mu_c \mathbb{N}_c \mathbb{X}^{ref H}(n)E^c(n)$ , where  $\mu_c$  is diagonal; and  $\mathbb{N}_c$  is a diagonal matrix representing the constrain on the gradient, whose  $(m, m)^{\text{th}}$  element is set to be  $|\gamma_m|^4$ . This adaptation essentially fall in line with SAF, and can be optimized according to [75].

### 3.6 Implementation Complexity

From Fig. 3.2, the proposed implementation requires two pairs of PAC / PSC and three IPEs. The PAC takes in  $D$  pieces of data and computes  $M$  outputs, while the PSC takes in  $M$  pieces of data and computes  $D$  outputs. For every  $D$  inputs, the low pass prototype filter for both PAC and PSC; two  $M$ -point FFTs; and corresponding IPEs are

operated once. Let the low pass prototype filter for an  $M$ -path PAC and PSC have  $L_A$  and  $L_S$  taps (real coefficients) per polyphase arm respectively. Then the two prototype filters consume  $2M(L_A + L_S)$  real multiplies for complex input signal. Using Radix-2 algorithm, the  $M$ -point FFT computation for PAC/PSC together costs  $2 \times 4 \times \frac{M}{2} \log_2 M$  real multiplies. Finally, each IPE costs  $4 \times M$  real multiplies. Therefore the number of operations per input data is written as:

$$\begin{aligned} \left( \frac{\text{ops}}{\text{input}} \right)_D &= 2 \times \frac{1}{D} \left[ 2M(L_A + L_S) + 2 \times 4 \times \frac{M}{2} \log_2 M \right] + 3 \times \frac{1}{D} \times 4M \quad (3.26) \\ \left( \frac{\text{ops}}{\text{input}} \right)_{D=\frac{M}{2}} &= 8(L_A + L_S) + 16 \log_2 M + 24 \end{aligned}$$

Equation 3.26 shows the total workload for two pairs of PAC/PSC and three IPEs. Clearly, the workload is on the order of  $\log_2 M$  (or the FFT workload) plus a constant polyphase and IPE filtering cost. Consider a practical example, setting  $L_A = L_S = 10$  will result LPPFs with more than 80 dB dynamic range; and  $M = 256$  well equalizes a multipath channel with normalized delay spread equals to 5 (will later be shown in the simulation section), i.e., ratio of RMS channel delay spread and symbol period. Plugging in these numbers we find the ops/input is 312 for  $D = M/2$  implementation. This number corresponds to the power consumption of a 156 tap FIR filter processing complex input data. Yet, we have done matched filtering, linear and nonlinear equalization. Comparing to the ATSC-8VSB [76] system, which has 6 MHz wide signal and requires total linear and nonlinear equalizer length over 400 taps, our proposed methods is clearly far more efficient. Moreover, Eq. 3.22 to Eq. 3.25 states finite path equalization error energy is inversely proportional to  $M^4$ . Now, we see that increasing  $M$  is at the cost of FFT which is a much economical way comparing with the FIR approach. Furthermore, we should not neglect that the proposed structure operates on the deeply decimated input rate; while the FIR approach operates on the input rate, which is a well-known bottleneck for wideband filtering.

### 3.7 Simulation Results

To further consolidate the performance of the proposed two-stage equalizer, several representative examples are prepared. We first examine the adaptive behavior of the two equalizers under a stationary channel. Then, we show the equalizers' achievable MMSE level for a given channel. Lastly, we present the bit error rate (BER) results based on frequently used channel models. In all of our simulation results, unless otherwise mentioned, the polyphase arm length for both PAC and PSC are set to 10 taps; the time domain prototype filter for shaping / MF is a pair of identical SRRC filters of 64-tap long, sampled at 2 samples per symbol, with roll-off factor 0.25; and, we do not assume perfect 1st stage linear equalizer (LE) tentative symbol decisions.

Experiment based on Fig.3.2 over tapped delay channel:  $(0.7982 - j0.0346) + (0.5701 - j0.3401)z^{-3} - (0.0959 + j0.0914)z^{-6} - (0.028 + j0.0353)z^{-9}$  is conducted; the modulation scheme is QPSK with 20 dB  $E_b/N_0$ ; and the simulation is based on an  $M = 256$ ,  $D = 128$ , PR-NMDFB. The channel's magnitude response along with the averaged received signal's power spectrum is shown in subplot 1 of Fig. 3.3. Clearly, the channel introduced two deep notches (over 20 dB) to the received signal. Subplot 2 of Fig. 3.3 shows the signal spectrum obtained after the LE along with the theoretical optimal LE weights and the adaptively converged equalizer weights. As expected, the LE cannot recover the channel notch. Subplot 3 shows the averaged signal spectrum after the ISI canceller; along with the theoretical and the adaptively converged canceller weights. The ISI canceller tends to only response to the channel notches, and the signal spectrum is "flattened" after the ISI cancellation. Fig. 3.4 shows the learning curves for the two equalizers. These curves were obtained by recording the symbol errors between the input and output of the two memory-less detectors. In addition, the learning curve of the ISI canceller's is produced with a stationary linear equalizer, i.e., after the LE weights are converged. We have set the LE step size to be  $\mu_f = \mu_f \mathbf{I}$ , where  $\mu_f = \frac{0.02}{P_0}$  and  $P_0$  is the received signal power on 0<sup>th</sup> path, i.e.,  $0.5\sigma_s^2 |\gamma_0|^2 + \sigma_n^2$ . Similarly,  $\mu_c = \mu_c \mathbf{I}$  and  $\mu_c = \frac{0.02}{\bar{P}_0}$ , where  $\bar{P}_0$  is the reference signal power on the 0<sup>th</sup> path, i.e.,  $0.5\sigma_s^2 |\gamma_0|^4$ . Note, other choices of  $\mu_f, \mu_c$ ; and signal power acquisition methods can also be applied [75]. We can see clearly from Fig. 3.4 that the ISI canceller's learning curve is roughly 3 dB lower than the LE for this particular channel, which is about 50 % reduction in

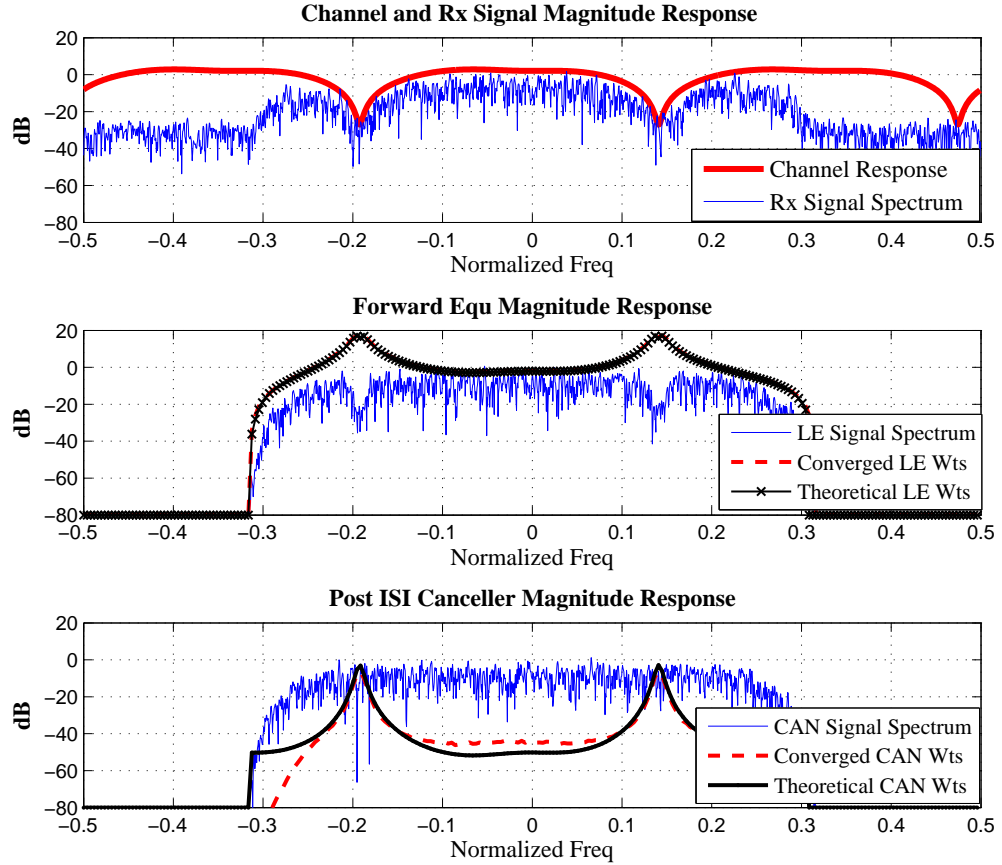


**Figure 3.3:** Signal and Equalizer Magnitude Responses

symbol error energy.

Fig. 7 shows the MMSE behavior of the proposed equalizers over another stationary channel with multiple sharp nulls (over 10 dB), whose impulse response is:  $0.8638 + j0.4319Z^{-6} + j0.2591Z^{-12} + j0.008638Z^{-18}$ . This example is simulated based on an  $M = 240$ ,  $D = 80$  triangular shaped PR- NMDFB; with QPSK symbol energy set to be . Note that, the linear equalization part requires a pair of PAC & PSC, plus one IPE. The number of real multiplies per input data spent on PAC & PSC filtering is  $6(L_A + L_S)$ , which is 120. The 240-point FFT can be designed via Good Thomas algorithm costs 1100 real multiplies for complex input (Table 2-6 of [48]) ; two 240-point FFT operate once for every  $D = 80$  inputs, which is 27.5 real multiplies per input. The

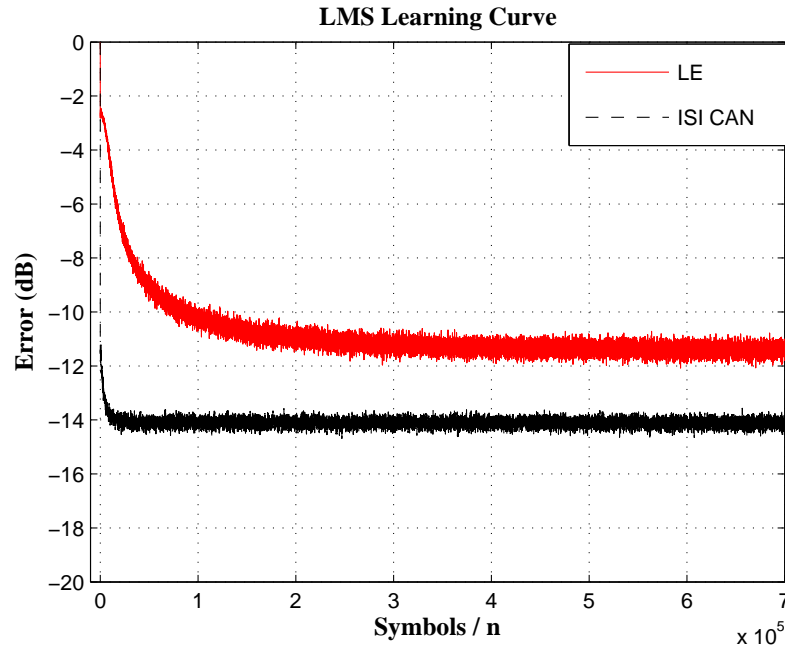


**Figure 3.4:** Learning Curve of the Linear / Non-Linear Equalizers

IPE costs 12 real multiplies per input. In total, the NMDFB implementation costs 159.5 real multiplies per input sample, which roughly corresponds to a real coefficient FIR filter with 80 taps processing complex data. Therefore, we included the MMSE performance of an 80-tap FIR LE in subplot 1 of Fig.3.5 for comparison. Subplot 1 of Fig. 3.5 reports the recorded MMSEs for simulated 80-Tap, 240-Tap FIR LEs; simulated 240-path PR-NMDFB based LE; estimated MMSE bound according to Eq.3.23; and optimal MMSE LE based on Eq. 3.13. We can see the MMSE of 240-path LE is very close to the optimal achievable result; and our derived estimated MMSE well predicts the simulation results. Similar, subplot 2 of Fig.3.5 shows the MMSEs for 240-path ISI canceller (assuming perfect 1<sup>st</sup> stage tentative symbol decisions). We find the simulated MMSE aligns with the optimal infinite long equalizer MMSE (from Eq.3.18) from 0 dB to 30 dB; and deviate afterwards. Lastly, the estimated MMSE (from Eq.3.25) well bounds the simulated MMSE results.

The next example is the BER performance over another fixed low delay spread channel but having a highly distorted, low pass shaped frequency response, used by authors in [4] (Fig. 6 in [4]). Our BER result, Fig.3.6, is obtained by assuming perfect

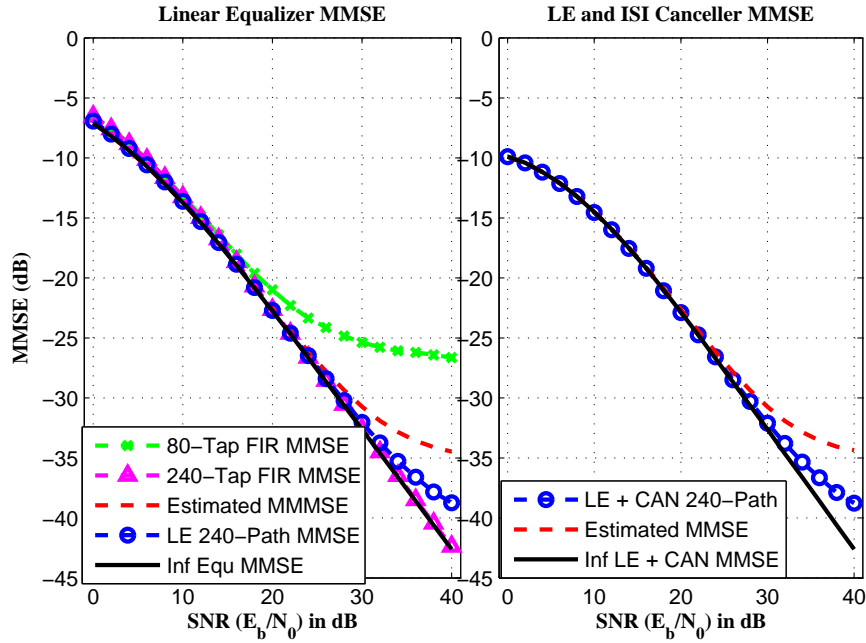


**Figure 3.5:** MMSE Performance of Proposed Equalizers

channel knowledge (as assumed in [4]); the optimal two-stage equalizer weights were directly applied. The blue crossed curve is the best result given by [4] under 512-point FFT IBD FE. The red triangled and the black circled curves are the LE and ISI canceller results respectively based on a 256-path,  $D = 128$ , PR-NMDFB structure. In this example, our ISI canceller has very similar BER performance to the SD-IBDFE [4]. Yet, our scheme does not rely on parameter estimation; has no redundancy in transmitted signal.

We next present the BER results averaged over statistical channel models. Consider QPSK signal with 50 MHz symbol rate communicating over ITU-R M.1225 indoor office channel B [77]. The ITU-B channel has RMS delay spread of 100 ns, meaning the normalized delay spread is  $\tau_{rms}/T = 5$ ; and a total delay of 700 ns. Fig. 3.7 shows the BER performance averaged over  $10^3$  channel realizations, with 95 % confident level. We have simulated both 256-path and 128-path PR-NMDFB in this example. The curve named "MFB" is the matched filter bound [78], offering the ideal BER performance. The theoretical and simulated BER for conventional OFDM without water-filling are also included for comparison. The theoretical BER of conventional OFDM is the same with the well-known flat Rayleigh fading result, Eq. (68) of [79]. The simulated OFDM

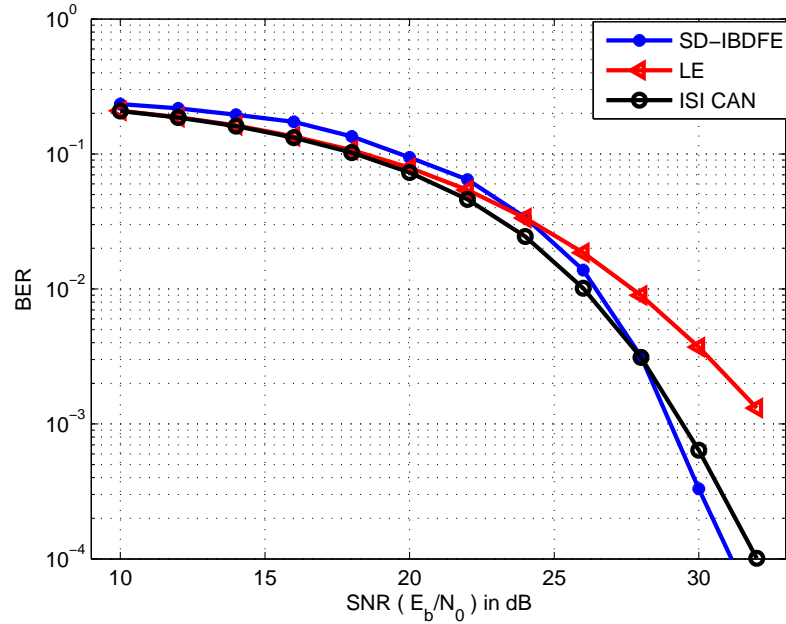


**Figure 3.6:** BER Performance over Low Delay Spread, Highly Distorted Channel [4]

uses 256-point FFT, 64-point CP, which is a scaled version of the 802.11a standard [80]; and experiences the same channel realizations with PR-NMDFB simulation. We found with sufficiently large number of PR-NMDFB paths, our equalizer out performs theoretical best achievable conventional OFDM BER. And we must keep in mind that, the OFDM error floor in practice is dominated by carrier offset, and channel estimation error [79]. As expected, the 256-path PR-NMDFB outperforms 128-path due to less equalization error. The ISI canceller results are seen to offer 1 dB gain at high SNR. The reason we do not see dramatic performance advantage of the ISI canceller is because: 1). Tentative decisions at output of LE are non-ideal. 2). Not all channel realizations exhibit deep nulls.

Our final example is the BER results over 802.11 AC channel model, Medbo model B [81], for typical large open space and office environments. Let us consider very high throughput QPSK signal with 100 MHz symbol rate, which falls in "system bandwidth  $80\text{ MHz} \leq W \leq 160\text{ MHz}$  [81]", with power delay profile spacing 2.5 ns. This channel has RMS delay spread 100 ns, (normalized delay spread  $\tau_{rms}/T = 10$ ); total delay 790 ns. Fig.3.8 reports the BER performance for 256-path and 512-path

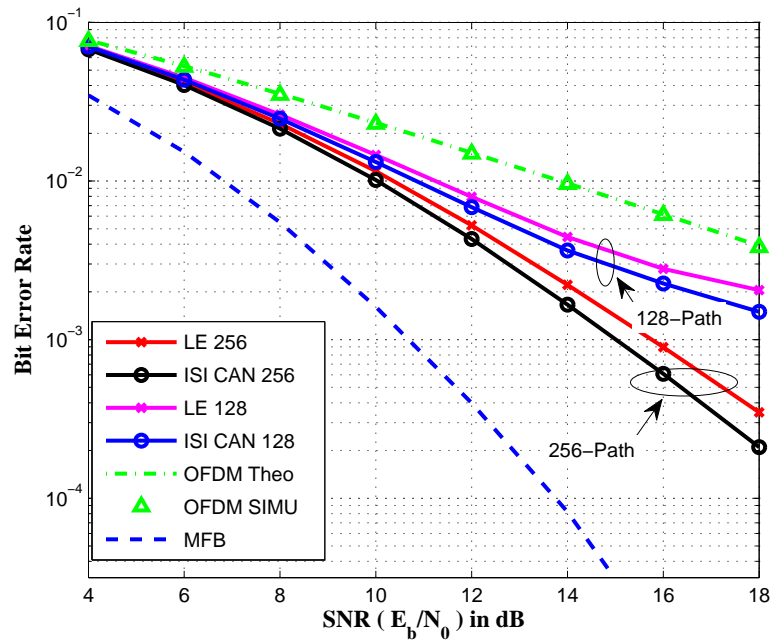


**Figure 3.7:** 50MHz Symbol Rate QPSK Signal BER Results Over ITU-B Channel

PR-NMDFB averaged over  $10^3$  realizations. Again the conventional OFDM BER and MFB are included for comparison. The simulated conventional OFDM based on scaled 802.11 standard [80] uses 512-point FFT and 128-point CP. The BER results shown in Fig.3.8 follows similar trend to Fig.3.7. except for the fact that larger NMDFB paths is needed to accommodate larger channel delay spread; and the ISI canceller, for this channel model, provides approximately 2 dB SNR gain in the high SNR region.

Based on the averaged BER experiments, it is clearly that the proposed modem structure is capable of wirelessly delivering large amount of data utilizing legacy QAM waveform, which has well controlled characteristics on synchronization and PAPR. It is well known that, one needs water-filling to further improve the BER of OFDM system, which also requires very accurate channel state information (CSI), as well as receiver feedback. The proposed scheme, on the other hand, does not require these conditions, which further reduces the implementation complexity. Moreover, in the case of large channel delay spread, given the carrier synchronization and the PAPR problems were well solved, the OFDM based technique still requires very long CP or guard interval

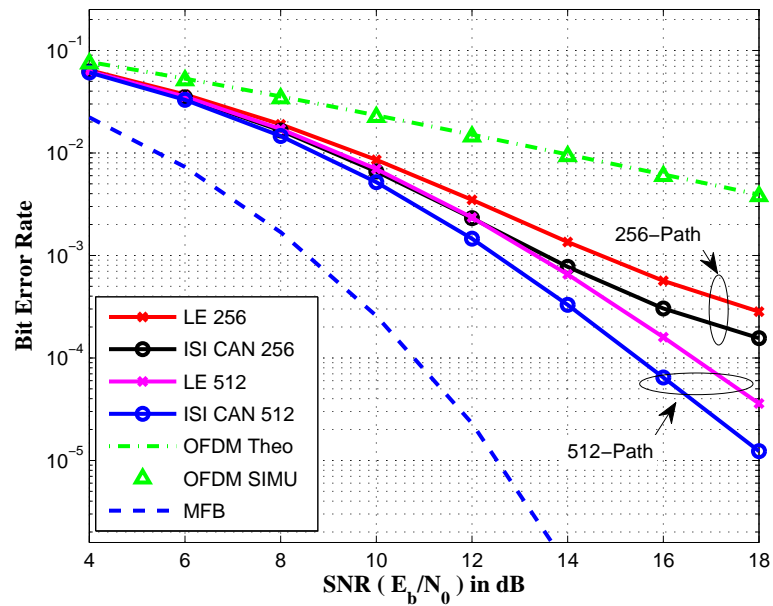


**Figure 3.8:** 100MHz Symbol Rate QPSK Signal BER Results Over 802.11 AC Medbo Model B

duration for each block, which has no advantage in throughput comparing with PR-NMDFB processing.

### 3.8 Acknowledgment

Chapter 3, in part, is currently being prepared for submission for publication of the material:

- Xiaofei Chen, fred harris, Bhaskar Rao and Elettra Venosa, "Equalizers for Wide-band Digital Receivers Based on Non-Maximally Decimated Filter Bank"

## **Chapter 4**

# **Filter Bank Selection Diversity and Linear Equalization Over Highly Frequency Selective Channels for Single Carrier Transmission**

## 4.1 Introduction

Modern communication systems require wideband communication over highly dispersive frequency selective channels. The multi-carrier (MC) transmission, e.g., OFDM [14], has captured major attention due to its simple equalization scheme and its low processing speed feature, i.e., serial to parallel conversion. These important characteristics allow one to build very broadband systems in a cost effective manner. However, as pointed out in [6], the OFDM based MC systems suffer from a number of drawbacks, such as cyclic prefix (CP) overhead, high peak to average power ratio (PAPR), sensitivity to carrier frequency offset; and these facts limit the system's throughput, power consumption, and bit error rate (BER) performances. On the other hand, the legacy single carrier (SC) signal, i.e., square root raised cosine (SRRC) shaped QAM waveform, has these problems well controlled. Yet, legacy waveforms require very long equalizers, i.e., the ATSC-8VSB [76] has 6 MHz wide signal bandwidth; and requires an equalizer with total length exceeding 400 taps, the longest equalizer ever deployed. Moreover, the diversity techniques are not well supported for SC transmissions over frequency selective channels. In 1992, authors in [82] developed the optimum diversity receiver structure over a frequency selective channel, as shown in Fig. 4.1, which has been later recognized as an MRC in [83]. The received signals from the  $L$ -branch independent antennas are first matched filtered (matched to the shaping pulse and the channel) and then summed to form the combined signal. The combined signal is then sent to a tapped delay line equalizer to produce desired symbol outputs subject to either zero forcing (ZF) or minimum mean square error (MMSE) criteria.

The direct implementation of Fig. 4.1 does not only require significant hardware resources on filtering, but also need precise channel knowledge for each branch. Comparing to MC techniques where filtering is FFT based and channel gains can be extracted from the preamble, the SC transmission at first glance seems very disadvantaged in broadband wireless communication. The authors in [83] first introduced filter bank (FB) based MRC concept to non-CP SC system, which is a direct filter bank (FB) implementation of the optimal maximal ratio combining (MRC) receiver (Fig. 4.1). The FB diversity combining receiver can be generalized via Fig. 4.2. The idea is to use analysis filter bank (AFB), whose polyphase form is named as polyphase analysis chan-

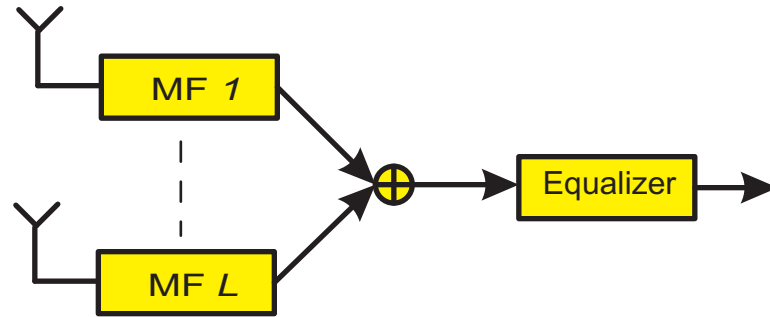


**Figure 4.1:** Optimum Combiner / Linear Equalizer Structure

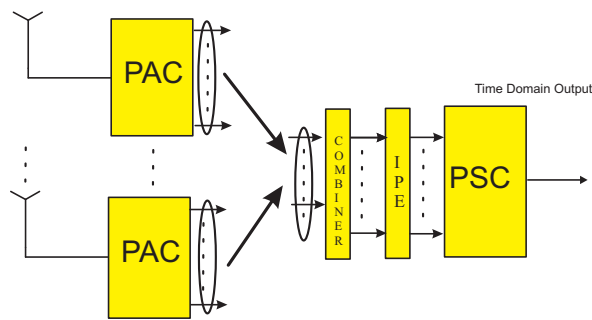


**Figure 4.2:** Filter Bank Based Diversity Combining Model

nelizer (PAC), to interface with each receiver's antenna; and then perform combining in the PAC transformed domain. Since [83] followed the MRC criteria, the PAC outputs are first matched filtered (in FB transformed domain) and then combined. The combined signal is then equalized via the intermediate processing element (IPE). Finally, the equalized signal is transformed back to time domain via synthesis filter bank (SFB), whose polyphase form is called polyphase synthesis channelizer (PSC). Although MRC is optimal, it requires precise channel knowledge to perform combining, which is a significant limitation in practical implementation. We shall propose FB selection method, whereby the signal with highest power is selected across the diversity branches and no channel information is needed. In addition, in the past work [83] numerical results were provided to evaluate FB based MRC. We shall provide a more rigorous performance analysis over both the FB selection and the optimal MRC.

The organization of this chapter is: section 2 presents signal model; section 3 derives the combining technique; section 4 gives simulation results; section 5 draws

conclusion.

## 4.2 Signal Model

Let us consider an  $M$ -path PR-NMDFB model, with analysis and synthesis prototype filter denoted as  $a(n)$  and  $g(n)$  respectively. The  $m^{\text{th}}$  AFB filter is  $a_m(n) = a(n)e^{j\frac{2\pi}{M}mn}$ , whose Z-transform is  $A_m(z) = A\left(e^{-j\frac{2\pi}{M}}z\right) = A(W_M^m z)$ , and  $W_M \triangleq e^{-j\frac{2\pi}{M}}$ . Similarly, the  $m^{\text{th}}$  SFB filter is  $g_m(n) = g(n)e^{j\frac{2\pi}{M}mn}$ , whose Z-transform is  $G_m(z) = G\left(e^{-j\frac{2\pi}{M}}z\right) = G(W_M^m z)$ . Then, following the NMDFB theory developed in Chapter. 2 we define the AFB matrix and SFB column as:

$$\mathbb{A} = \begin{pmatrix} A(zW_M^0 W_D^0) & \cdots & A(zW_M^0 W_D^{D-1}) \\ \vdots & \ddots & \vdots \\ A(zW_M^{M-1} W_D^0) & \cdots & A(zW_M^{M-1} W_D^{D-1}) \end{pmatrix}_{M \times D} = [A_{M \times 1} \bar{\mathbb{A}}_{M \times (D-1)}]_{M \times D}$$

and the SFB vector:  $\mathbf{G}(z) = [G(zW_M^0) \dots G(zW_M^{M-1})]^T$ ; IPE diagonal matrix:  $\mathbb{K} = \text{diag}\{k_0, \dots, k_{M-1}\}$ ;

We now examine a baseband equivalent system for a QAM signal with complex notation for the in-phase ( $I$ ) and quadrature ( $Q$ ) branches, e.g.,  $\text{Re}(\cdot)$  and  $\text{Im}(\cdot)$  respectively. Denoting the  $k^{\text{th}}$  complex QAM data symbol as  $S_k$ , with symbol period  $T$  seconds. We assume the data symbols are stationary and uncorrelated,  $[S_k S_{k'}] = \sigma_s^2 \delta_{kk'}$ , where  $\delta_{kk'}$  is the Kronecker delta function. At the transmitter (Tx), the symbol stream first experiences 1-to-2 zero packing / up-sampling process and then were passed onto a square-root raised cosine (SRRC) digital shaping filter  $h_{tx}(n)$ ; and assume perfect digital to analog conversion, the emitted signal has power spectral density (PSD)  $\frac{1}{2}\sigma_s^2 |H_{tx}(\Omega)|^2$ , where  $\Omega$  is the analog frequency; and  $H_{tx}(\Omega)$  is Fourier transform of the shaping pulse. Denote the complex base-band equivalent channels for a  $L$ -branch receiver as  $h_l^c(t)$ , for  $l = 1, 2, \dots, L$ . The additive white noise  $n_l(t) = n_l^I(t) + jn_l^Q(t)$  of two-sided power spectral density  $\frac{N_0}{2}$  W/Hz per complex components is introduced at the output of each independent channel. The received  $l^{\text{th}}$  branch continuous signal is written as:

$$r_l(t) = \sum_{k=-\infty}^{\infty} S_k h_l^{tc}(t - kT - t_l) + n_l(t) \quad (4.1)$$

where,  $h_l^{tc}(t) \triangleq h^{tx}(t) * h_l^c(t)$  and  $t_l$  is the channel delay or the sampler phase. In this paper, we assume the channel  $h_l^c(t)$  is free of linear phase component, and set  $t_l = 0$ . Digitizing the received signal at sampling speed  $T_S = T/2$ , i.e., 2 samples-per-symbol, we find digitized signal as:

$$r_l(n) = \sum_{k=-\infty}^{\infty} S_k h_l^{tc}(n - 2k) + n_l(n) \quad (4.2)$$

Here we assume the noise variance on all  $L$ -branches are the same and equal to  $\sigma_n^2$ . The decimated by  $D$  and frequency translated output signal observed at the  $m^{\text{th}}$  AFB output on the  $l^{\text{th}}$  diversity branch is:

$$x_{m,l}(n) = (\downarrow D) \left[ \sum_k S_k h_{m,l}^a(n - 2k) e^{-j\theta_m n} + v_{m,l}(n) e^{-j\theta_m n} \right] \quad (4.3)$$

where,  $h_{m,l}^a(n) \triangleq h_l^{tc}(n) * a_m(m)$ , and  $v_{m,l}(n) \triangleq n_l(n) * a_m(n)$ . The Discrete Time Fourier Transform (DTFT) of  $h_{m,l}^a(n)$  is denoted as  $H_{m,l}^a(\theta) = H^{tx}(\theta) H_l^c(\theta) A_m(\theta)$ . Assuming the number of AFB is large, i.e.,  $M \rightarrow \infty$ , the bandwidth of BPF  $A_m(\theta)$  becomes arbitrarily narrow. The DTFT of  $h_{m,l}^a(n)$  can be rewritten as:

$$H_{m,l}^a(\theta) \approx \gamma_m \beta_{m,l} A_m(\theta) \xrightarrow{IDTFT} \gamma_m \beta_{m,l} a_m(n) \approx h_{m,l}^a(n) \quad (4.4)$$

where,  $\gamma_m = H^{tx}(\theta_m)$ ,  $\beta_{m,l} = H_l^c(\theta_m)$ ; and Eq. 4.3 can be written as:

$$x_{m,l}(n) = e^{-j\theta_m n D} \left[ \sum_k S_k \gamma_m \beta_{m,l} \bar{a}_m(n - 2k) + \bar{v}_{m,l}(n) \right] \quad (4.5)$$

where,  $\bar{a}_m(n) = a(nD)$  and  $\bar{v}_m(n) = v(nD)$ .

### 4.3 Diversity Combining and Channel Equalization

Examining Eq. 4.5, one can observe that the AFB has transformed wideband SC signal onto a collection of narrow band signals and this is true when  $M$  is sufficiently large for a given frequency selective channel. With this assumption, the multipath channel becomes a complex scalar gain  $\beta_{m,l}$  for the  $m^{\text{th}}$  AFB output on the  $l^{\text{th}}$  diversity branch. The diversity combining for frequency selective channel can now be readily defined based on the existing narrow band diversity concepts. For the  $l^{\text{th}}$  branch, define  $X_l(n) \triangleq [x_{0,l}(n), \dots, x_{M-1,l}(n)]^T$  as the AFB outputs;  $\beta_l(n) \triangleq [\beta_{0,l}, \dots, \beta_{M-1,l}]^T$  as the channel gain;  $\mathbb{W}_l \triangleq \text{diag}\{w_{0,l}, \dots, w_{M-1,l}\}$  as the complex scalar weights applied to AFB outputs. Thus, the diversity combined signal is  $X(n) \triangleq [x_0(n), \dots, x_{M-1}(n)]^T$  is written as:

$$X(n) = \sum_l \mathbb{W}_l^H X_l(n) \quad (4.6)$$

Based on Eq. 4.6, one immediately recognizes from narrow band combining concepts that setting  $\mathbb{W}_l = \text{diag}\{\beta_{0,l}, \dots, \beta_{M-1,l}\}$  produces the MRC [8]. However, the MRC requires precise channel knowledge, which is difficult to obtain for non-CP SC systems. Therefore, our focus naturally turns to the FB based selection diversity. Take the  $m^{\text{th}}$  AFB output for example; one can select the signal with the highest power among the  $L$  available branches. And the combiner's weights can be represented as:

$$w_{m,l} = \begin{cases} 1 & \text{if } |\beta_{m,l}| = \max(|\beta_{m,1}|, \dots, |\beta_{m,L}|) \\ 0 & \text{Otherwise} \end{cases} \quad (4.7)$$

It is clear that, regardless of the combining rule, the mechanism i.e., Fig.4.2, essentially generates a new channel that is supposed to enhance the overall system performance. This new channel  $\hat{B}$ , expressed as  $M$ -by-1 vector, can be expressed as:

$$\hat{B} = \sum_l \mathbb{W}_l^H B_l = [\hat{\beta}_0, \dots, \hat{\beta}_{M-1}]^T \quad (4.8)$$

For the MRC, the  $m^{\text{th}}$  entry of  $\hat{B}$  is:  $\hat{\beta}_m = \sum_l |\beta_{m,l}|^2$ ; and for the selection diversity them<sup>th</sup>

entry of  $\hat{B}$  is  $\hat{\beta}_m = \beta_m^{Max}$ , where  $\beta_m^{Max}$  is the channel gain associated with the signal that has the highest power across the  $L$  branches. The combined signal observed on the  $m^{\text{th}}$  AFB path is written as

$$x_m(n) = e^{-j\theta_m n D} \left[ \sum_k S_k \gamma_m \hat{\beta}_m \bar{a}_m(n-2k) + \bar{u}_m(n) \right] \quad (4.9)$$

where the noise term  $\bar{u}_m(n) = \sum_l w_{m,l}^* \bar{v}_{m,l}(n)$

Assuming a perfect copy of the matched filtered signal free of channel and noise is available, denoted as  $x_m^{ref}(n)$ :

$$x_m^{ref}(n) = e^{-j\theta_m n D} \sum_k S_k |\gamma_m|^2 \bar{a}_m(n-2k) \quad (4.10)$$

And we denote reference signal column vector  $X^{ref}(n) \triangleq [x_0^{ref}(n), \dots, x_{M-1}^{ref}(n)]^T$ . In practice, the reference signal is produced via decision directed process, a standard process in equalizer design ???. The MMSE linear equalizer is produced by solving the following optimization problem:

$$\arg \min_{\mathbf{K}} \mathbf{J}(\mathbf{K}) = \arg \min_{\mathbf{K}} E \left\| \mathbf{K}^H X(n) - X^{ref}(n) \right\|_2^2$$

where  $\mathbf{K} \triangleq \text{diag}\{k_0, \dots, k_{M-1}\}$  is the to be determined equalizer's coefficient. Since the AFB has decoupled the input signal into  $M$  outputs. The optimization problem can be solved by examining one channel, say the  $m^{\text{th}}$  channel. In the case  $M \rightarrow \infty$ , the equalizer weight for the  $m^{\text{th}}$  channel can be solved by minimizing the following function:

$$\arg \min_{k_m} J_m(k_m) = \arg \min_{k_m} E \left\| k_m^* x_m(n) - x_m^{ref}(n) \right\|_2^2 = \arg \min_{k_m} E \left[ \epsilon_m^f \epsilon_m^{f*} \right] \quad (4.11)$$

where  $\epsilon_m^f \triangleq k_m^* x_m(n) - x_m^{ref}(n)$ . After simple steps, the optimum coefficient  $k_m^{\text{opt}}$  can be written as:

$$k_m^{\text{opt}} = \frac{E \{x_m(n) x_m^{\text{ref}*}(n)\}}{E \{x_m(n) x_m^*(n)\}}$$

And, one may calculate quantities:

$$\begin{aligned}
E \{ \bar{v}_m(n) \bar{v}_m^*(n) \} &= \sigma_n^2 \sum_k |\bar{a}_m(n-k)|^2 = \sigma_n^2 \eta_1 \\
\sigma_u^2 = E \{ \bar{u}_m(n) \bar{u}_m^*(n) \} &= \begin{cases} \sigma_n^2 \eta_1 & \text{Selection Combining} \\ \sigma_n^2 \eta_1 \sum_l |\beta_{m,l}|^2 & \text{MRC} \end{cases} \\
E \{ x_m(n) x_m^*(n) \} &= |\gamma_m|^2 |\hat{\beta}_m|^2 \sigma_s^2 \eta_2 + \sigma_u^2 \\
E \{ x_m(n) x_m^{\text{ref}*}(n) \} &= |\gamma_m|^2 \gamma_m \hat{\beta}_m \sigma_s^2 \eta_2
\end{aligned}$$

where  $\eta_1 \triangleq \sum_k |\bar{a}_m(n-k)|^2$ ;  $\eta_2 \triangleq \sum_k |\bar{a}_m(n-2k)|^2$ . Note,  $\eta_1$  is the decimated AFB prototype filter norm; we also have  $\eta_2 = \frac{\eta_1}{2}$ , i.e.,  $\bar{a}_m(2k)$  is the two path polyphase partition of  $\bar{a}_m(k)$ . We then find the optimum  $k_m^{\text{opt}}$  as

$$k_m^{\text{opt}} = \frac{\gamma_m \hat{\beta}_m}{|\hat{\beta}_m|^2 + \frac{\sigma_n^2 \eta_1}{\sigma_s^2 \eta_2 |\gamma_m|^2}} \quad (4.12)$$

Examine Eq. 4.12, the term  $\gamma_m$  is the fixed SRRRC part; and the rest is the MMSE equalizer based on channel  $\hat{\beta}_m$ . The path-wise MMSE can be found by plugging Eq.4.12 into Eq. 4.11, we have

$$J_m(k_m^{\text{opt}}) = \frac{\sigma_n^2 |\gamma_m|^2 \eta_1}{|\hat{\beta}_m|^2 + \frac{\sigma_n^2 \eta_1}{\sigma_s^2 \eta_2 |\gamma_m|^2}} \quad (4.13)$$

And, one can use corresponding  $\hat{\beta}$  and  $\sigma_u^2$  to produce the equalizer coefficient for selection combining and MRC.

$$\begin{aligned}
J_m^{\text{SEL}}(k_m^{\text{opt}}) &= \frac{\sigma_n^2 |\gamma_m|^2 \eta_1}{|\beta_m^{\text{Max}}|^2 + \frac{\sigma_n^2 \eta_1}{\sigma_s^2 \eta_2 |\gamma_m|^2}} \\
J_m^{\text{MRC}}(k_m^{\text{opt}}) &= \frac{\sigma_n^2 |\gamma_m|^2 \eta_1}{\sum_l |\beta_{m,l}|^2 + \frac{\sigma_n^2 \eta_1}{\sigma_s^2 \eta_2 |\gamma_m|^2}}
\end{aligned}$$

Clearly,  $J_m^{SEL}(k_m^{opt}) \geq J_m^{MRC}(k_m^{opt})$ , since  $|\beta_m^{Max}|^2 \leq \sum_l |\beta_{m,l}|^2$ . And, the total MMSE is simply defined as:  $J_{min}^{SEL} \triangleq \sum_m J_m^{SEL}(k_m^{opt})$  and  $J_{min}^{MRC} \triangleq \sum_m J_m^{MRC}(k_m^{opt})$ .

$$J_{min}^{SEL} \triangleq \sum_m J_m^{SEL}(k_m^{opt}) \quad (4.14)$$

$$J_{min}^{MRC} \triangleq \sum_m J_m^{MRC}(k_m^{opt})$$

## 4.4 Simulation Results

Detailed simulation on MMSE based on single channel realization will be conducted to verify the derived results and BER result averaged over statistical channel model will also be provided.

### 4.4.1 MMSE Study over Single Channel Realization

A 240-path;  $D = 80$ ; 8 taps per polyphase arm low pass prototype filter; PR-NMDFB is constructed to perform diversity combining and linear equalization. The input signal is SRRC shaped QPSK sampled at 2 samples per symbol with 25 % roll off factor. The channel on the 1<sup>st</sup> branch, denoted as "1<sup>st</sup> Chan" has impulse response  $0.8638 + j0.4319z^{-6} + j0.2591z^{-12} + j0.008638z^{-18}$ ; the channel on the 2<sup>nd</sup> branch, denoted as "2<sup>nd</sup> Chan" has impulse response  $0.8352 - 0.5429z^{-11} - j0.0835z^{-22} + j0.0251z^{-33}$ . Fig. 4.3 shows the magnitude response of the two channels along with the combined channel via MRC and selection criteria based on Eq.4.8.

Fig.4.4 shows the theoretically achievable MMSE (i.e.,  $J_{min}^{SEL}$  and  $J_{min}^{MRC}$  obtained from Eq. 4.14) denoted as "SEL Opt" and "MRC OPT"; and simulated MMSE for selection, MRC, 1<sup>st</sup> Chan and 2<sup>nd</sup> Chan. Clearly the 2-branch diversity techniques outperform non diversity receivers by 4dB to 5 dB. In the realistic Eb/N0 range, i.e., from 0 dB to 30 dB, we found the MMSE of selection diversity is only 1.25 dB worse than MRC. The result shows the FB based selection technique is more than acceptable given the fact it does not require any channel knowledge.

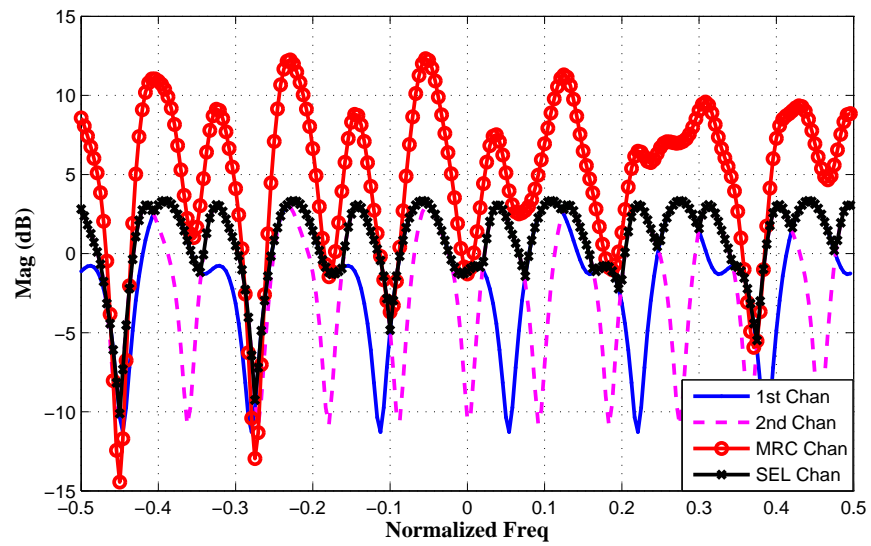


**Figure 4.3:** Magnitude response 1<sup>st</sup> Chan, 2<sup>nd</sup> Chan and Combined Channels

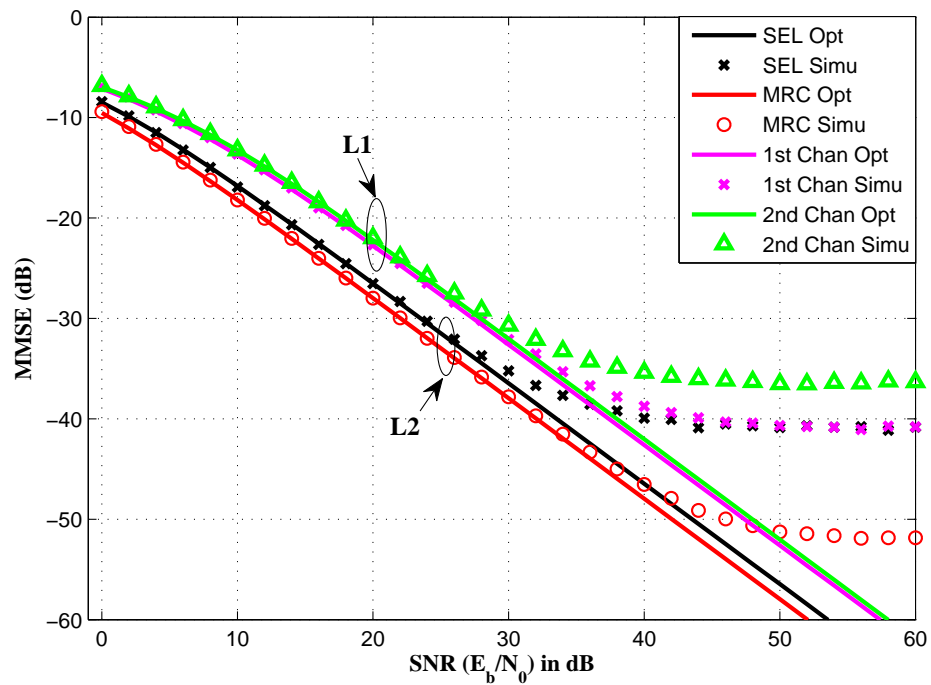


**Figure 4.4:** MMSE after Linear Equalization for 1<sup>st</sup> Chan, 2<sup>nd</sup> Chan and Combined Channels

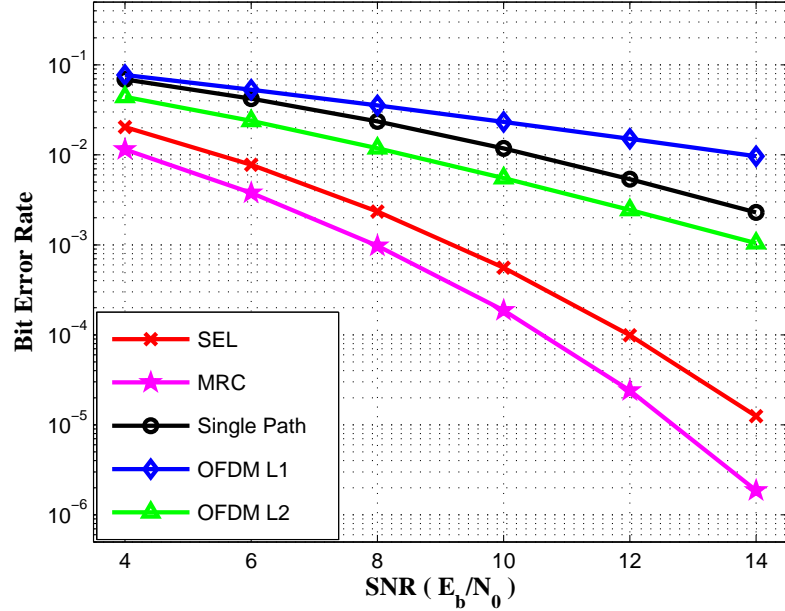


**Figure 4.5:** BER over ITU-B Channel with 50 MHz Symbol Rate

#### 4.4.2 BER Results over Statistical Channel Model

Consider QPSK signal with 50 MHz symbol rate communicating over ITU-R M.1225 indoor office channel B [77]. The ITU channel B has RMS delay spread of 100 ns, meaning the normalized delay spread is  $\tau_{rms}/T = 5$ . Fig.4.5 shows the BER performance averaged over  $10^3$  channel realizations. And, we can see the MRC has approximately 1 dB  $E_b/N_0$  advantage over FB selection approach. And, the diversity technique out performs single branch receiver by more than 4 dB. We also included the flat fading QPSK BER for 1 and 2 branches for comparison, which equals to conventional OFDM BER [79]. We can see the SC has lower BER than conventional OFDM.

#### 4.4.3 Implementation Complexity

The FB based diversity receiver has  $L$  PACs and 1 PSC. It has  $L$  IPEs associated with each PAC performing the combining; and 1 IPE perform equalization and SRRC filtering. The  $M = 240$ ,  $D = 80$ , PR-NMDFB has low pass prototype filters of 1920 taps, or 8 taps per polyphase arm, which supports 90 dB dynamic range. For every 80

complex inputs, all PAC, PSC operate once  $L + 1$  polyphase filters and 240-pt FFT) and uses  $\frac{L+1}{80} [1920 \times 2 + 1100 + 240 \times 4] = (L + 1) 73.75$  real multiplies, where the 240-pt complex FFT costs 1100 real multiplies [Table 2-6, [48]]. Setting  $L = 2$ , the count is 222, corresponding to an FIR filter with 111 taps processing complex data; yet we have done both diversity combining and channel equalization. The legacy FIR approach, however, requires more filters and certainly more computation to achieve the same task.

## 4.5 Acknowledgment

Chapter 4, in full, contains material that appears in the following article, accepted for publication:

- fred harris, Xiaofei Chen, Elettra Venosa, Bhaskar Rao, "Filter Bank Selection Diversity and Linear Equalization Over Frequency Selective Channels for Sinagle Carrier Transmission", International Conference on Acoustics, Speech, and Signal Processing (ICASSP) 2014 IEEE.

## **Chapter 5**

# **Non-Maximally Decimated Filter Bank Based Single Carrier Receiver: A Pathway to Next Generation Wideband Communication**

## 5.1 Introduction

The wireless technology has experienced significant growth in the past decades; and we have seen generations of wireless communication systems increased their bandwidth and data rates by more than an order of magnitude per generation. Current systems offer 100 Mbit/s data rates in 20 MHz bandwidth links. We can expect future generation wireless systems to offer 1 Gbit/s data rates with 500 MHz bandwidth links. As the demands for high data rate communication grows, the conventional methods, i.e., shaped QAM, become seemingly incapable of dealing with highly dispersive channels in a cost-effective manner. The legacy receivers often require building several overlapped FIR filters to parallelly perform synchronization, matched filtering as well as channel equalization. As the signal bandwidth grows comparable to the hardware's clock rate, any FIR filtering becomes extremely expensive. Meanwhile, the frequency selective channel requires very sophisticated equalizers, which adds more difficulties to fit the legacy QAM waveform into today's communication systems. To overcome this problem, many broadband techniques [10] such as spread spectrum and multicarrier transmission were introduced. Although the OFDM technique [14] suffers from problems like high peak to average power ratio (PAPR), sensitive to carrier frequency offset [6] and time and frequency guard span, it still becomes dominate because of its simple equalizer structure for highly frequency selective channels. An unappreciated advantage of OFDM is its fast Fourier transform (FFT) based block processing nature [14], which not only takes advantage of FFT's efficiency but also slows down the hardware processing speed, i.e., serial/parallel conversion at the transmitter (Tx) and receiver (Rx).

The modern research towards wideband communication systems can be generally categorized as: 1). Block based transmission with cyclic prefix (CP) occupied guard interval. This includes the conventional OFDM systems, discrete Fourier transform (DFT) precoded OFDM single carrier modulation [6, 7, 50, 4, 51]. 2). Non-block based, continuous streaming signal format, without CP or guard interval. This includes filter bank (FB) based solutions such as filter bank multicarrier / offset QAM (FBMC / OQAM) [57, 84, 85]; and filter bank single carrier (FBSC) transmission [86, 61, 62, 63]. The FBSC transmission is not well studied compared to FBMC, but is believed to have significant influence in future high through transmissions such as backhaul modems. In

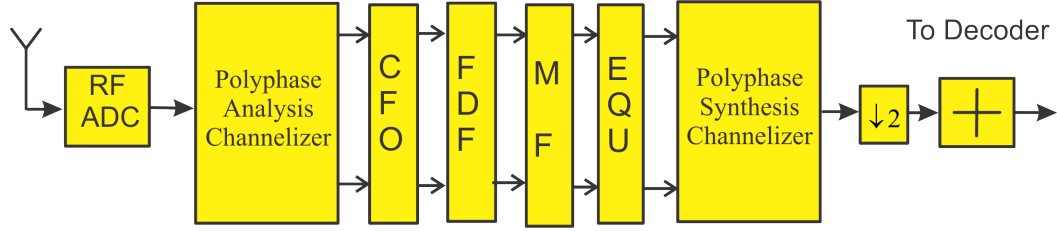


**Figure 5.1:** High Level Architecture of FBMC Receiver

this chapter, we shall focus on developing a unified receiver structure for FBSC transmissions. Fig. 5.1 shows a Perfect Reconstruction - Non-maximally Decimated Filter Bank (PR-NMDFB) based FBSC receiver embeds the carrier frequency offset (CFO) removal; fractional delay filter (FDF) for finding the correct symbol timing; matched filter (MF); and equalization process in between the polyphase analysis channelizer (PAC) and polyphase synthesis channelizer (PSC). Those signal processing tasks were previously implemented in the time domain; and we will show they can also be implemented in the FB transformed domain as independent intermediate processing elements (IPEs). Since the signals presented at PAC outputs are highly decimated, the IPE processing demonstrates impressive workload reduction compared to the conventional time domain methods.

Several authors have studied the FBSC from equalization perspectives and have shown the equalization task is closely related to subband adaptive filtering (SAF) [60]. Authors in [61] show the preliminary examples on FB based channel identification. Author in [86] demonstrated the design of fractionally spaced equalizer (FSE) via NMDFBs (oversampled FBs). We address the design of FBSC from the synchronization perspective. In particular, we will introduce the recently proposed [64] PR-NMDFB based digital filtering concept which allows us to carry out much more rigorous performance analysis towards FBSC compared to the past works [86, 61, 62, 63]. We will present the NMDFB based carrier frequency recovery; symbol timing recovery; and matched filtering (MF) process. These independent tasks were not discussed in the past works on FBSC. The novelty of our approach is: 1) present the PR-NMDFB filtering based formulation for FBSC; 2) Propose the synchronization techniques for FBSC in the FB transformed domain. To our best knowledge, these topics were not presented before or

studied in depth.

The organization of this chapter is: Sec. II presents the carrier frequency recovery technique; Sec. III solves the symbol time recovery problem; Sec. IV performs the complexity analysis; Sec. V presents simulation results; and Sec VI draws the conclusion. And, we shall continue using the PR-NMDFB notations established in Chapter 3 and 4.

## 5.2 PR-NMDFB Based Carrier Frequency Recovery

The conventional maximum likelihood carrier recovery approaches [17, 87, 88], as shown in Fig. 5.2, requires implementing a pair of bandedge (BE) filters that operate in parallel with the square-root raised cosine (SRRC) filter. The two BE filters are centered on received signal's left and right transition bands. The carrier recovery is achieved by balancing the signal energy observed at the output of two BE filters. The offset correction process is achieved via a digital phase locked loop (PLL) and a direct digital synthesizer (DDS). As derived in [87], the optimal BE or frequency matched filter has frequency response equal to the frequency derivative of the SRRC MF, shown in Fig. 5.3a. Due to the difficulty of designing optimal BEs' sharp transition band, sub-optimal BE filter is often used, as shown in Fig. 5.3b, which makes BE filters have the same length as the SRRC MF filter. As the signal's bandwidth grows, not only the power consumption of these three filters grows, but it also adds difficulty to lay out high speed circuits running at speed of many times the input rate.

Let us examine a baseband equivalent system for a QAM signal with complex notation for the in-phase ( $I$ ) and quadrature ( $Q$ ) branches, e.g.,  $\text{Re}(\cdot)$  and  $\text{Im}(\cdot)$  respectively. Denoting the  $k^{\text{th}}$  complex QAM data symbol as  $S_k$ , with symbol period  $T$  seconds. Let the transmitter's SRRC shaping pulse be  $h_{tx}(t)$  and additive noise  $n(t) = n_I(t) + n_Q(t)$ . Thus the received and digitized signal with sampling speed  $T_s = \frac{1}{f_s} = \frac{T}{2}$ , i.e., 2 samples-per-symbol is written as:

$$r(n) = e^{j(\omega_c n + \psi)} \sum_{k=-\infty}^{\infty} S_k h_{tx}(n - 2k - \tau) + n(n) \quad (5.1)$$

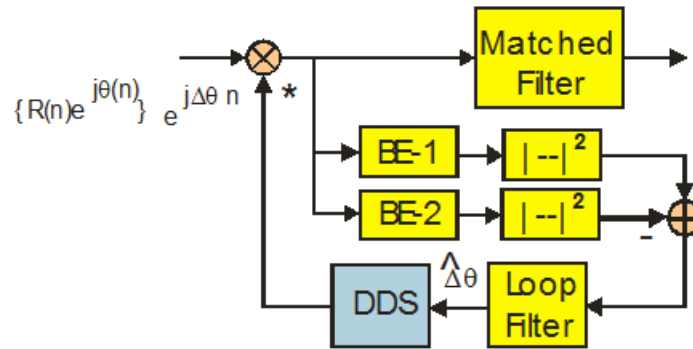
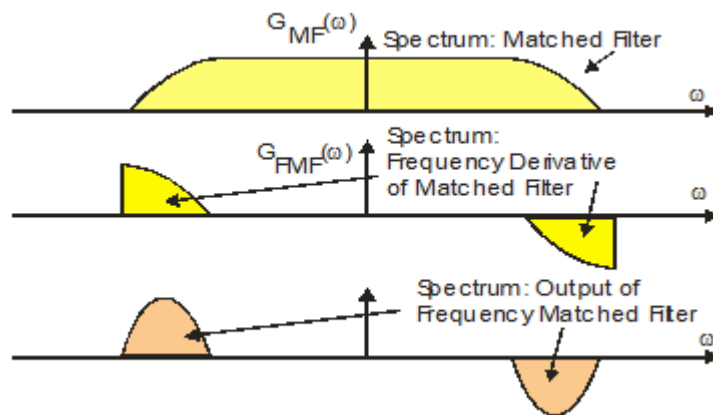
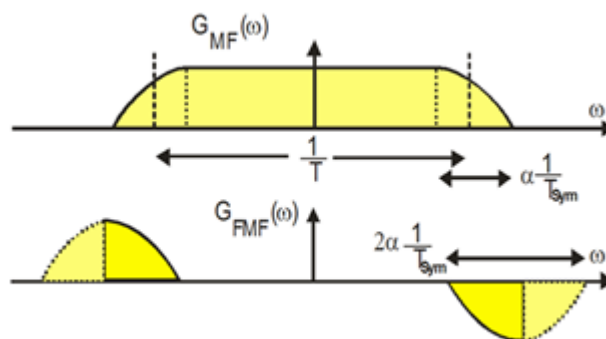


**Figure 5.2:** Band Edge Filter Frequency Locked Loop



(a)



(b)

**Figure 5.3:** (a).Spectra of SRRC MF, Corresponding Frequency MF, and Spectral Response of their Cascade; (b).Suboptimal BE Filters

where  $e^{j(\omega_c n + \psi)}$  is the residue CFO and phase offset after down conversion; and  $\tau$  is the imperfect sampler phase. Note, we do not consider the multipath channel effects in this chapter; the equalization for FBSC is treated in Chapter 3.

Fig. 5.4 shows the proposed CFO recovery scheme via an  $M$ -path decimation by  $D$  PR-NMDFB structure. The CFO and constellation phase offset removal is achieved via dedicated IPEs embedded in between the receiver's PAC and PSC along with other filtering tasks such as matched filtering and equalization. The IPE based CFO correction converts the high speed time domain DDS into a collection of low speed DDSs working in the channelizer transformed domain. The BE filters can surely be implemented via the NMDFB filtering property along with the receiver's MF and equalizer. Moreover, since the BE filters [87] were oversampled (see Fig. 5.3b) and only the BE output signal energy is needed, they can be synthesized onto reduced sample rate via PSC with much less paths as depicted in Fig. 5.4. The constellation phase offset removal is a decision directed process and happens after the CFO correction. It uses the same IPE as used in the CFO loop; and it is relatively simple to design. In this chapter, we only focus on developing the BE filtering and CFO correction process; we will derive the operating conditions of IPE based CFO correction and we will show the design of PR-NMDFB based BE filters.

### 5.2.1 CFO Correction in FB Transformed Domain

To compensate the CFO, the signals presented at the output of PAC shall be de-rotated by  $e^{-j\omega_c n D}$ . Let us only consider the CFO correction IPE and ignore other IPEs for now, i.e. setting  $\mathbb{K} = I$ . The Z-transform of the output signal  $z(n)$  after frequency shift IPE is written as:

$$\begin{aligned} Z(z) &= \frac{1}{D} \mathbf{G}_{1 \times M}^T(z) \mathbb{K}_{M \times M} \mathbb{A}_{M \times D}(ze^{j\omega_c}) \mathbf{R}_{D \times 1}(ze^{j\omega_c}) \\ &= \frac{1}{D} T_S^{\mathbb{K}}(z) R(ze^{j\omega_c}) + \frac{1}{D} \mathbf{T}_A^{\mathbb{K}}(z) \bar{\mathbf{R}}(ze^{j\omega_c}) \end{aligned} \quad (5.2)$$

where  $\mathbb{A}_{M \times D}(z)$  is the analysis filter bank (AFB) matrix:

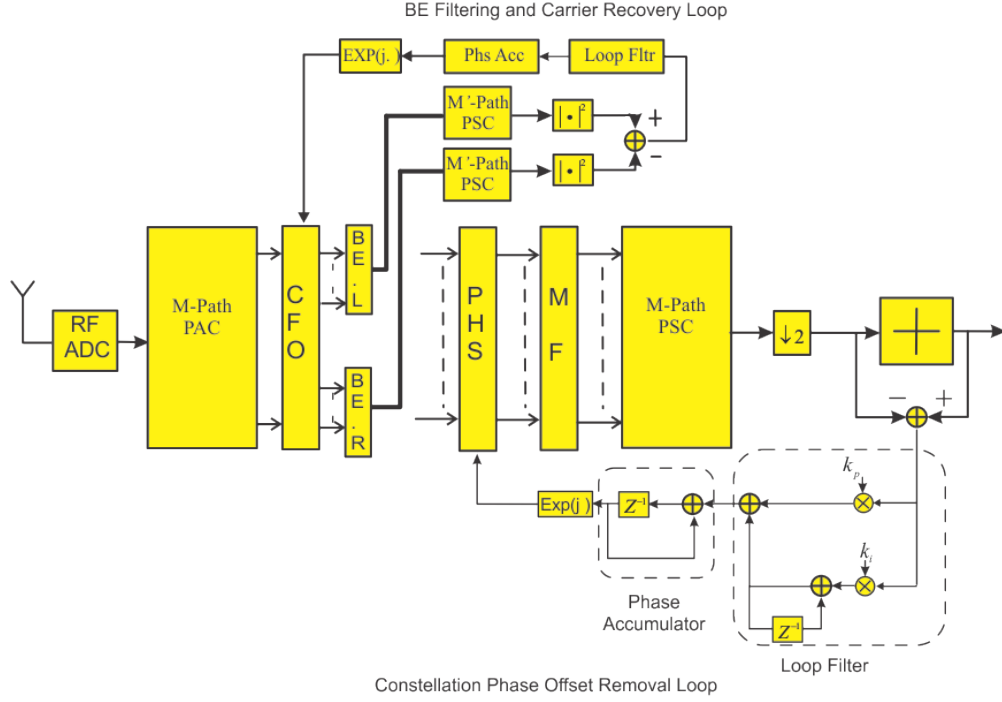


**Figure 5.4:** FB Transformed Domain CFO Recovery

$$\mathbb{A} = \begin{pmatrix} A(zW_M^0 W_D^0) & \cdots & A(zW_M^0 W_D^{D-1}) \\ \vdots & \ddots & \vdots \\ A(zW_M^{M-1} W_D^0) & \cdots & A(zW_M^{M-1} W_D^{D-1}) \end{pmatrix}_{M \times D} = [A_{M \times 1} \bar{A}_{M \times (D-1)}]_{M \times D}$$

$\mathbf{G}_{1 \times M}(z)$  is synthesis filter bank (SFB) vector:  $\mathbf{G}(z) = [G(zW_M^0) \dots G(zW_M^{M-1})]^T$ , and  $\mathbf{R}(z) = [R(zW_D^0), R(zW_D^1), \dots, R(zW_D^{D-1})]^T = [R(zW_D^0) \bar{\mathbf{R}}(z)]^T$  is the modulated versions of the input signal;  $T_S^{\mathbb{K}}(z) \triangleq \mathbf{G}_{1 \times M}^T(z) \mathbb{K}_{M \times M} \mathbf{A}_{M \times 1}(ze^{j\omega_c})$  is the signal transfer function;  $\mathbf{T}_A^{\mathbb{K}}(z) \triangleq \mathbf{G}_{1 \times M}^T(z) \mathbb{K}_{M \times M} \bar{\mathbf{A}}_{M \times (D-1)}(ze^{j\omega_c})$  is the aliasing transfer function.

The aliasing cancellation condition is satisfied if  $\mathbf{T}_A^{\mathbb{K}}(z) = 0$ , which can be translated to:  $A(zW_D^d e^{j\omega_c}) G(z) = 0, \forall d = 1, \dots, D-1$ . It should be noted that the aliasing cancellation comes from the NMDFB prototype filter design and is unaffected by scalar diagonal matrix  $\mathbb{K}$ . The frequency translated PR condition is satisfied if  $T_S^{\mathbb{K}}(z) = \sum_{m=0}^{M-1} A(zW_M^m e^{j\omega_c}) G(zW_M^m) = z^{-nD}$ . This condition is met if the composite response  $A(ze^{j\omega_c}) G(z)$  produces Nyquist pulse  $H^{NYQ}(z)$ , or its frequency shifted version  $H^{NYQ}$

$(ze^{j\omega_c})$ . We can design either  $A(z)$  or  $G(z)$  to be a Nyquist pulse and let the other filter be a low pass filter that passes the Nyquist pulse unaltered. Eq. 5.3, 5.4 shows shows the impact of the two options; and we can see both choices produce the frequency shifted version of the input signal when  $\mathbb{K} = I$  as along as the PR, and aliasing cancellation conditions are met.

$$A(ze^{j\omega_c})G(z) = H^{NYQ}(ze^{j\omega_c}) \Rightarrow T_s^{\mathbb{K}}(z) = \sum_{m=0}^{M-1} K_m H^{NYQ}(zW_M^m e^{j\omega_c}) \quad (5.3)$$

$$A(ze^{j\omega_c})G(z) = H^{NYQ}(z) \Rightarrow T_s^{\mathbb{K}}(z) = \sum_{m=0}^{M-1} K_m H^{NYQ}(zW_M^m) \quad (5.4)$$

Fig. 5.5 depicts the example of the analysis and synthesis low pass prototype filter (LPPF) for an  $M$ -path, decimation by  $D = \frac{M}{3}$ , PR-NMDFB that matches Eq. 5.4. The analysis LPPF is assigned to be a low pass filter while the synthesis LPPF is chosen to be a triangular shaped Nyquist pulse. For  $D = \frac{M}{3}$ , the PAC outputs have sample rate  $\frac{3 \times f_s}{M}$ , or range from  $-\frac{3\pi}{M}$  to  $\frac{3\pi}{M}$  given  $f_s = 2\pi$ . Seen from Fig.5.5, one can frequency shift the analysis LPPF without raising aliasing energy inside the "Aliasing Free Shift Region". However, the aliasing error will occur if we shift into the "Aliasing Penalty Shift Region", i.e., CFO  $\omega_c$  approaches  $\frac{\pi}{M}$ . Clearly this aliasing error is due to the transition band of the analysis LPPF as depicted in Fig.5.5. Note that, a maximum frequency shift by  $\frac{\pi}{M}$  is all we need to achieve full range center frequency change, i.e.,  $\omega_c \in \left[-\frac{f_s}{2}, \frac{f_s}{2}\right]$  in PR-NMDFB based FBMC receiver. This is because one can cyclic shift the PAC outputs to account for CFO greater than half of the NMDFB channel spacing, recall the path / channel spacing is  $\frac{2\pi}{M}$  in an  $M$ -path PR-NMDFB. Furthermore, it can be easily prove that the "Aliasing Penalty Shift Region" can be completely eliminated by having  $D = \frac{M}{4}$ , yet reducing the decimation rate for this option also raises the system's workload.

## 5.2.2 CFO Detection in FB Transformed Domain

The CFO detection is based on a pair of BE filters centered on left and right of the received signal's transition bands. And they can be efficiently integrated in the NMDFB structure via spectral shaping IPEs. As shown in [87], the target spectrum of

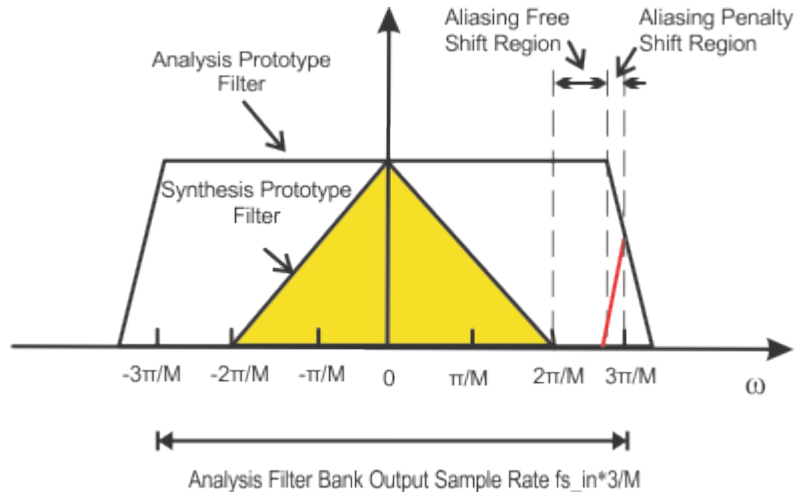


**Figure 5.5:** Analysis and Synthesis Low Pass Prototype Filter (LPPF)

the two BE filters is the frequency derivative of the SRRC shaping filter's left and right transition bands. To synthesize an NMDFB based BE filter, one simply sets the target spectrum  $S(\omega)$  to be the ideal BE filter spectrum with IPE gain  $K_m = S(\omega_m)$ . Unlike the conventional time domain implementation (Fig. 5.3b) in which suboptimal, symmetrically extended BE filters have to be built to avoid designing sharp filter transition bands, the PR-NMDFB based filter allows us to directly synthesize the ideal BE filter spectrum and produce near optimal frequency response as shown in Fig. 5.3a. And, we will further demonstrate this in the simulation section.

Serving as the error detector within a PLL, the input signal to the BE filter must already be frequency shifted or error compensated as shown in Fig.5.2. Re-examine Eq. 5.3, 5.4 and consider a non-trivial IPE, i.e.,  $\mathbb{K} \neq I$ , Eq. 5.3 corresponds to filter the input data and then deliver the heterodyned output; whereas Eq. 5.4 maps to first heterodyne the input signal and then apply the filtering. Clearly, the arrangement in Eq. 5.4 matches the requirement of a loop control system. Therefore, the NMDFB implementation requires the analysis LPPF to be a low pass filter; and synthesis LPPF to be any Nyquist pulse, i.e., Fig. 5.5. Another detail which is worth noting is that the conventional BE design produces an oversampled filter, see Fig. 5.3. The oversampling ratio is related to the SRRC filter's transition bandwidth or the roll-off factor. Mapping to the NMDFB implementation, this means only a certain group of entries of BE filter's

IPE matrix  $\mathbb{K}_{M \times M}$  is non-zero. Equivalent of saying, only a portion of FB channels are needed to synthesize a BE filter. Therefore, an  $M'$ -path, reduced size PSC is used to only synthesize the FB channels that fall into the signal's left or right transition bands. This saves computational resources and increases the efficiency of the proposed architecture.

### 5.3 PR-NMDFB Based Symbol Timing Recovery

The goal of a symbol timing synchronizer is to sample the MF output at optimum instant for the  $k^{\text{th}}$  symbol. The conventional analog solution controls a sample-and-hold circuit located at the output of the analog MF to identify the optimum sampling instant. It is also well know that [89, 90] the log-likelihood function for unknown timing phase  $\tau$  for equally likely  $S_k \in \{+1, -1\}$  is:

$$\Lambda(\tau) = \sum_k \ln \left[ \cosh \left( \frac{2E}{N_0} \right) y(kT + \tau) \right]$$

where  $E$  is the symbol energy;  $N_0$  is power spectral density W/Hz of zero-mean Gaussian noise; and  $y(kT + \tau)$  is the analog MF output. The estimated timing offset  $\hat{\tau}$  that maximizes  $\Lambda(\tau)$  is the timing phase that forces the derivative of  $\Lambda(\tau)$  to zero.

$$\sum_k \tanh \left( \frac{2E}{N_0} y(kT + \tau) \right) \frac{d}{dt} y(kT + \tau) = 0$$

Often, the  $\tanh(\cdot)$  function is replaced by its small signal approximation  $\tanh(x) \approx x$  for low signal to noise ratio (SNR) and  $\tanh(x) \approx \text{sign}(x)$  for high SNR. Authors in [89] proposed full digital timing recovery techniques based on polyphase FB and have shown various timing error detection (TED) methods via FBs. In this chapter, we adopt the TED formed by taking the product between the MF output and the derivative MF output, i.e., Fig. 10 of [89]. The derivative MF is produced by taking derivative to the time domain SRRC impulse response; this should not be confused with BE filter which is formed by taking frequency domain derivative to SRRC spectra.

The time domain TED [89], requires building one FIR SRRC MF and one time domain derivative SRRC MF. The product of the two filters forms the TED which then drives a PLL. The PLL then tunes the FDF to find the best symbol timing. The NMDFB implementation of the TED together with the FDF is shown in Fig. 5.6, where the IPEs

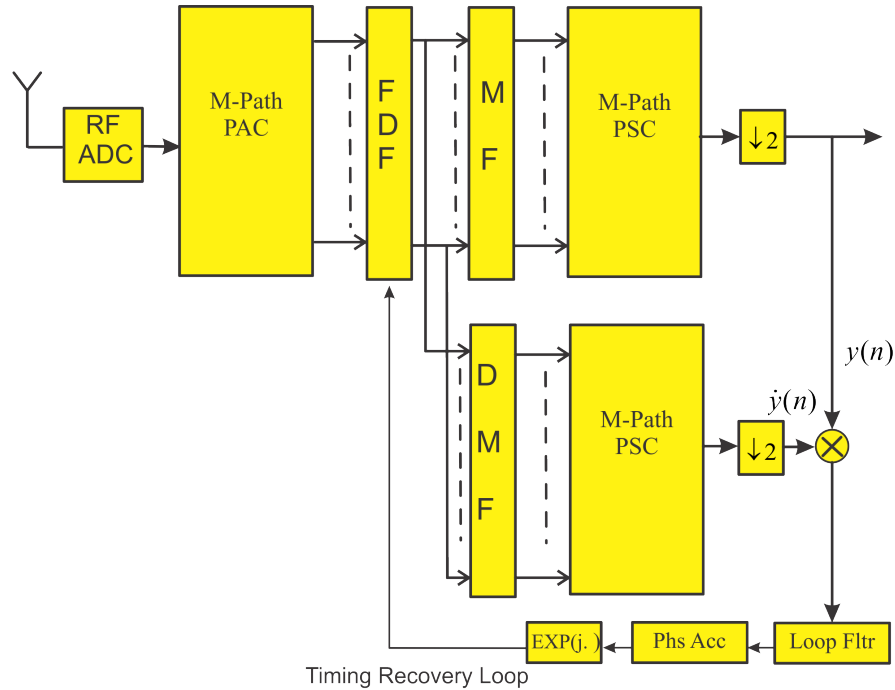


**Figure 5.6:** FB Transformed Domain Symbol Timing Recovery

are used to synthesize the FDF, MF and the derivative MF. Their target spectrums can be readily obtained from the previously developed NMDFB filtering property in Chapter. 2. Seen from Fig. 5.6, one PAC, two PSCs are used to produce the time domain MF, derivative MF as well as the FDF. We shall show detailed workload analysis in the next section.

## 5.4 Full NMDFB based FBMC Receiver and Complexity Analysis

The complete block diagram of the FBMC receiver is shown in Fig. 9. We can see the entire signal processing is embedded between in the PAC and PSC transformed domain; and all filtering tasks are implemented based on the NMDFB filtering property via dedicated IPEs. In this section, we would like to analyze the workload for the FBMC receiver and compare it to its time domain antecedent counterpart.

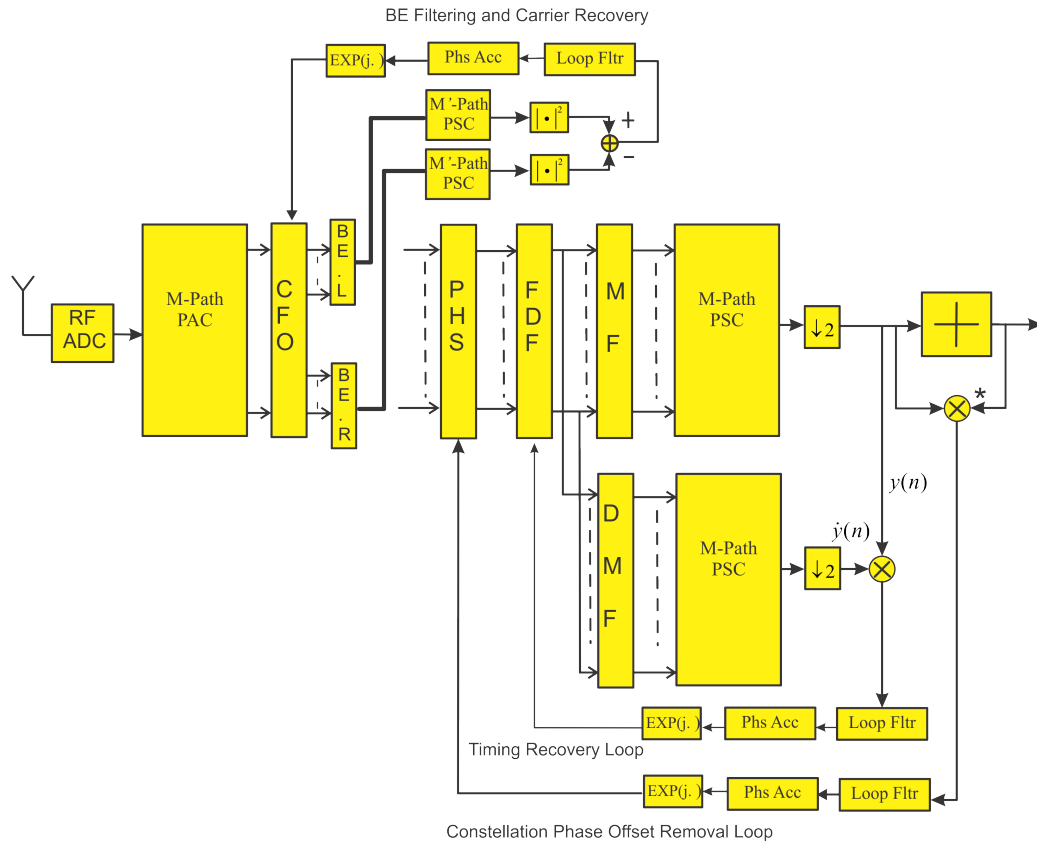


**Figure 5.7:** Proposed FBSC Receiver Block Diagram

Examining Fig.5.7, the FBSC receiver contains one  $M$ -path PAC; two  $M$ -path PSC; two reduced size  $M'$ -path PSC; five  $M$ -entry IPEs; and two reduced size  $M'$ -entry IPEs. Let all LPPFs have  $L$  taps (real coefficient) per polyphase arm, i.e., the LPPF length for  $M$ -path PAC (or  $M$ -path PSC) is  $M \times L$ ; the LPPF length for  $M'$ -path PSC is  $M' \times L$ . Take the  $M$ -path, decimation by  $D$ , PAC for example: a block of  $D$  pieces of data enter the PAC, and its LPPF operates once, and so does its  $M$ -point FFT. Therefore, the workload in terms of number of multiplies per input complex (I-Q pair) sample, for an  $M$ -path, decimation by  $D$ , PAC is calculated as:  $\frac{1}{D} [2ML + \langle M \text{ Pnt FFT} \rangle]$ , where  $\langle M \text{ Pnt FFT} \rangle$  denotes the number of multiplies required for an  $M$ -point FFT processing complex inputs. In addition, the workload for an  $M$ -entry complex coefficient IPE is:  $\frac{4M}{D}$ .

For an  $M$ -path, decimation by  $D$  arrangement, every block of  $D$  pieces of data coming in, all the PACs, PSCs and IPEs operate once. Therefore, the total workload count in terms of number of multiplies per input complex sample is:

$$(\text{ops})_{\text{input}} = \frac{1}{D} [6ML + 4M'L + 20M + 8M' + 3\langle M \text{ Pnt FFT} \rangle + 2\langle M' \text{ Pnt FFT} \rangle] \quad (5.5)$$

Eq. 5.5 is the total workload count for the proposed FBSC receiver. It should be noted that, it also includes the fractional spaced equalizer, which is essentially another IPE that can be combined with the MF IPE (See Chapter 3). The conventional time domain implementation requires building at least four FIR filters: SRRC MF, two BE filters (for carrier recovery), and one derivative MF (for timing recovery) [89]. These four filters often have the same length (Suboptimal BE filter designed as Fig. 5.3b) with the SRRC filter. Therefore, the workload count for time domain implementation is:

$$(\text{ops})_{\text{input}} = 8N \quad (5.6)$$

where  $N$  is the length of the SRRC filter. We now assign practical parameters to Eq. 5.5, 5.6 to make further comparison. A 65-tap, i.e.,  $N=64$ , SRRC filter with 25% roll off factor is used for time domain implementation. Therefore, based on Eq.5.6 the conventional FIR approach costs 520 real multiplies per complex input. In the FBSC

solution, we use  $M = 240$ ,  $M' = 42$  and  $D = \frac{M}{3} = 80$ , triangular shaped PR-NMDFB with LPPF length  $L = 8$ . And our observation shows it can well equalize multipath channels with normalized R.M.S delay spread  $\frac{\tau_{rms}}{T} = 5$ . The 240-point and 42-point complex FFT cost 1100 and 152 real multiplies respectively [48]. Plugging in those parameters into Eq. 5.5, we find the workload count for FBSC receiver is 270 real multiples per complex input. Those numbers show the PR-NMDFB based FBSC solution offers 48% workload reduction only for the synchronization part. And this workload reduction did not account for the linear equalization which is required in the conventional FIR approach; notice that, on the other hand, the equalization task has already been included in Eq. 5.5. Furthermore, as will be shown in the simulation section, the 65-tap SRRC only gives 43 dB stop band performance; however the PR-NMDFB offers 100 dB dynamic range, an improvement by 56 dB.

## 5.5 Simulation Results

This section presents the simulation results of the proposed FBSC receiver. We shall first examine the PR-NMDFB implemented filters and compare them with the FIR based designs. Then we will demonstrate the behaviors of the proposed CFO recovery loop and symbol timing recovery loop.

### 5.5.1 PR-NMDFB Implemented Filters

The frequency response of a SRRC filter with 25% roll off synthesized via a 240-path, decimation by 80 PR-NMDFB is shown in Chapter 2.6.4. We have seen the proposed solution produces over 50 dB more stop-band performance; and with much smaller in-band ripple. We next show the frequency response of the synthesized BE filters. Fig. 5.8 shows the FIR based time domain implementation of the suboptimal 65-tap BE filters (upper subplot) and the PR-NMDFB based BE filters (lower subplot). Comparing the two, we find the PR-NMDFB implements extremely sharp filter transitions and achieve near optimal BE filter design [87]. Note that the smallest transition band of a triangular shaped PR-NMDFB is  $\frac{\pi}{M}$ , half of the NMDFB channel spacing. Clearly, the proposed approach offers close to optimal design of BE filters.

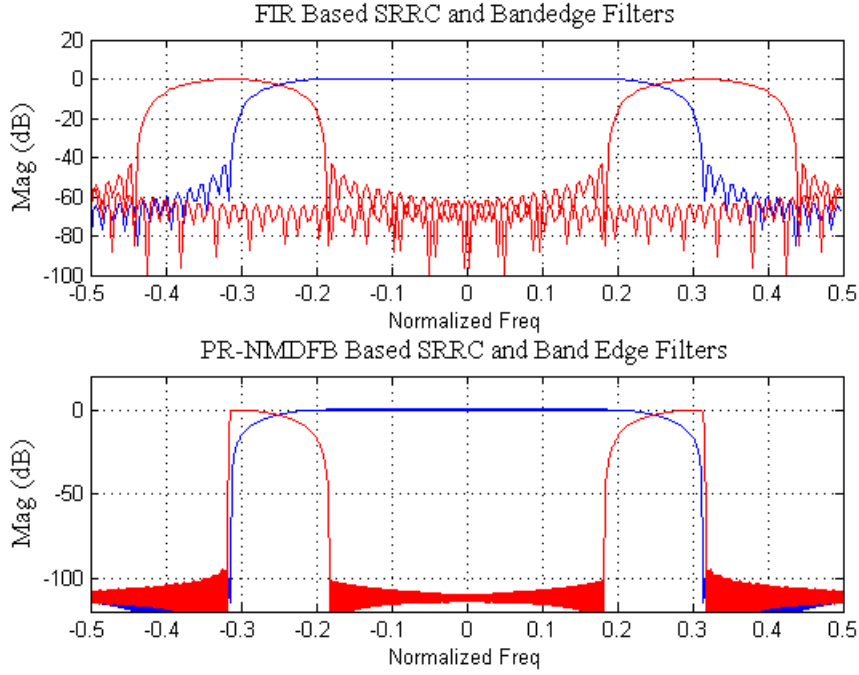


**Figure 5.8:** Time and Channelizer Domain MF, and BE Filters

Fig.5.9 shows the result for delaying the impulse response by 0, 0.5, and -0.5 samples via 240-path PR-NMDFB. The left column figures show the impulse responses, while the right column figures show the magnitude responses. Note that, we have subtracted the parasitic delay  $n_D$  caused by PAC / PSC from the impulse responses. Thus we see the impulse response for delaying by 0 sample sits on index 0. And, the impulses for delaying by  $\pm 0.5$  samples become sampled Nyquist pulses. The magnitude responses for delaying by  $\pm 0.5$  samples are seen to have very slightly larger in-band distortions comparing to delaying by 0 sample. This is due to the use of IPE to approximate the complex sinusoid of the phase shifters. Clearly, the worst case distortion happens when delaying by  $\pm 0.5$ , since all one need is fractional delay within one sample.

## 5.5.2 Carrier Frequency Offset (CFO) Recovery Results

The CFO and constellation phase offset removal is simulated based on QPSK signal with 25 dB Eb/N0. The CFO is set to  $\omega_c = 0.2 \frac{2\pi}{M}$ , or 20% of the NMDFB channel

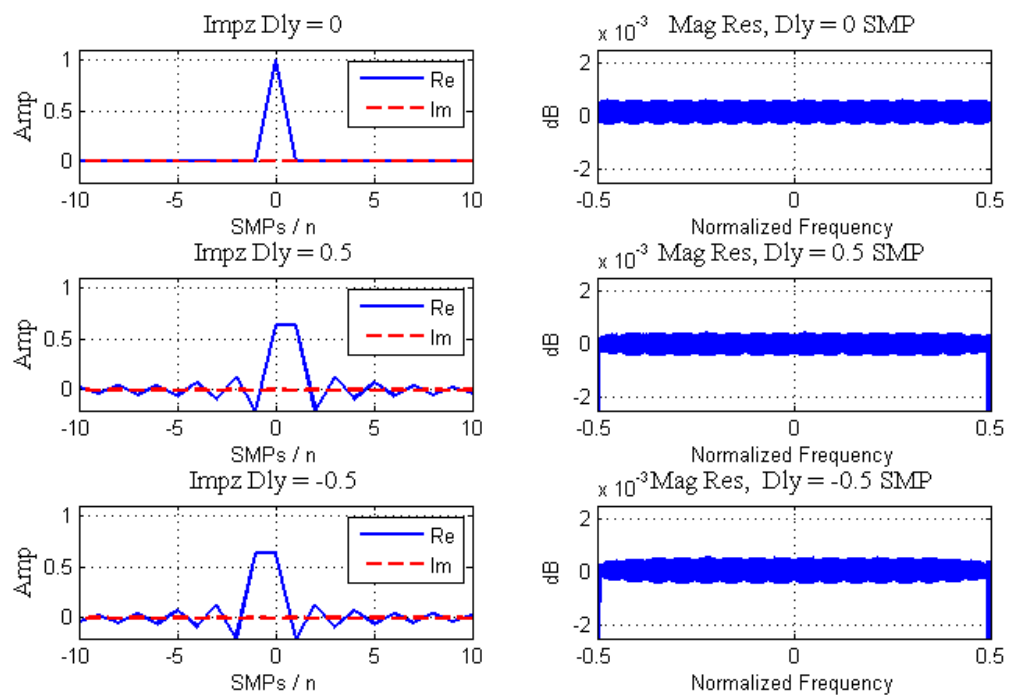


**Figure 5.9:**  $M = 240$ ,  $D = 80$ , PR-NMDFB Implemented FDF

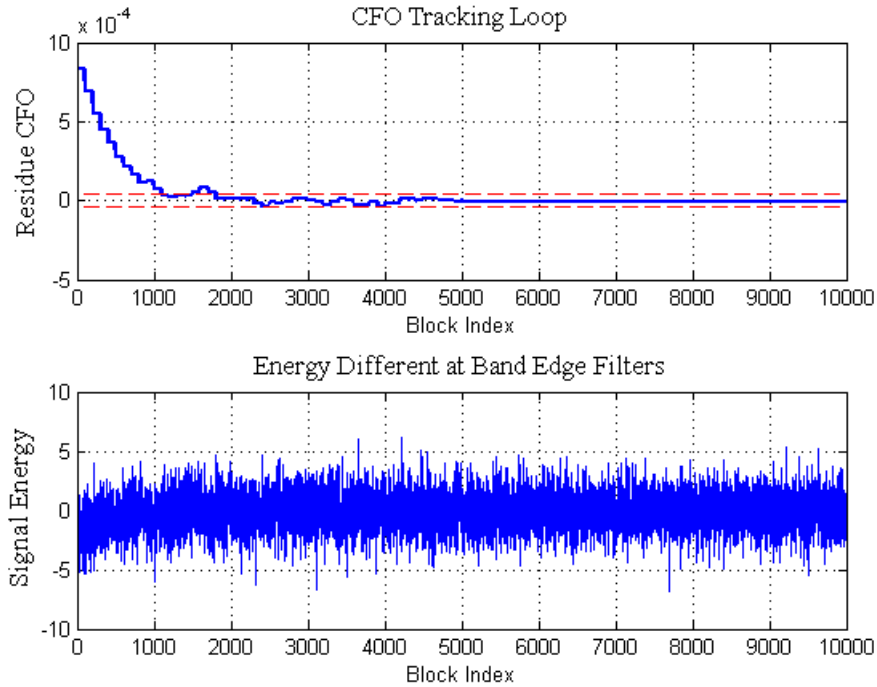


**Figure 5.10:** CFO Tracking Loop Profile

spacing. Fig. 5.10 shows the CFO tracking loop dynamics. The horizontal axis is plotted in terms of block index, recall the NMDFB receiver takes in data samples in block of  $D$ , and in this example  $D = 80$ . We can see the PLL pulls the CFO to a very small value by balancing the signal energy from the two BE filters. Upon the convergence of the CFO loop, the constellation phase offset correction loop, Fig. 5.11, began to work, which tracks the small residue CFO based on decision directed criterion. The signal constellations taken before and after the convergence of the phase offset correction loop are shown in Fig. 5.12.

### 5.5.3 Symbol Timing Recovery Results

The symbol timing recovery is simulated under the same setup as the carrier recovery. The initial timing offset  $\tau$  is set to be  $0.5T_s$ . Fig. 5.13 shows the phase accumulator profile of the timing recovery PLL; and we can see the steady state is reached in about 100 blocks, or 8000 samples. The lower subplot of Fig. 5.13 shows the input

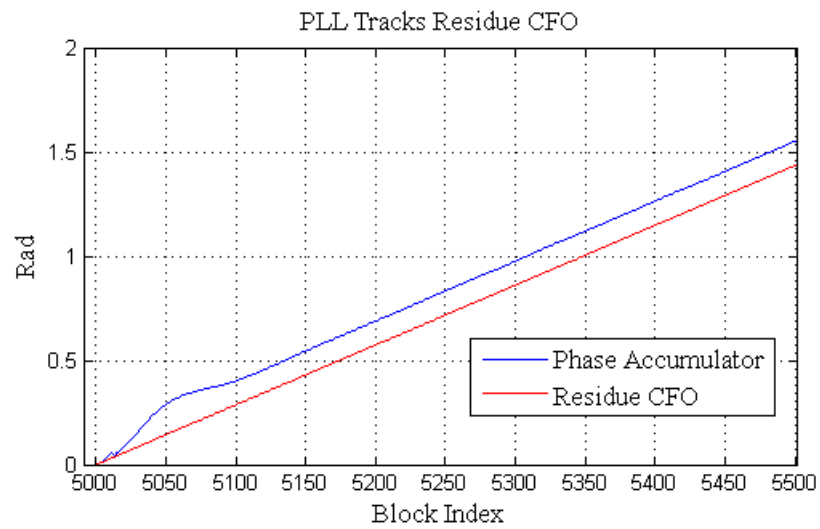


**Figure 5.11:** Constellation Phase Offset Removal Tracking Loop Profile

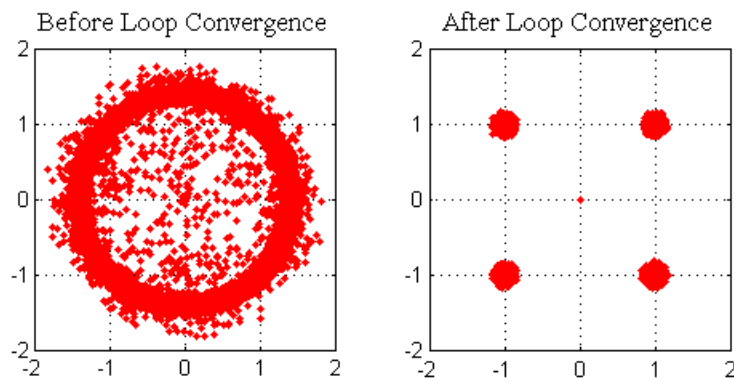


**Figure 5.12:** Constellation Before and After the Convergence of the Constellation Phase Offset Removal Loop

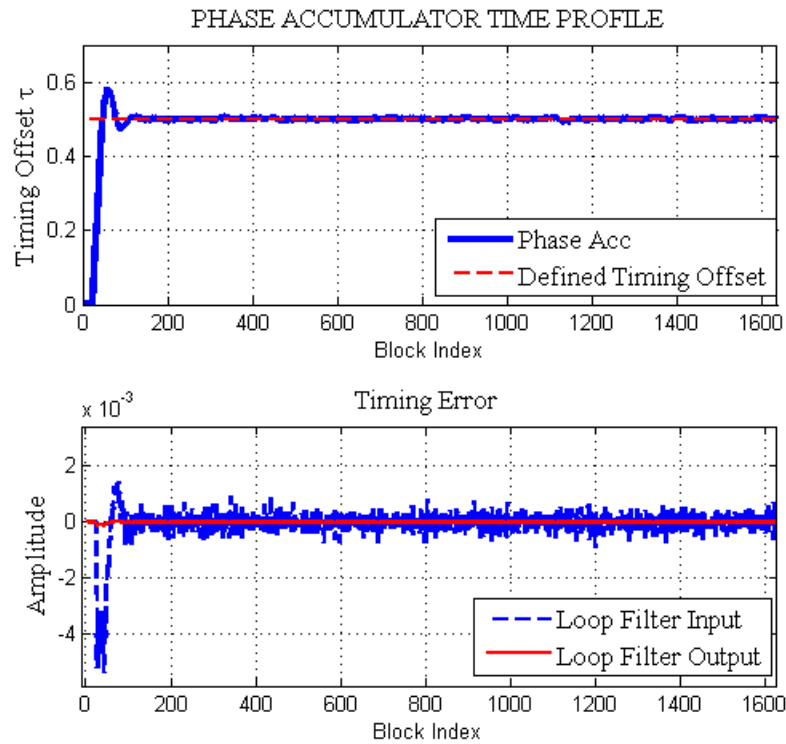


**Figure 5.13:** Symbol Timing Recovery Loop Profile

and output signals at the loop filter and we see the timing error is driven to zero by the PLL. Fig. 5.14 shows the QPSK constellation before / after the convergence of timing loop, which further confirms the functionality of the proposed approach.

## 5.6 Acknowledgment

Chapter 5, in full, contains material that appears in the following articles (both accepted and published):

- Xiaofei Chen, fred harris, Elettra Venosa and Bhaskar Rao, "Non-Maximally Decimated Filter Bank Based Single Carrier Receiver: A Pathway to Next Generation Wideband Communication", accepted by EURASIP Journal on Advances in Signal Processing.

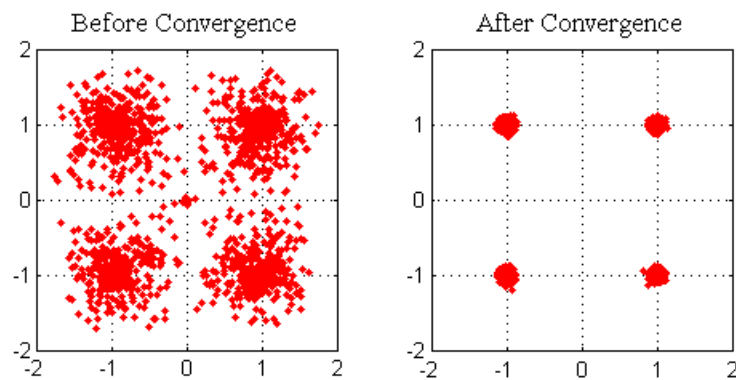


**Figure 5.14:** Constellation Before and After the Convergence of the Symbol Timing Recovery Loop

- fred harris, Xiaofei Chen, Elettra Venosa, "A carrier recovery architecture for next generation wideband modems," Global Conference on Signal and Information Processing (GlobalSIP), 2013 IEEE, vol., no., pp.1262,1265, 3-5 Dec. 2013
- fred harris, Elettra Venosa, Xiaofei Chen, Chris Dick, "Band edge filters perform non data-aided carrier and timing synchronization of software defined radio QAM receivers," Wireless Personal Multimedia Communications (WPMC), 2012 15th International Symposium on , vol., no., pp.271,275, 24 - 27 Sept. 2012

## **Chapter 6**

# **Multi-Channel Channelization Technique**

## 6.1 Introduction

In order to solve the spectrum scarcity problem and improve the spectrum usage efficiency, the modern communication requires future radios to be "smart" and re-configurable. For instance, a cognitive radio (CR) receiver should be able to detect the unused spectrum or "white space" and communicate with those unused spectrum fragments. On the other hand, a CR receiver should be able to simultaneously receive multiple signals having arbitrary bandwidths and randomly located center frequencies as illustrated in Fig. 6.1. This requirement impose great challenges to the current state of art, whereby most of the digital receivers today are dedicated to a single frequency band.

Today's digital receiver has to perform the first tier tasks of filtering, spectral translation and analog-to-digital conversion to reverse the first tier processing tasks performed at the transmitter [91]. The receiver must also perform a number of second tier tasks not present in the transmitter. These tasks are needed for estimating unknown parameters of the received signal such as amplitude, frequency and timing alignment. Fig. 6.2 shows the block diagram of the first and second tier processing in a typical digital receiver. It samples the output of the analog intermediate frequency (IF) filter and down converts the IF centered signal to base-band with a digital down converter (DDC). The base-band signal is then down sampled by a decimating filter and finally processed in the matched filter to maximize the signal-to-noise ratio (SNR) of the samples presented to the detector. The digital signal processing (DSP) portion of this receiver includes carrier alignment, timing recovery, channel equalization, automatic gain control, SNR estimation, signal detection and interference suppression blocks. Because the receiver contains analog hardware components, it also incorporates a number of third tier DSP blocks to suppress the undesired artifacts formed by the imperfect analog blocks. The digital data section of the receiver shown in Fig. 6.2 is matched to the bandwidth and center frequency of the signal that has to be demodulated. For simultaneously down converting multiple signals with different bandwidths, centered on different center frequencies, it is necessary to replicate the sampled data section of the receiver. The more signals we want to simultaneously down convert, the more sampled data sections we need to implement. This is surely not a suitable option for a modern CR or Software

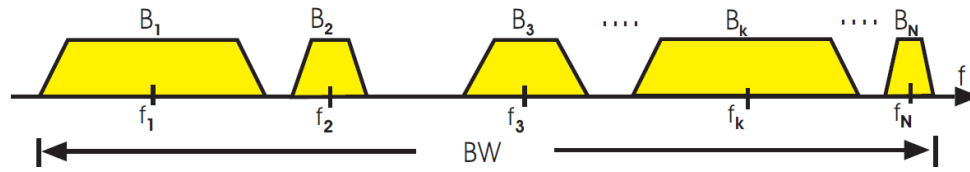


**Figure 6.1:** Possible Received Signal Spectrum

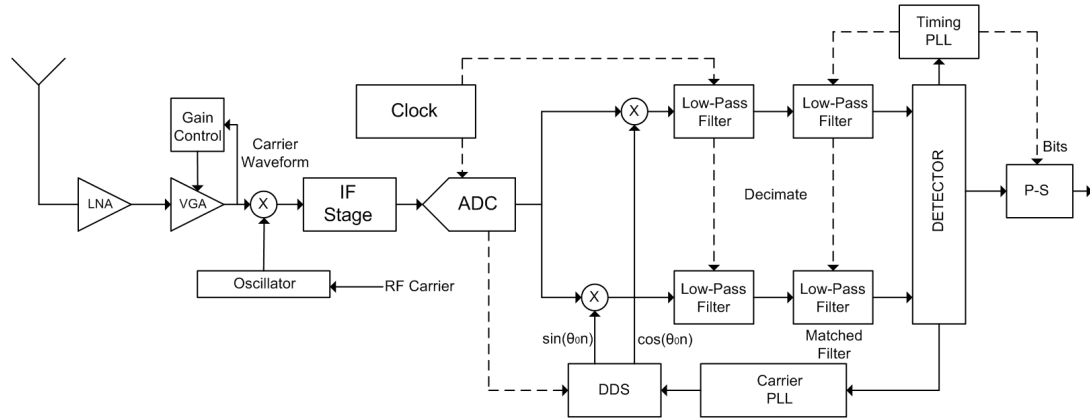


**Figure 6.2:** Block Diagram of Primary Signal Processing in a Typical Digital Receiver

Defined Radio (SDR) receiver that should guarantee maximum flexibility while minimizing both workload and power consumption [92], [93], [94], [95], [96], [97], [98], [99], [100], [12], [101].

The conventional channelization solution is designed for  $M$  equally spaced channels; and this problem is efficiently solved via multirate Transmultiplexer, or  $M$ -Path critically sampled polyphase channelizer [17], whose block diagram is shown in Fig. 6.3. The conventional Transmultiplexer delivers  $M$  outputs, with output sampling frequency as well as channel spacing equal to  $\frac{f_s}{M}$ , where  $f_s$  is the signal sampling frequency at the input to the transmultiplexer. Although the critically sampled Transmultiplexer exhibits advantages in complexity, it suffers from some critical limitations. First of all, the received signals must be equally spaced; then their bandwidth must be smaller than  $\frac{f_s}{M}$ . These limiting conditions pose huge flexibility restrictions to the receiver; and can hardly be applied in future's sophisticated communication environments.

In this chapter, we present a novel channelizer architecture [102], [103], [104],

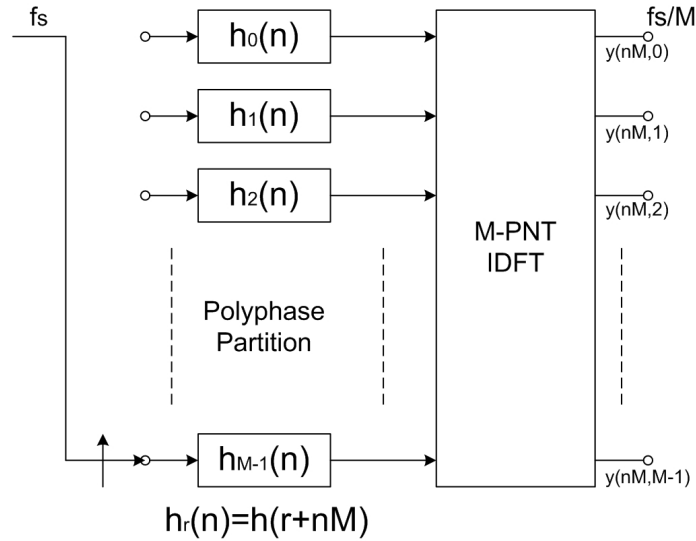


**Figure 6.3:** Block Diagram of the Standard M-path Polyphase Channelizer; M-Port Input Commutator, M-Path Partitioned Filter and M-Point IDFT

[105], [106], [107] that enables CR to simultaneously receive multiple signals with arbitrary bandwidths and center frequencies. Following the analog-to-digital converter, it simultaneously down converts multiple signals with arbitrary bandwidth and randomly located center frequencies avoiding the need of replicating the receiver's digital data section. The sampling frequency of the ADC has to be selected according to the Nyquist low-pass sampling criteria for the highest frequency involved. The core of the proposed digital channelizer is polyphase analysis channelizer (PAC) and polyphase synthesis channelizer (PSC) introduced in Chapter 2. When operating under  $D = \frac{M}{2}$  mode, where  $D$  is PAC decimation factor and  $M$  is the number of channels in the PAC; the PAC is able to deliver  $M$  output spectral fragments whose original input center frequencies are  $k \frac{f_s}{M}$  for the  $k = 0, 1, \dots, M - 1$ , where  $f_s$  is the input signal's sampling rate. Since  $D = \frac{M}{2}$ , the PAC outputs are twice oversampled w.r.t the PAC's channel spacing, i.e., the sampling frequency for each spectral fragments is  $\frac{2f_s}{M}$ . A post PAC, connected with a channel configuration block, when necessary, filters the output ports of the analysis channelizer for extracting, from the base-band shifted channels, the spectra, or their fragments, belonging to different signals. Upon sufficient spectral decomposition, a finite collection of PSCs that are smaller dual versions of the PAC, recombine the spectral fragments

belonging to signals with bandwidth wider than the PAC channel bandwidth. Complex heterodynes are used for correcting the residual frequency offsets due to the completely arbitrary center frequency positioning of the received signals. Arbitrary interpolators are used, at the end of the proposed chain, for providing the two samples-per-symbol needed for the further processing stages.

The rest of the chapter is organized as follows: in Section 2, we present the complete block diagram of the proposed receiver. In Section 3, the spectral decomposition process based on the modified M/2-to-1 PAC is introduced. In this same section we also give the PR prototype filter specifications; Nyquist filters are required as low-pass prototype to avoid energy losses during the signal processing. In Section 4 we explain the motivations for introducing the post analysis block, along with the small synthesis channelizers. In Section 5 the arbitrary interpolator design issues are discussed. In Section 6, we show the simulation results that demonstrate the effectiveness of the complete down converter chain. Conclusions and suggestions for future developments are derived in Section 7.

## **6.2 Channelization via Polyphase Analysis Channelizer (PAC) and Polyphase Synthesis Channelizer(PSC) Processing**

As discussed earlier, a critically decimated Transmultiplexer imposes two restrictions for the received signals: 1) signals must be equally spaced 2) signal bandwidth must be smaller than  $\frac{f_s}{M}$ . Note that, the Transmultiplexer by itself is a critically decimated PAC which delivers  $M$ -spectral slices. If one can perfectly re-assemble all or any portion of these  $M$ -spectral fragments via PSC, then these two restrictions vanish. However, perfectly re-assembling the spectral fragments at the output of the PAC requires non-trivial modifications to the legacy Transmultiplexer. The reason is illustrated in Fig. 6.4. The subplot 1 of Fig. 6.4 demonstrates the input / output channel spectrum of a critically decimated PAC. The channel spacing is  $\frac{f_s}{M}$  and the output rate is also  $\frac{f_s}{M}$ . Since one can not build a perfect brick wall filter, certain aliasing (red portion) must occur. There-

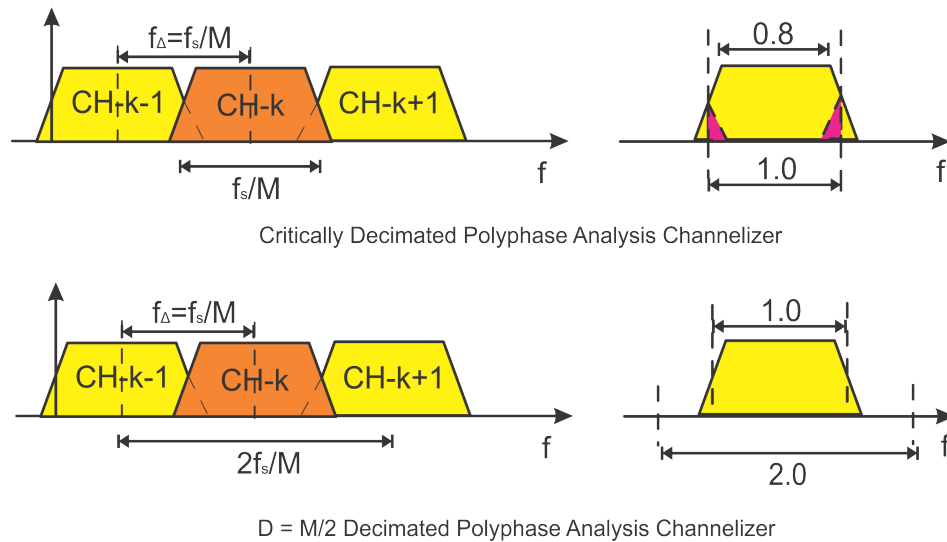


**Figure 6.4:** PAC Output Sample Rate Relative to Channel Spacing

fore, the critically decimated Transmultiplexer only supports signal bandwidth smaller than  $\frac{f_s}{M}$ ; plus, all channels must be equally spaced seating inside the aliasing free region. Two modifications are made to overcome the restrictions posed by the legacy Transmultiplexer: 1) use oversampled PAC, i.e.,  $D = \frac{M}{2}$  to avoid the aliasing. 2) use Nyquist pulse as the PAC's low pass prototype filter (LPPF) to allow perfect reconstruction (PR) of any spectral portions. This modified channelizer is illustrated in subplot 2 of Fig. 6.4. The Nyquist filter presents the interesting property that its band edge gain is 0.5 (or 6 dB) and the transition bandwidths are symmetric about the band edge. By using this PR filter as LPPF in the PAC, we place  $M$  of them across the whole spanned spectrum with each filter centered on  $k\frac{f_s}{M}$ . All adjacent filters exhibit 6 dB overlap at their band-edges. The channelizer working under this configuration is able to collect all the signal energy across its full operating spectrum range even if the signals occupy more than one adjacent channel and/or reside in the channel's overlapping transition bandwidths.

According to this analogy, the modified channelizer based on joint PAC and PSC processing is drawn in Fig. 6.5. The received spectrum containing multiple signals with arbitrary bandwidth and center frequencies is first fed into the  $D = \frac{M}{2}$  PAC. The PAC then decomposes the spectrum into  $M$ -slices. Since the PAC is oversampled and Nyquist LPPF is used, its outputs contain all the necessary information that we need to

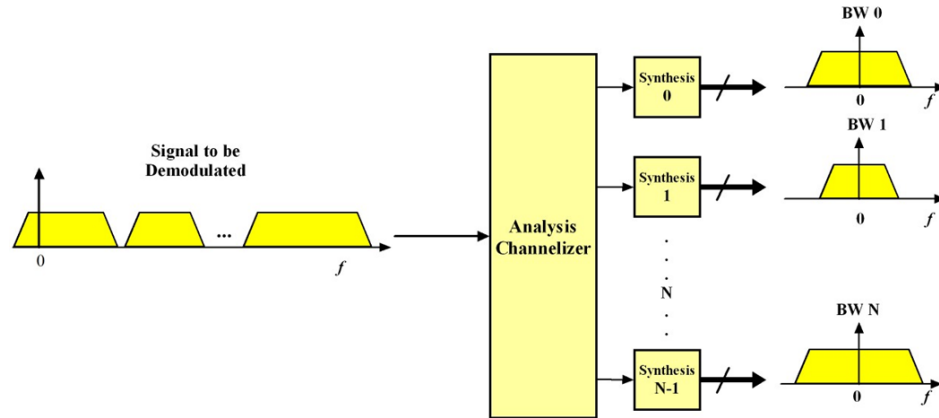


**Figure 6.5:** High Level Block Diagram of the Proposed Channelizer

reconstruct each signal within the span of the received spectrum. After PAC, a collection of reduced path PSCs are needed to reassemble the spectrum portions of interests, i.e., the portions that contain signal energy. Note that, the PSCs only need to reassemble the signals of interests, which may only cover, say 2 to 3 channels of the PAC outputs. Therefore, the number of PSC paths can be much smaller compared to the PAC.

### 6.3 Proposed Multi-Channel Channelizer Receiver

Figure. 6.6 shows the complete block diagram of the proposed receiver chain. The input signal is first processed by an  $M$ -path, decimate by  $D$  PAC. It simultaneously down converts all the channels to base-band presenting an output sampling rate equals to twice of the channel spacing, i.e.,  $\frac{2f_s}{2}$ . Note that, in practice, with limited PAC path size / resolution  $M$ , one could still encounter the situation that some of the PAC channels pick up two or more signals, or spectral content belong to different signals. If this happened, further processing is needed to separate signals at the output of the PAC. The post filtering process is performed in the post analysis block that is connected to a channel configuration block which provides the receiver with the necessary information about the input signal bandwidths and center frequencies. Different options can be implemented for simplifying the design of the post analysis block. One of the possible options is to decrease the bandwidth of the PR prototype low-pass filter, i.e.,

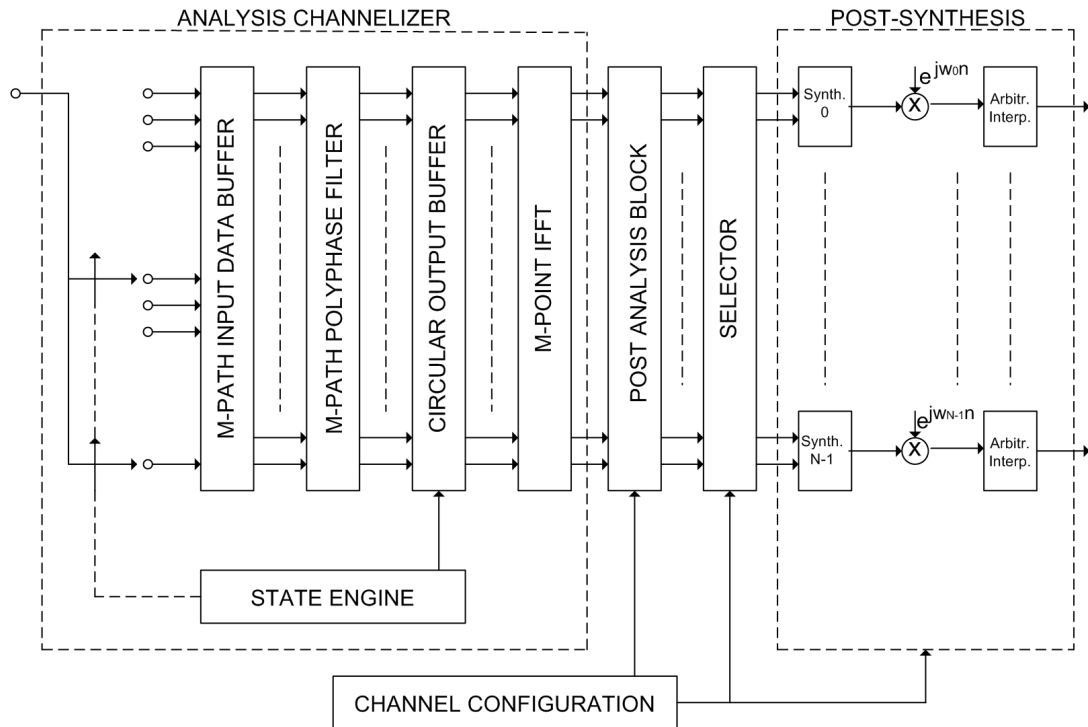


**Figure 6.6:** Block Diagram of the Proposed Receiver; PAC, Post Analysis Block, PSC, Complex Frequency Rotators and Arbitrary Interpolators

increasing resolution  $M$ . By designing the channel spacing and bandwidth to accommodate the most likely expected signal bandwidth, one can minimize the possibility of having more than one signal in each channel. It is also possible to modify the PAC for having a more convenient frequency positioning of the aliased channels. The optimal choice, of course, depends on the receiver application as well as the workload requirements. After post analysis block, most of the signals with bandwidths narrower than the channel bandwidth are already down converted by means of the channelization process. However the spectra wider than the channel bandwidth, or the spectra that, as a consequence of the arbitrary center frequency positioning, are processed by two or more adjacent PAC channels, have been fragmented and their segments have all been aliased to the first Nyquist zone; these segments need to be recomposed before being translated to DC. The recomposition of spectral fragments is the task performed by the PSC. They are small 2-to- $P_n$  PSC in which the IFFT size,  $P_n$ , is properly chosen in order to span the

bandwidth of the  $n^{\text{th}}$  received signal spectrum. We summarize the reason for including the reduced size PSCs as: at the output of the  $D = \frac{M}{2}$  PAC, all the signals have been down sampled and their spectra, or their spectral fragments, have been translated to the first Nyquist zone by the channelizing process. In order to reassemble the segments into a wider bandwidth super channel, the time series from each segment must be up sampled and frequency shifted to their appropriate positions so that they can be added together for forming the time series corresponding to the wider bandwidth assembled signal. These are the functions performed by the synthesizers following the PSC.

Upon finishing synthesizing all the signals of interests via PSC, the residue frequency offset compensation and sample rate conversion are needed to produce DC centered signal with proper sampling frequency.

### 6.3.1 Post Analysis Block and PSC

At the output of the first tier PAC, all the channels have been aliased to base-band. As a consequence, the channelized segments of the received spectrum have been aliased to the first Nyquist zone. The following three options that enclose all the possible cases of bandwidths positioning in the channelized spectrum, have to be considered and solved, by further processing the first tier PAC outputs.

1. The PAC output channel could contain only one signal spectrum whose bandwidth is narrower than the channel bandwidth. The carrier frequency of the signal, generally, does not coincide with the center frequency of the channel.
2. The PAC output channel could contain two or more spectra, or also their fragments, belonging to different signals. These spectra are arbitrary positioned in the channel bandwidth.
3. The PAC output channel could contain only one spectral fragment belonging to one of the received signals whose bandwidth is larger than the PAC channel spacing.

In the first option, at the output of the PAC, the signal that is entirely contained in one of the PAC output channels resides in the first Nyquist zone. Eventually the receiver has to compensate the frequency offsets derived from its arbitrary center frequency positioning and to resample it for obtaining the desired output sampling rate, i.e., two samples-per-symbol for QAM signal. The complex frequency rotators and the

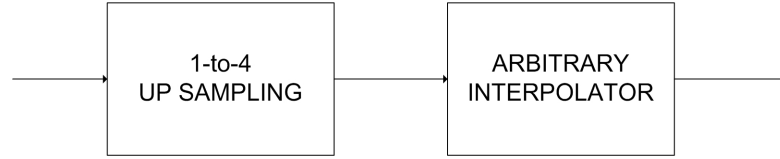


**Figure 6.7:** Two Stage Arbitrary Interpolator

arbitrary interpolators perform these tasks at the end of the receiver chain.

In the case two or more spectra are processed by one single PAC channel, more tasks need to be performed before frequency offset compensation and arbitrary interpolation. One needs to separate, by filtering, the bands, or their fragments, belonging to different signals before processing all of them independently. The separation task is performed by the post analysis block. It is essentially another channelization process that filters, from every base-band aliased channel, the bands belonging to different signals.

In the third case, that concerns the signals with bandwidths wider than the channel spacing, the first tier PAC partitions the signal into several fragments and aliases every fragments to base-band. In order to recombine them we must first, up sample each input time series and second, translate them onto their proper spectral region. We can then form the sum to obtain the super channel representation of the original signal bandwidth. Those are exactly the tasks performed by the PSC.

### 6.3.2 Arbitrary Interpolator

In this section we present the polyphase arbitrary interpolator structure used for delivering desired signal sample rate for the second and third tier processing tasks in a digital receiver. It is well known that the dynamic range of an arbitrary interpolator should match the system's quantization noise level [17]. The error due to the linear interpolation process is not observable if it is below the noise level attributed to the signal quantization process. Since the error due to the  $b$ -bit quantized signal is  $2^{-b}$ , the interpolation error or, equivalently, the residual spectral artifacts level has to be below this threshold. In other words, if the oversampling factor,  $N$ , satisfies

$$\left[ \frac{1}{2N} \right]^2 \leq \frac{1}{2^b}$$

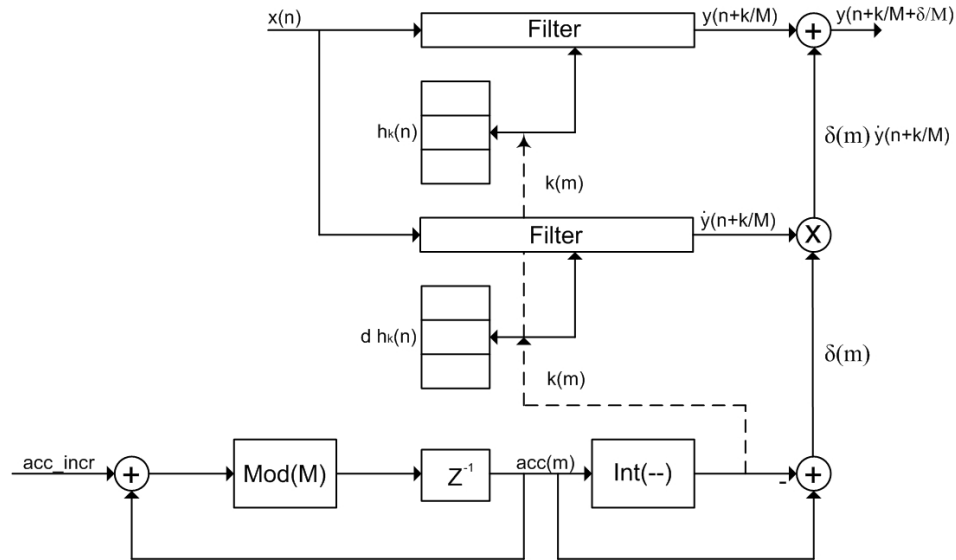


**Figure 6.8:** Polyphase Arbitrary Linear Interpolator

then the interpolation error will not be noticeable. Thus, for 16-bit data set, one needs to oversample by a factor of 128. To interpolate the signal by a factor  $N = 128$ , we break the up sampling process of the base-band centered spectra in two stages. As depicted in Fig. 6.7, we perform an initial 1-to-4 up sampling followed by 1-to-32 up sampling obtained by using the polyphase arbitrary linear interpolator shown in Fig. 6.8. The initial 4-times oversampling effectively reduces the length of the polyphase filters used in the polyphase arbitrary linear interpolation which significantly reduces the total workload of this structure. More details on this topic can be found in [17].

## 6.4 Simulation Results

Consider the received composite spectrum containing 12 non-equally spaced QAM signals with 5 different bandwidths. In particular, the signal constellations are 4-QAM, 16-QAM, 64-QAM and 256-QAM while the signal bandwidths are 1.572132 MHz, 3.892191 MHz, 5.056941 MHz, 5.360537 MHz and 11.11302 MHz respectively. Note we have used two different signal bandwidths for the 256-QAM constellation (5.360537 MHz and 11.11302 MHz). Each QAM signal is shaped by square-root raised cosine filter with 20% excess bandwidth. Fig. 6.9 shows the received spectrum with

input sampling frequency 192 MHz. In particular, the upper subplot of Fig. 6.9 shows, superimposed on the composite received spectrum, the 48 channels of the PAC. It is easy to recognize that the received spectra are arbitrarily located. Their center frequencies do not coincide with the channel center frequencies. The lower subplot of Fig.6.9 shows the enlarged view of one of the received signals. The arbitrary signal positioning is the reason for which the PAC by itself is not able to directly down convert signals to DC. The IFFT transform size of the PAC is  $M = 48$  with an output sample rate of 8 MHz.

Figure. 6.10 shows the impulse response and the magnitude response of the designed PAC LPPF Nyquist filter. It is designed to have 48 samples per symbol. Its length is 1200 taps while its stop band attenuation is  $-80$  dB. Note that, since this filter is  $M$ -path partitioned, the length of each filter arm in the  $M$ -path bank is only 25 taps.

The 48 spectra, at the output of the PAC, are depicted in Fig. 6.11. The PAC has partitioned the entire received spectrum into 48 segments. It is easy to recognize in this figure the different spectra composing the received signal. Note that, because of the arbitrary frequency positioning, it is possible that signals having bandwidths narrower than the channelizer's channel spacing occupy more than one PAC channel outputs.

Before delivering the PAC outputs to the synthesis channelizers, we need to separate, if necessary, by filtering, those spectra that belong to different signals lying in the same PAC output channel. An example of this is represented by channel 30 in Fig. 6.11. It contains fragments of two spectra belonging to different signals. The filter design in the post analysis block, of course, depends on the bands that have to be resolved. An example of post analysis filters along with the filtered signals, for the 30<sup>th</sup> PAC channel, is shown in Fig. 6.12. In particular, the signal spectra and the filters used for separating them are shown in the upper subplot while the separated spectra are shown in the lower subplots.

At the output of the post analysis block, signals with bandwidths narrower than the PAC channel spacing and lying in a single PAC channel, can be directly delivered to the complex heterodyne that translates them to DC. All other signals, the ones with bandwidths wider than the PAC channel spacing and the ones with bandwidths narrower than the PAC channel spacing but resides across two PAC channels, need to be processed by the reduced size PSCs. In the example of Fig. 6.9, four of the received spectra,

the narrowest ones, are directly sent to the frequency rotators to compensate frequency offsets. Eight of them are processed through the PSCs. The IFFT sizes  $P_n$ , with  $n = 0, 1, 2$  of the synthesizers we selected to process the three remaining bandwidths are:  $P_0 = 6$ ,  $P_1 = 4$  and  $P_2 = 2$  points. These sizes are the minimum possible chosen to satisfy Nyquist sampling criterion for each output signal. Note that because of the structure of the PSC, we can only have an even number of IFFT points. At the output of the PSC, all the signal fragments are recombined in base-band but may have a residual frequency offset that needs to be compensated. The signal spectra, before frequency offset compensation are shown in Fig. 6.13. It is clearly visible that some of the signals are not centered at DC (the red line in Fig. 6.13 represents the signals' center frequency). We compensate these frequency offsets by using complex frequency rotators.

When all signals are properly channelized and DC centered, the arbitrary interpolator shall resample all signals to the desired output rate for the rest of the signal processing task. In this example, we resample each signal to 2 samples-per-symbol. The interpolated, DC shifted signals are shown in Fig. 6.14. We also match-filtered each of the twelve channelized and reconstructed QAM signals and present their constellations in Fig. 6.15, here we see that all of the QAM constellations are perfectly reconstructed which demonstrates the correct functionality of the proposed receiver.

## 6.5 Acknowledgment

Chapter 6, in full, contains material that appeared in the following three published articles:

- fred harris, Elettra Venosa, Xiaofei Chen "Multirate Signal Processing for Software Radio Architectures", Academic Press Library in Signal Processing: Volume 1: Signal Processing Theory and Machine Learning
- fred harris, Elettra Venosa, Xiaofei Chen, and Bhaskar Rao, "Polyphase analysis filter bank down-converts unequal channel bandwidths with arbitrary center frequencies," Analog Integrated Circuit and Signal Processing, vol. 71, no. 3, pp. 481 - 494, 2012.

- fred harris, Chris Dick, Elettra Venosa and Xiaofei Chen, "M-Path Channelizer with Arbitrary Center Frequency Assignments", Wireless Personal Multimedia Communications (WPMC), 2010 13th International Symposium on.

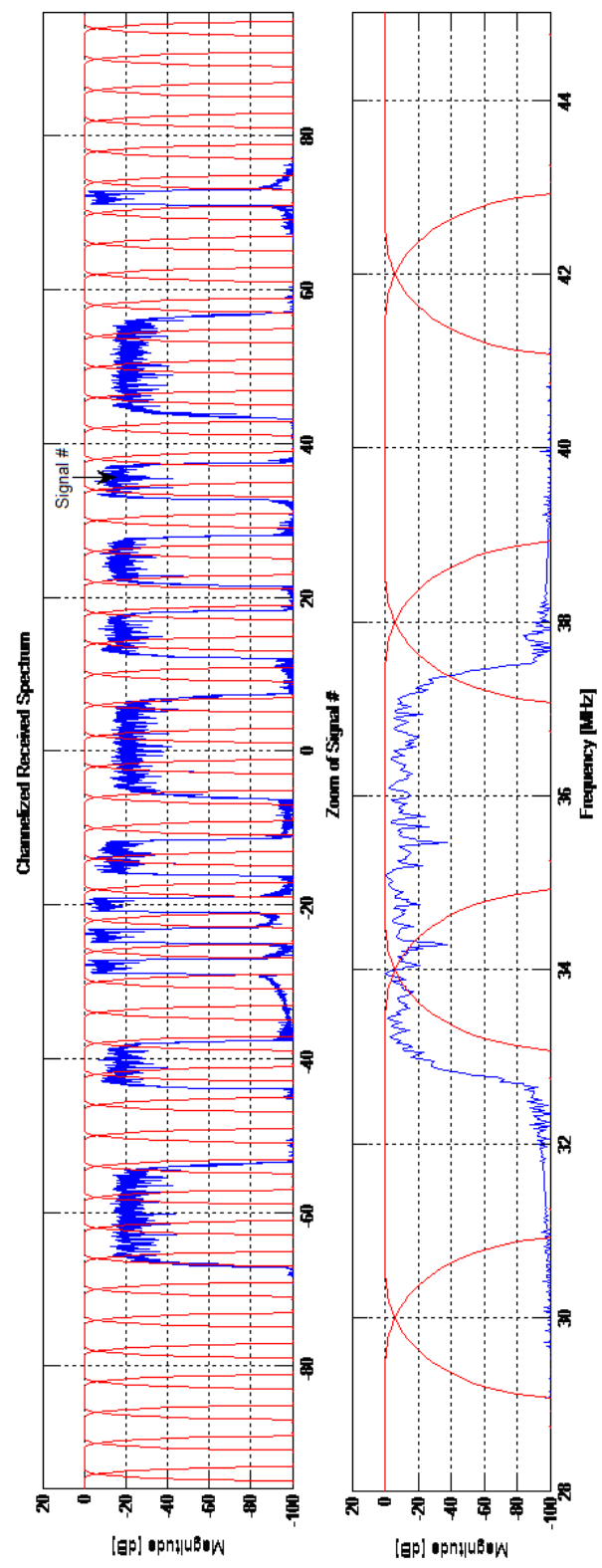
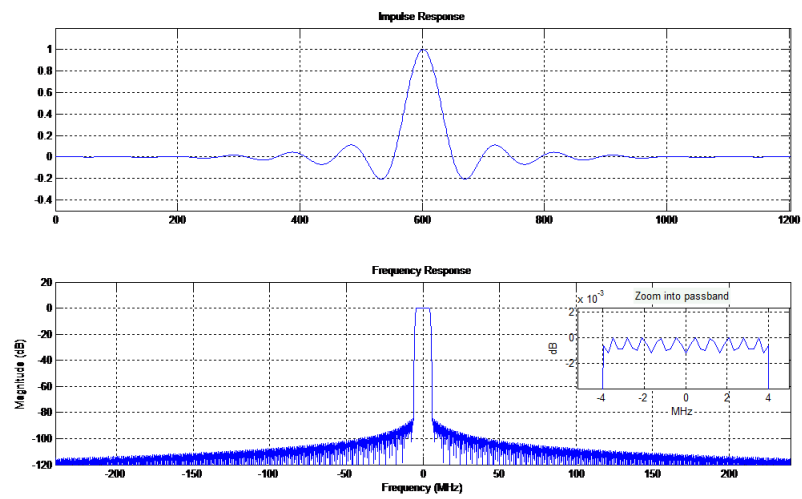


Figure 6.9: Channelized Received Spectrum and Zoom of One of the Received Signals



**Figure 6.10:** PAC Low Pass Prototype Filter: Nyquist Pulse

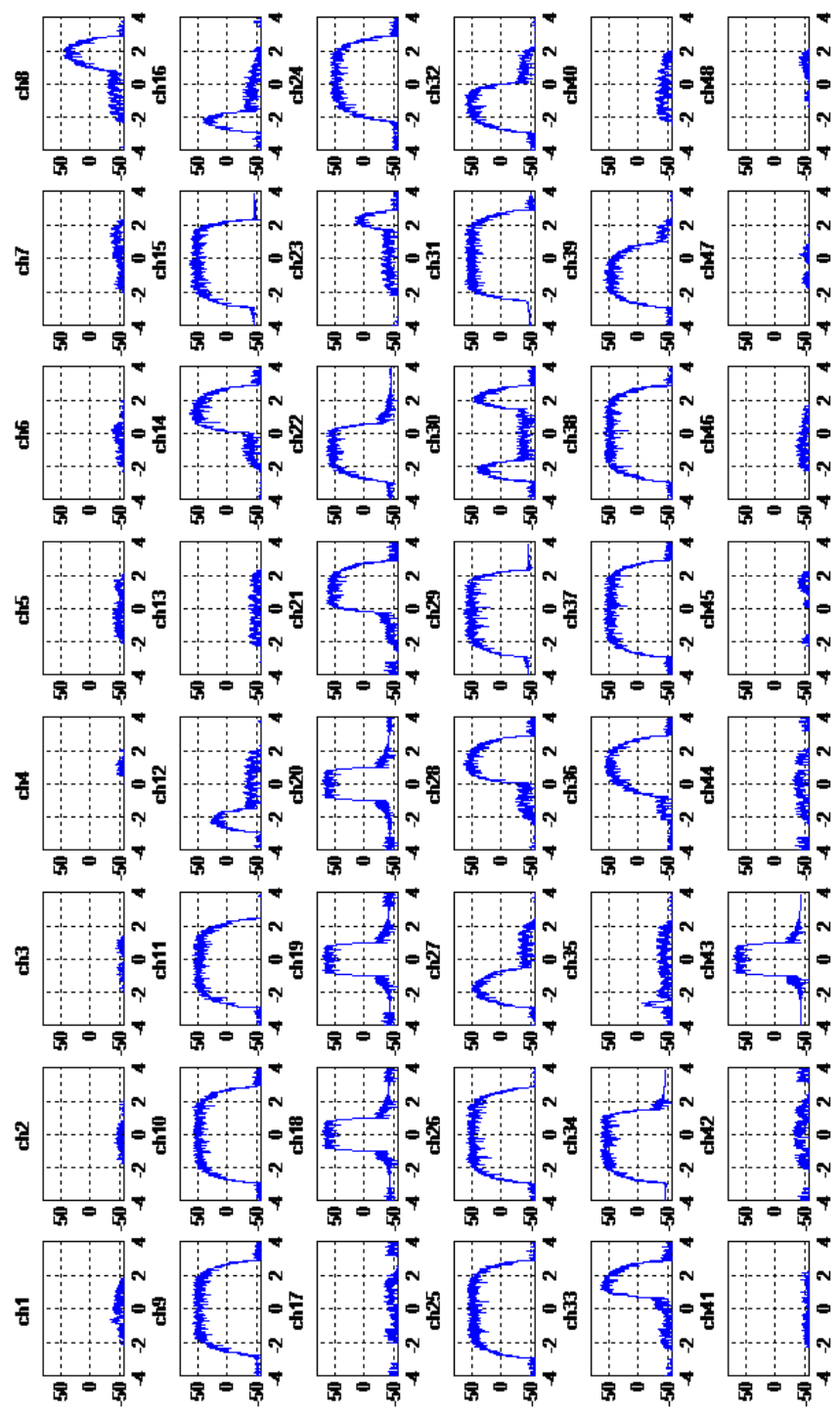


Figure 6.11: PAC Output Signal Spectrum

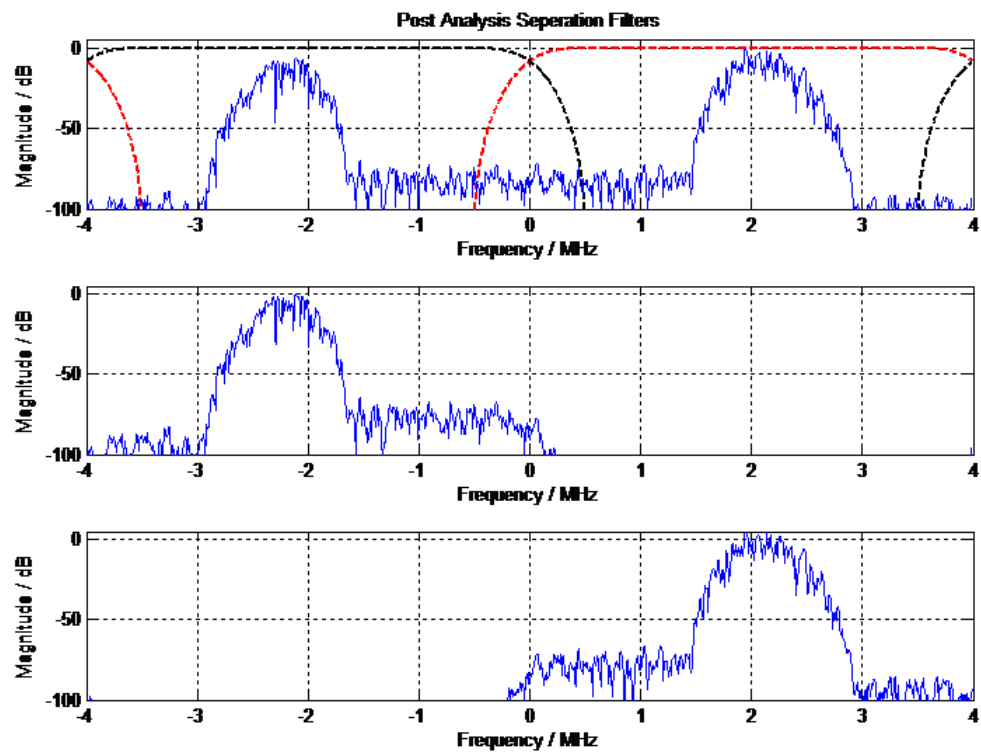
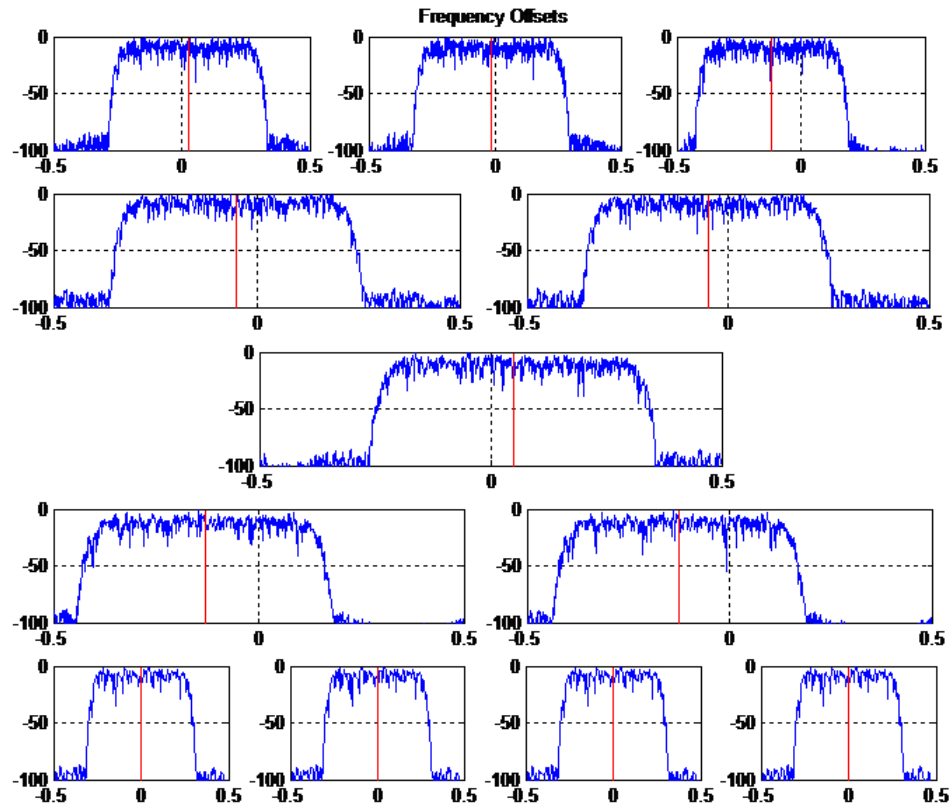
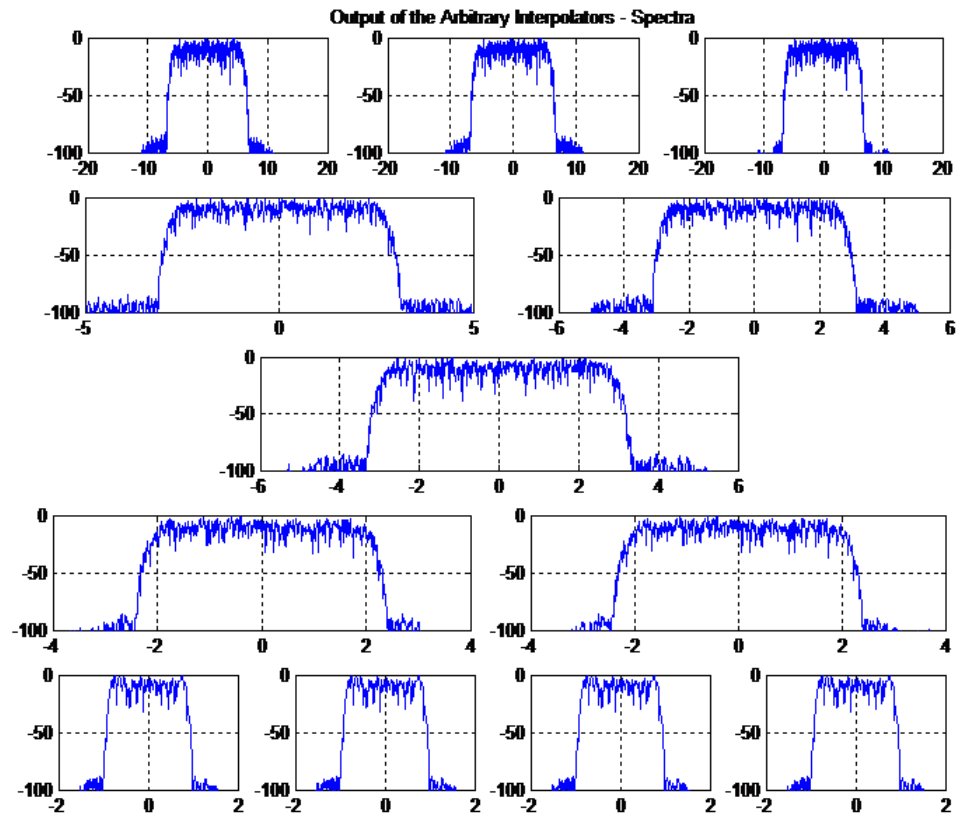


Figure 6.12: Post Analysis Filters and Filtered Signals for Channel 30 of the PAC



**Figure 6.13:** Log Magnitude of Synthesizer Outputs with Frequency Offsets in the Normalized Frequency Domain



**Figure 6.14:** Log Magnitude of the Heterodyned and Interpolated Spectra in the Frequency Domain [MHz]

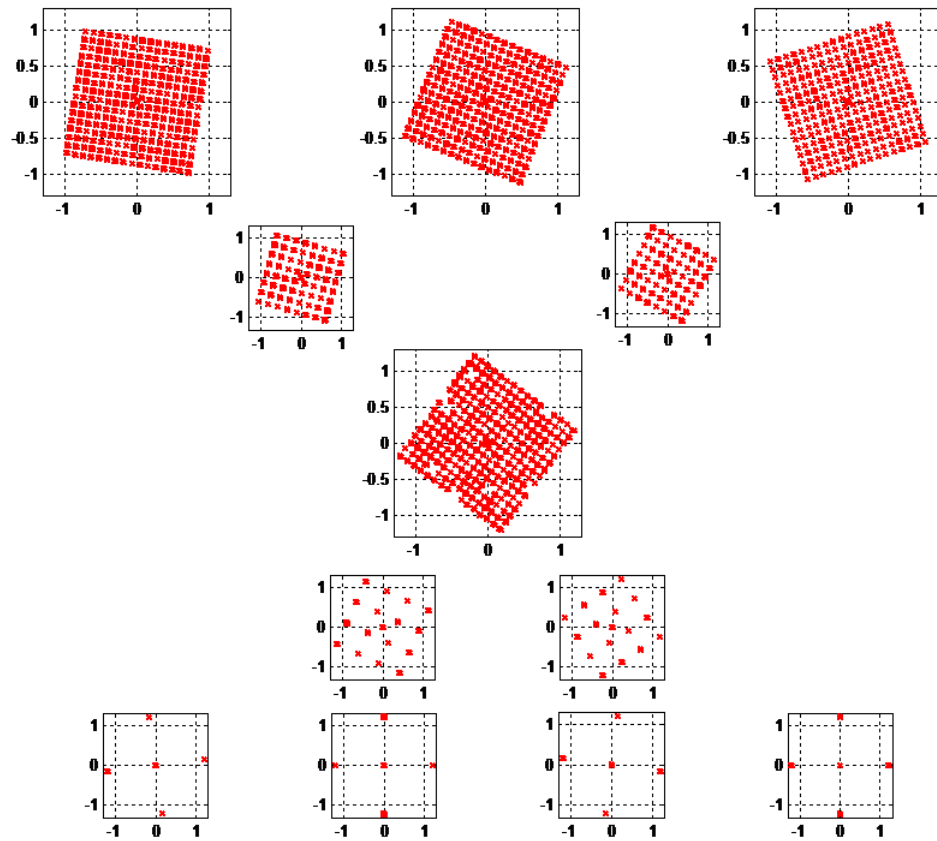


**Figure 6.15:** Matched-Filtered and Timing Recovery Signal Constellation

# **Chapter 7**

## **Conclusions**

In this dissertation, a set of NMDFB based wideband signal processing solutions are proposed to tackle various signal processing problems occurred when the signals' sample rates are comparable to the hardware's clock rate. The proposed novel filtering approach not only exhibits low speed processing characteristic but also ties its workload to FFT. We also explored the opportunity of using NMDFB based filters as a receiver. It is shown that the NMDFB based filter can efficiently perform linear / non-linear equalization tasks as FIR filters do, but in a much economical fashion. We also demonstrated the carrier, and timing synchronization techniques for an NMDFB based receiver. Despite for replacing the FIR filters with NMDFB based filters, we also presented the new features offered by NMDFB that are previously unavailable. This includes using NMDFB filter as a wideband diversity combiner and using NMDFB to perform channelization tasks. We summarize the benefits of the proposed wideband solutions in the following areas:

- **Wideband Digital Filtering:** The NMDFB based filter utilizes the spectral shaping method to synthesize any spectral responses with a controlled level of accuracy. The major benefit of this type of filter is its low power and low clock rate nature. In addition, the NMDFB based filter supports multiple cascade time variant and invariant filtering at the cost of one filter. This feature makes it a strong candidate for performing a chain of signal processing tasks, e.g., signal processing chain inside a modem.
- **Wideband Equalizer:** As discussed in Chapter III, with trivial modification the NMDFB filters can perform both linear and non-linear equalization to very wideband single carrier QAM signals. We have shown the proposed equalizer has workload related to the workload of FFT. Therefore, the receiver's complexity is on the same order of OFDM system. This fact made the idea of wideband single carrier QAM transmission feasible. Plus, one can take advantage of all the nice properties in QAM waveform and still enjoy the efficiency of the frequency domain equalization.
- **Diversity Combiner for Wideband Single Carrier Signals:** The diversity combining is a crucial technique for reliable communication. As discussed in Chapter

IV, the NMDFB based filters servers naturally as a wideband signal combiner. Moreover, it enables the filter bank selection combining technique, whose performance is very close to the optimal MRC approach but does not need prior channel knowledge.

- **Synchronization of Single Carrier Signal:** The conventional approach for synchronizing the single carrier signal requires building multiple FIR filters running in parallel extracting and monitoring the synchronization characteristics. For wideband signals, the FIR approach becomes unaffordable and power inefficient. The proposed synchronization approach takes advantage of the efficiency of NMDFB filters and finishes the synchronizations tasks in between the analysis and synthesis filter bank. This arrangement is shown to be a lot more efficient and hardware friendly than the existing solutions.
- **Channelization Technique:** The channelization technique holds the essential key to future's communication system. This dissertation proposed a complete and elegant solution for channelizing multiple signals with arbitrary formats, arbitrary center frequencies, and arbitrary bandwidths.

We have started with the digital filtering problem and proposed a set of solutions dealing with the challenges occurred in wideband signal processing. The proposed solutions are shown to be much capable of performing key signal processing tasks that are required by the upcoming future's communication systems.

# Bibliography

- [1] T. Karp and N. J. Fliege, "Modified dft filter banks with perfect reconstruction," *IEEE Trans. Circuits Syst. II*, vol. 46, no. 11, pp. 1404–1414, Dec 1999.
- [2] f. j. harris, X. Chen, E. Venosa, and C. Dick, "Wideband 160-channel polyphase filter bank cable tv channeliser," *Signal Processing, IET*, vol. 5, pp. 325–332, June 2011.
- [3] f. j. harris, E. Venosa, X. Chen, and B. D. Rao, "Polyphase analysis filter bank down-converts unequal channel bandwidths with arbitrary center frequencies," *Analog Integr Circ Sig Process*, vol. 71, no. 3, pp. 481–494, 2012.
- [4] M. Magarini, L. Barletta, and A. Spalvieri, "Efficient computation of the feedback filter for the hybrid decision feedback equalizer in highly dispersive channels," *IEEE Trans. Wireless Commun*, vol. 11, no. 6, pp. 2245–2253, June 2012.
- [5] G. Fettweis, F. Guderian, and S. Krone, "Entering the path towards terabit/s wirelesslinks," in *Design, Automat. Test Eur. Conf. Exhibit.*, 2011, pp. 1–6.
- [6] N. Benvenuto, R. Dinis, D. Falconer, and S. Tomasin, "Single carrier modulation with nonlinear frequency domain equalization: an idea whose time has come again," *Proc. IEEE*, vol. 98, no. 1, pp. 69–96, Jan 2010.
- [7] S. Tomasin and N. Benvenuto, "Iterative design and detection of a dfe in the frequency domain," *IEEE Trans. Commun*, vol. 53, no. 11, pp. 1867–1875, 2005.
- [8] J. Proakis, *Digital Communications*. McGraw-Hill Education, 2007.
- [9] D. Falconer, "History of equalization 1860-1980," *IEEE Commun. Mag*, vol. 49, no. 10, pp. 42–50, Oct 2011.
- [10] S. Ariyavisitakul, D. Falconer, F. Adachi, and H. Sari, "Guest editorial - wireless broadband techniques," *IEEE J. Select. Areas Commun*, vol. 17, no. 10, pp. 1709–1710, Oct 1999.
- [11] G. Fettweis. (2011) How to keep 100b transistors busy for cellular communications and beyond. [Online]. Available: <http://www.comm.ntu.edu.tw/>

filedownload.php?filename=Gerhard+Fettweis+at+NTU+DistLecturer+2010+05+17.pdf&filepath=./NewsUploadDir/2010\_05\_19\_03\_06\_21\_0.pdf

- [12] J. Mitola, "Cognitive radio architecture evolution," *Proc. IEEE*, vol. 97, no. 4, pp. 626–641, 2009.
- [13] A. V. Oppenheim and R. W. Schaffer, *Digital Signal Processing*. Prentice-Hall, 1987.
- [14] V. N. Richard and R. Prasad, *OFDM wireless multimedia communication*. Artech House, 2000.
- [15] D. Falconer, S. L. Ariyavisitakul, A. Benyamin-Seeyar, and B. Eidson, "Frequency domain equalization for single-carrier broadband wireless systems," *IEEE Commun. Mag*, vol. 40, no. 4, pp. 58–66, Apr 2002.
- [16] J. G. Proakis and D. G. Manolakis, *Digital Signal Processing*. Pearson Prentice Hall, 2007.
- [17] f. j. harris, *Multirate Signal Processing for Communication Systems*. Prentice Hall, 2004.
- [18] P. P. Vaidyanathan, "Theory and design of m channel maximally decimated quadrature mirror filters with arbitrary m, having perfect reconstruction property," *IEEE Trans. Acoust., Speech, Signal Processing*, vol. ASSP-35, pp. 476–492, Apr 1987.
- [19] T. A. Ramstad and J. P. Tanem, "Cosine-modulated analysis-synthesis filter bank with critical sampling and perfect reconstruction," in *Proc. IEEE Int. Conf. ASSP*. IEEE, 1991, pp. 1789–1792.
- [20] Y. Lin and P. P. Vaidyanathan, "Linear phase cosine modulated maximally decimated filter banks with perfect reconstruction," *IEEE Trans. Signal Processing*, vol. 42, pp. 2525–2539, Nov 1995.
- [21] M. Vetterli and D. Le Gall, "Perfect reconstruction fir filter banks: Some properties and factorizations," *IEEE Trans. Acoust., Speech, Signal Processing*, vol. 37, no. 7, pp. 1057–1071, July 1989.
- [22] V. K. Jain and R. E. Crochiere, "Cosine-modulated analysis-synthesis filter bank with critical sampling and perfect reconstruction," in *Proc. IEEE Int. Conf. ASSP*. IEEE, 1983, pp. 5.10–5.10.
- [23] P. P. Vaidyanathan, *Multirate Systems and Filter Banks*. Prentice Hall, 1993.
- [24] G. Strang and T. Q. Nguyen, *Wavelets and filter banks*. Wellesley-Cambridge Press, 1997.

- [25] N. J. Fliege, *Multirate Digital Signal Processing*. Wiley, 1994.
- [26] P. N. Heller, T. Karp, and T. Q. Nguyen, "A general formulation of modulated filter banks," *IEEE Trans. Signal Process*, vol. 47, no. 4, pp. 986–1002, Apr 1999.
- [27] T. Q. Nguyen, "Near-perfect-reconstruction pseudo-qmf banks," *IEEE Trans. Signal Process*, vol. 42, no. 1, pp. 65–67, Jan 1994.
- [28] S. S. Yin, S. C. Chan, and K. M. Tsui, "On the design of nearly-pr and pr fir cosine modulated filter banks having approximate cosine-rolloff transition band," *IEEE Trans. Signal Process*, vol. 42, no. 1, pp. 65–67, Jan 1994.
- [29] G. Doblinger, "A fast design method for perfect-reconstruction uniform cosine-modulated filter banks," *IEEE Trans. Signal Process*, vol. 60, no. 12, pp. 6693–6697, Dec 2012.
- [30] T. D. Tran, "M-channel linear phase perfect reconstruction filter bank with rational coefficients," *IEEE Trans. Circuits Syst. I, Fundam. Theory Appl*, vol. 49, no. 7, pp. 914–927, July 2002.
- [31] R. B. Casey and T. Karp, "Performance analysis and prototype filter design for perfect-reconstruction cosine-modulated filter banks with fixed-point implementation," *IEEE Trans. Circuits Syst. II*, vol. 52, no. 8, pp. 452–456, Aug 2005.
- [32] H. Bolcskei and F. Hlawatsch, "Oversampled cosine modulated filter banks with perfect reconstruction," *IEEE Trans. Circuits Syst. II*, vol. 45, no. 8, pp. 1057–1071, Aug 1998.
- [33] Z. Cvelkovic and M. Vetterli, "Oversampled filter banks," *IEEE Trans. Signal Process*, vol. 46, no. 5, pp. 1245–1255, May 1998.
- [34] H. Bolcskei, F. Hlawatsch, and H. Feichtinger, "Frame-theoretic analysis of oversampled filter banks," *IEEE Trans. Signal Process*, vol. 46, no. 12, pp. 3256–3268, Dec 1998.
- [35] J. M. de Haan, "Filter bank design for subband adaptive filtering," Ph.D. dissertation, University of Karlskrona and Ronneby, 2001.
- [36] A. Viholainen, J. Alhava, and M. Renfors, "Efficient implementation of 2 x oversampled exponentially modulated filter banks," *IEEE Trans. Circuits Syst. II*, vol. 53, no. 10, pp. 1138–1142, Oct 2006.
- [37] D. Pinchon and P. Siohan, "Oversampled paraunitary dft filter banks: A general construction algorithm and some specific solutions," *IEEE Trans. Signal Process*, vol. 59, no. 7, pp. 3058–3070, July 2011.
- [38] T. Tanaka, "A direct design of oversampled perfect reconstruction fir filter banks," *IEEE Trans. Signal Process*, vol. 54, no. 8, pp. 3011–3022, Aug 2006.

- [39] L. Chai, J. Zhang, and Y. Sheng, "Optimal design of oversampled synthesis fbs with lattice structure constraints," *IEEE Trans. Signal Process*, vol. 59, no. 8, pp. 3549–3559, Aug 2011.
- [40] Y. C. Lim and Y. Lian, "Frequency response masking approach for digital filter design: Complexity reduction via masking filter factorization," *IEEE Trans. Circuits Syst. II*, vol. 41, no. 8, pp. 518–525, Aug 1994.
- [41] Y. C. Lim and R. Yang, "On the synthesis of very sharp decimators and interpolators using the frequency-response masking technique," *IEEE Trans. Signal Process*, vol. 53, no. 4, pp. 1387–1397, Apr 2005.
- [42] L. Rosenbaum, P. Lowenborg, and H. Johansson, "Cosine and sine modulated fir filter banks utilizing the frequency-response masking approach," in *Proc. IEEE Int. Symp. Circuits Syst.* IEEE, 2003, pp. III–882 –III–885.
- [43] Z. U. Sheikh and H. Johansson, "Efficient wide-band fir lti systems derived via multi-rate techniques and sparse bandpass filters," *IEEE Trans. Signal Process*, vol. 60, no. 7, pp. 3859–3863, July 2012.
- [44] f. j. harris, E. Venosa, X. Chen, and B. D. Rao, "Variable bandwidth m-path filter with fixed coefficients formed by m-path polyphase filter engines," in *Proc. Circuit Theory and Design, 20th European Conf. on.* IEEE, 2011, pp. 29–31.
- [45] D. G. Manolakis, V. K. Ingle, and S. M. Kogon, *Statistical and adaptive signal processing: spectral estimation, signal modeling, adaptive filtering and array processing.* Artech House, 2005.
- [46] L. R. Rabiner and B. Gold, *Theory and Application of Digital Signal Processing.* Prentice-Hall, 1975.
- [47] f. j. harris, "Performance and design of farrow filter used for arbitrary resampling," in *Proc. 13th Int. Conf. DSP.* IEEE, 1997, pp. 595–599.
- [48] C. S. Burrus and T. W. Parks, *DFT/FFT and convolution algorithms: theory and implementation.* Wiley, 1984.
- [49] R. Shafik, S. Rahman, and A. R. Islam, "On the extended relationships among evm, ber and snr as performance metrics," in *Proc. IEEE ICECE.* IEEE, 2006, pp. 408–411.
- [50] G. Huang, A. Nix, and S. Armour, "Feedback reliability calculation for an iterative block decision feedback equalizer," in *Vehicular Technology Conference Fall (VTC 2009-Fall).* IEEE, Sept 2009, pp. 1–5.
- [51] C. Zhang, Z. Wang, C. Pan, S. Chen, and L. Hanzo, "Low-complexity iterative frequency domain decision feedback equalization," *IEEE Trans. Veh. Technol*, vol. 60, no. 3, pp. 1295–1301, March 2011.

- [52] G. B. Giannakis, "Filterbanks for blind channel identification and equalization," *IEEE Signal Process. Lett.*, vol. 4, no. 6, pp. 184–187, 1997.
- [53] A. Scaglione, G. B. Giannakis, and S. Barbarossa, "Redundant filterbank precoders and equalizers part i: Unification and optimal designs," *IEEE Trans. Signal Process.*, vol. 47, no. 7, pp. 1988–2006, 1999.
- [54] G. Gu and E. F. Badran, "Optimal design for channel equalization via the filterbank approach," *IEEE Trans. Signal Process.*, vol. 52, no. 2, pp. 536–545, 2004.
- [55] P. K. S. Carson and N. Q. Truong, "Design of oversampled filter bank based widely linear oqpsk equalizer," in *Proc. IEEE Int. Conf. ASSP*. IEEE, April 2007, pp. III-861–III-864.
- [56] D. S. Waldhauser, L. G. Baltar, and J. A. Nossek, "Mmse subcarrier equalization for filter bank based multicarrier systems," in *Signal Processing Advances in Wireless Communications SPAWC 2008*. IEEE, July 2008, pp. 525–529.
- [57] T. Ihalainen, A. Ikhlef, J. Louveaux, and M. Renfors, "Channel equalization for multi-antennafbmc/oqam receivers," *IEEE Trans. Veh. Technol.*, vol. 60, no. 5, pp. 2070–2085, 2011.
- [58] B. Farhang-Boroujeny, "Ofdm versus filter bank multicarrier," *IEEE Signal Process. Mag.*, vol. 28, no. 3, pp. 92–112, 2011.
- [59] C. Hu and Y. Liao, "Efficient mimo ds-usb downlink chip-level mmse equalization using subband adaptive interference mitigation techniques," *Trans. Veh. Technol.*, vol. 61, no. 8, pp. 3783–3790, 2012.
- [60] B. Farhang-Boroujeny, *Adaptive filters: theory and applications*. Wiley, 1998.
- [61] S. Weiss, S. R. Dooley, R. W. Stewart, and A. K. Nandi, "Adaptive equalization in oversampled subbands," *Electron. Lett.*, vol. 34, no. 15, pp. 1452–1453, 1998.
- [62] Y. Yang, T. H. Stitz, M. Rinne, and M. Renfors, "Mitigation of narrowband interference in sc transmission with filter bank equalization," in *Circuits and Systems, 2006. APCCAS 2006. IEEE Asia Pacific Conference on*. IEEE, Dec 2006, pp. 748–751.
- [63] Y. Yang, T. Ihalainen, M. Renfors, and M. Rinne, "Noise predictive turbo equalization for a filter bank based receiver in a sc transmission system," in *Vehicular Technology Conference Fall (VTC 2007-Spring)*. IEEE, April 2007, pp. 2389–2393.
- [64] X. Chen, f. j. harris, E. Venosa, and B. D. Rao, "Non-maximally decimated analysis/synthesis filter banks: Applications in wideband digital filtering," *IEEE Trans. Signal Process.*, vol. 62, no. 4, pp. 852–867, 2014.

- [65] S. Weiss, M. Rupp, and L. Hanzo, "A fractionally spaced dfe with subband decorrelation," in *34th Asilomar Conf. Signals, Syst., Comput.* IEEE, 2000, pp. 1767–1771.
- [66] H. Mohamad, S. Weiss, M. Rupp, and L. Hanzo, "A performance comparison of fullband and different subband adaptive equalisers," in *11th IEEE Signal Processing Workshop on Statistical Signal Processing.* IEEE, Aug 2001, pp. 567–570.
- [67] A. Stamoulis, G. B. Giannakis, and A. Scaglione, "Block fir decision-feedback equalizers for filterbank precoded transmissions with blind channel estimation capabilities," *IEEE Trans. Commun.*, vol. 49, no. 1, pp. 69–83, 2001.
- [68] K. Berberidis and P. Karaivazoglou, "An efficient block adaptive decision feedback equalizer implemented in the frequency domain," *IEEE Trans. Signal Processing.*, vol. 50, no. 1, pp. 2273–2285, 2002.
- [69] A. Gersho and T. L. Lim, "Adaptive cancellation of intersymbol interference for data transmission," *Bell Syst. Tech. J.*, vol. 70, no. 1, pp. 1997–2021, 2002.
- [70] E. Biglieri, A. Gersho, R. D. Gitlin, and T. L. Lim, "Adaptive cancellation of nonlinear intersymbol interference for voiceband data transmission," *IEEE J. Sel. Areas Commun.*, vol. 52, no. 5, pp. 765–777, 1984.
- [71] S. Weiss, A. Stenger, R. W. Stewart, and R. Rabenstein, "Steady-state performance limitations of subband adaptive filters," *IEEE Trans. Signal Process.*, vol. 49, pp. 1982–1991, 2001.
- [72] H. Mohamad, S. Weiss, and M. Rupp, "Mmse limitations for subband adaptive equalisers," in *36th Asilomar Conf. Signals, Syst., Comput.* IEEE, 2002, pp. 1233–1237.
- [73] S. U. H. Qureshi, "Adaptive equalization," *Proc. IEEE*, vol. 73, no. 9, pp. 1349–1387, 1985.
- [74] K. Wesolowski, "On the performance and convergence of the adaptive canceller of intersymbol interference in data transmission," *IEEE Trans. Commun.*, vol. 33, pp. 425–432, 1985.
- [75] J. J. Shynk, "Frequency-domain and multirate adaptive filtering," *IEEE Signal Processing Mag*, vol. 9, no. 1, pp. 14–37, 1992.
- [76] E. Nemer, "Effective multi-mode equalization for atsc receivers," in *Consumer Communications and Networking Conference, 2006.* IEEE, 2002, pp. 854–858.
- [77] Guidelines for evaluation of radio transmission technologies for imt-2000. [Online]. Available: [http://www.itu.int/dms\\_pubrec/itu-r/rec/m/R-REC-M.1225-0-199702-1!!PDF-E.pdf](http://www.itu.int/dms_pubrec/itu-r/rec/m/R-REC-M.1225-0-199702-1!!PDF-E.pdf)

- [78] F. Ling, "Matched filter-bound for time-discrete multipath rayleigh fading channels," *IEEE Trans. Commun.*, vol. 43, pp. 710–713, 1995.
- [79] M. X. Chang and Y. T. Su, "Performance analysis of equalized ofdm systems in rayleigh fading," *IEEE Trans. Wireless Commun.*, vol. 1, no. 4, pp. 721–732, 2002.
- [80] R. Porat, "Introductory tgah proposal," Doc. IEEE 802.11-11/0069r0, Tech. Rep.
- [81] G. Breit, "Tgac channel model addendum," Doc. IEEE 802.11-09/0308r12, Tech. Rep.
- [82] P. Balaban and J. Salz, "Optimum diversity combining and equalization in digital data transmission with applications to cellular mobile radio-part i and ii: Theoretical considerations," *IEEE Trans. Commun.*, vol. 40, pp. 885–907, 1992.
- [83] T. Ihalainen, Y. Yuan, and M. Renfors, "Filter bank based frequency-domain equalizers with diversity combining," in *IEEE International Symposium on Circuits and Systems, 2008*. IEEE, 2008, pp. 93–96.
- [84] M. Caus and A. I. Perez-Neira, "Transmitter-receiver designs for highly frequency selective channels in mimo fbmc systems," *IEEE Trans. Signal Process.*, vol. 60, no. 12, pp. 6519–6532, Dec 2012.
- [85] T. Ihalainen, T. H. Stitz, M. Rinne, and M. Renfors, "Channel equalization in filter bank based multicarrier modulation for wireless communications," *EURASIP J. Advances Signal Proces.*, 2007.
- [86] Y. Yang, T. Ihalainen, M. Rinne, and M. Renfors, "Frequency-domain equalization in single-carrier transmission: filter bank approach," *EURASIP J. Advances Signal Proces.*, 2007.
- [87] f. j. harris, E. Venosa, X. Chen, and C. Dick, "Band edge filters perform non data-aided carrier and timing synchronization of software defined radio qam receivers," in *WPMC*. IEEE, Sept 2012, pp. 271–275.
- [88] C. Dick, f. j. harris, and M. Rice, "Synchronization in software radios. carrier and timing recovery using fpgas," in *Field-Programmable Custom Computing Machines, 2000 IEEE Symposium on*. IEEE, 2000, pp. 195–204.
- [89] f. j. harris and M. Rice, "Multirate digital filters for symbol timing synchronization in software-defined radios," *IEEE J. Sel. Areas Commun.*, vol. 19, no. 12, pp. 2346–2357, 2001.
- [90] L. E. Franks, "Carrier and bit synchronization in data communication: a tutorial review," *IEEE Trans. Commun.*, vol. 28, no. 8, pp. 1107–1121, 1980.

- [91] f. j. harris, C. Dick, and M. Rice, "Digital receivers and transmitters using polyphase filter banks for wireless communications," *IEEE Trans. Microwave Theory Tech.*, vol. 51, no. 4, pp. 1395–1412, 2003.
- [92] E. Buracchini, "The software radio concept," *IEEE Commun. Mag.*, vol. 38, no. 9, pp. 138–143, 2000.
- [93] f. j. harris and W. Lowdermilk, "Software defined radio: Part 22 in a series of tutorials on instrumentation and measurement," *IEEE Instrum. Meas. Mag.*, vol. 13, no. 1, pp. 23–32, 2010.
- [94] I. F. Akyildiz, W. Y. Lee, M. C. Vuran, and S. Mohanty, "Next generation/dynamic spectrum access/cognitive radio wireless networks: A survey," *Computer Networks Journal*, vol. 50, pp. 2127–2159, Sept 2006.
- [95] B. Wang and K. J. Liu, "Advances in cognitive radio networks: A survey," *IEEE J. Sel. Topics Signal Process.*, vol. 5, no. 1, pp. 5–23, February 2011.
- [96] A. Sahai, S. M. Mishra, R. Tandra, and K. A. Woyach, "Cognitive radios for spectrum sharing," *IEEE Signal Process. Mag.*, vol. 26, no. 1, pp. 140–145, Jan 2009.
- [97] T. Ulversoy, "Software defined radios: challenges and opportunities," *IEEE Communications Surveys and Tutorials*, vol. 12, no. 4, April 2010.
- [98] R. Bagheri, A. Mirzaei, and M. E. Heidari, "Software-defined radio receiver: Dream to reality," *IEEE Commun. Mag.*, vol. 44, no. 8, pp. 111–118, August 2006.
- [99] M. Sherman, A. N. Mody, R. Martinez, and C. Rodriguez, "Ieee standards supporting cognitive radio and networks, dynamic spectrum access, and coexistence," *IEEE Commun. Mag.*, vol. 46, no. 7, pp. 72–79, 2008.
- [100] J. Ma, G. Y. Li, and B. H. Juang, "Signal processing in cognitive radio," *Proc. IEEE*, vol. 97, no. 5, pp. 805–823, 2009.
- [101] R. Tandra, S. M. Mishra, and A. Sahai, "What is a spectrum hole and what does it take to recognize one?" *Proc. IEEE*, vol. 97, no. 5, pp. 824–848, 2009.
- [102] f. j. harris, C. Dick, X. Chen, and E. Venosa, "M path channelizer with arbitrary center frequency assignments," in *WPMC 2010*. IEEE, March 2010.
- [103] A. Eghbali, H. Johansson, and P. Lowenborg, "Reconfigurable nonuniform transmultiplexers based on uniform filter banks," in *Proc. IEEE Int. Symp. Circuits Syst.* IEEE, 2010.

- [104] T. Liu and T. Chen, "Design of multichannel nonuniform transmultiplexers using general building blocks," *IEEE Trans. Signal Process.*, vol. 49, no. 1, pp. 91–99, January 2001.
- [105] A. Eghbali, H. Johansson, P. Lowenborg, and H. G. Gockler, "Flexible dynamic frequency-band reallocation and allocation: from satellite based communication systems to cognitive radios," *Journal of Signal Processing Systems*, January 2009.
- [106] A. Eghbali, H. Johansson, and P. Lowenborg, "A multimode transmultiplexer structure," *IEEE Trans. Circuits Syst. II*, vol. 55, no. 3, pp. 279–283, March 2008.
- [107] E. Venosa, X. Chen, and f. j. harris, "Polyphase analysis filter bank down-converts unequal channel bandwidths with arbitrary center frequencies-design i," in *SDR 2010. SDR-WinnComm*, December 2010.